ANALYTICAL AND EXPERIMENTAL INVESTIGATION OF DYNAMIC AMPLIFICATION FACTOR FOR THE LOAD RATING OF REINFORCED CONCRETE BOX CULVERTS

by

Andrew C. Wells

A thesis submitted to the Faculty of the University of Delaware in partial fulfillment of the requirements for the degree of Master of Civil Engineering

Fall 2016

ANALYTICAL AND EXPERIMENTAL INVESTIGATION OF

DYNAMIC AMPLIFICATION FACTOR FOR THE LOAD RATING

OF REINFORCED CONCRETE BOX CULVERTS

by

Andrew C. Wells

Approved: _____

Harry W. Shenton III, Ph.D.
Professor in charge of thesis on behalf of the Advisory Committee

Approved: _____

Kalehiwot Nega Manahiloh, Ph.D.
Professor in charge of thesis on behalf of the Advisory Committee

Approved: _____

Harry W. Shenton III, Ph.D.
Chair of the Department of Civil & Environmental Engineering

Approved: _____

Babatunde A. Ogunnaike, Ph.D.
Dean of the College of Engineering

Approved: _____

Ann L. Ardis, Ph.D.
Senior Vice Provost for Graduate and Professional Education

ACKNOWLEDGMENTS

I would like to thank my parents, Chris and Karen Wells, for their unending support in all my endeavors. They have always done their best to put me in a position to succeed. For that I am eternally grateful. Their love and friendship are extremely valuable to me; and their support and encouragement have allowed me to pursue a variety of personal and professional interests that I would not have been able to otherwise. I am truly humbled by their commitment to me and my success.

I would also like to thank my many friends in the New Hampshire Section of the American Society of Civil Engineers (ASCE-NH). Much of my professional development up to this point has occurred while participating in ASCE-NH and I have always appreciated my relationships with people there. I feel very fortunate to call so many great engineers my friends. In particular, I would like to thank Hugh Scott, Darren Benoit and Tony Puntin for their encouragement and mentorship, without which many of my current opportunities would not have been realized.

Finally, I would like to thank my advisors, Dr. Harry Shenton and Dr. Kalehiwot Nega Manahiloh, for providing me with the opportunity to work on this research project, as well as Gary Wenczel and my fellow graduate students for their assistance throughout. I have gotten great satisfaction out of this investigation and it would not have been possible without them.

TABLE OF CONTENTS

LIST OF TABLES

LIST OF FIGURES

ABSTRACT

This thesis seeks to better understand the factors that influence the dynamic amplification of reinforced concrete box culverts (RCBC) resulting from moving traffic loads. Due to large discrepancies between observations made during inspections and the results of load rating many RCBC in the State of Delaware, it is believed that the dynamic amplification factor (*DAF*) is overconservative. The *DAF* is a ratio of a structure's dynamic response to its static response, used to amplify static loads to account for the maximum dynamic loading condition.

According to American Association of State Highway and Transportation Officials (AASHTO) provisions, *DAF* for RCBC is specified as 1.33 when zero meters of fill is present between the culvert and pavement, and decreases linearly to 1.00 when 2.44 m of fill is present. Two approaches are taken to investigate the adequacy of this specification. First, a parametric finite element analysis is conducted to examine the influence of fill depth, soil elastic modulus, span length, slab thickness and asphalt pavement thickness on *DAF*. In total 324 two-dimensional, plane-strain model configurations are analyzed. Second, five culverts representative of the Delaware Department of Transportation's inventory are instrumented and tested to investigate the behavior of in-service RCBCs.

Prior to the finite element analysis and field testing program, a literature review was conducted that revealed *DAF* to be extremely complex in nature. Particularly, it was noted that many studies examining structural dynamics have conflicting results due to the many factors that influence these systems.

The finite element analysis shows good agreement between the two-dimensional, numerical results and the theoretical solution to a single degree of

freedom (SDOF) system. This subsequently suggests that the dynamic amplification is related to the ratio of the applied load's pulse duration to the structure's natural period.

The maximum *DAF* calculated during the parametric study is 1.28. Based on the linear fit trend lines for each parameter, *DAF* has a positive relation with fill depth and pavement thickness, and a negative relation with soil elastic modulus, span length, and slab thickness. However, relative to fill depth and soil elastic modulus, span length, slab thickness and asphalt pavement thickness have little influence on *DAF*. The trend of increasing *DAF* with increasing fill depth is opposite those suggested by AASHTO specifications.

During field testing, the maximum *DAF* recorded for any culvert at the location of maximum static strain was 1.20. Two of the five culverts tested did not record *DAF* values greater than 1.05 at the location of maximum static strain. Contrary to the numerical results, field test results show fill depth to have a negative relation with *DAF* and slab thickness to have a positive relation. These differences may be due to the disparity between the limited number of field tests conducted and the number of model configurations analyzed. Additionally, the maximum fill depth of any culvert instrumented and tested is 0.5 m while the finite element analysis examined model configurations with up to 1.83 m of fill.

Depending on the statistic used, field tests do appear to corroborate trends suggested by AASHTO. However, based on the limited number of tests conducted and the contradictory results presented in the parametric finite element study it is difficult to elaborate on the extent to which that is true. The scope of field tests was limited to RCBC with less than 0.5 m of fill and with road surfaces in good condition. For

culverts within the range of these and other parameters tested in the field, a maximum *DAF* of 1.20 is recommended.

Chapter 1

INTRODUCTION

1.1 Overview of Bridge Load Rating

Under current Federal Highway Administration (FHWA) requirements, bridge owners are required to inspect bridges every two years (23 CFR § 650 C 2011). Inspection results must be reported and individual bridge components graded according to National Bridge Inspection (NBI) guidelines (FHWA 1995). In addition, it is required that states mathematically assess the ability of bridges and bridge-type structures to service traffic in keeping with statewide policies. The process of mathematically determining the fitness of bridges is known as load rating. In this process, each component of the structure must be evaluated individually according to the AASHTO Manual for Bridge Evaluation (AASHTO 2011). This manual, in conjunction with the AASHTO LRFD Bridge Design Specifications (AASHTO 2012), provides all necessary equations to determine the suitability of each individual component.

1.1.1 Rating Factor Calculation

The result of a load rating is a rating factor (*RF*), which is a ratio of a structural component's live load capacity to the live load demands placed on the component. AASHTO (2011) specifies *RF* as the structure's capacity less the factored dead load, divided by the factored live load. For each bridge, the component that receives the

lowest rating factor is considered to govern the entire structure and is therefore the only rating factor reported.

$$RF = \frac{C - \gamma_{DC}(DC) - \gamma_{DW}(DW) \pm \gamma_P(P)}{\gamma_{LL}(LL + IM)} \quad (1-1)$$

Where:

C = Capacity
DC = Dead load due to components
DW = Dead load due to the wearing surface and utilities
LL = Live load
P = Permanent load
γ_{DC} = Dead load components factor
γ_{DW} = Dead load wearing surface and utilities factor
γ_{LL} = Live load factor
γ_p = Permanent load factor
IM = Dynamic load allowance

In Equation 1-1 each of the load factors account for uncertainty within the system. Because the precise dead and live loads are not known, the load factors add an additional measure of conservatism to the load rating process.

Furthermore, the dynamic load allowance (*IM*) accounts for additional load effects resulting from moving traffic. As a vehicle crosses a bridge, it imparts a dynamic pulse through the structure that amplifies the vehicle's stationary weight. Since the live load input is a static load, meaning that it is representative only of vehicle weight, this factor is necessary to characterize the maximum load demand. However, *IM* is only applied to truck loads. The intended meaning of the live load factorization in Equation 1-1 is thus $\gamma_{LL}[LL_{Lane} + (1 + IM)LL_{Truck}]$, where LL_{Lane} is representative of passenger vehicles and LL_{Truck} represents the live load due to large commercial vehicles (tractor trailers, dump trucks, etc.).

1.1.2 Load Rating Outcomes

If a bridge receives a rating factor equal to or greater than one, it indicates that the structure can safely carry vehicles of equal or lower weight than those used during load rating. If a bridge receives a rating factor less than one, weight restrictions must be placed on the structure or the bridge may even be closed to traffic. The results of doing so can negatively impact the local and regional economy, cause inconveniences to local residents and restrict first responder access to certain areas. Consequently, the appropriate specification of load factors is critical for balancing the societal utility of bridges with public safety.

1.2 Description of Culverts

This research examines the behavior of reinforced concrete box culverts, which are similar to bridges in many ways and fall under the umbrella of bridges for design and load rating purposes. As such, culverts are designed and load rated in accordance with AASHTO (2011; 2012) specifications. Primarily, both bridges and culverts carry roadways over an encountered feature. However, culverts differ from bridges in that they generally have small span lengths, are intended to function at full hydraulic capacity and are typically covered by soil.

As defined in the National Bridge Inventory (FHWA 1995), bridges are defined as:

> A structure including supports erected over a depression or an obstruction, such as water, highway, or railway, and having a track or passageway for carrying traffic or other moving loads, and having an opening measured along the center of the roadway of more than 20 feet between undercopings of abutments or spring lines of arches, or extreme ends of openings for multiple boxes; it may also include multiple pipes, where the clear distance between openings is less than half of the smaller contiguous opening.

By contrast a culvert is defined as:

> [A] structure designed hydraulically to take advantage of submergence to increase hydraulic capacity. Culverts, as distinguished from bridges, are usually covered with embankment and are composed of structural material around the entire perimeter, although some are supported on spread footings with the streambed serving as the bottom of the culvert. Culverts may qualify to be considered "bridge" length.

1.3 Research Initiative and Objectives

Ideally, the load rating process should work such that rating factors are characteristic of observations made during inspection. If all bridge or culvert components show little to no signs of deterioration then a bridge or culvert should receive a high rating factor. Conversely, if a component is in poor condition a bridge or culvert should receive a low rating factor. However, many culverts receive low rating factors while showing little signs of distress. Consequently, it is believed that codified specifications may be overconservative. One possible source of this inconsistency is believed to be the *IM* factor which has been the subject of relatively little research in relationship to other load factors. This thesis explores the geometric and material properties that influence dynamic amplification, assess the adequacy of current specifications, and give recommendations regarding a possible reformulation of codified equations.

1.4 Research Approach

Fundamentally, the dynamic load allowance (*IM* or *DLA*) is a ratio of the dynamic response (R_{Dyn}) and static response (R_{Stat}). Experimentally, it can be determined using the equation (Beben 2013; Deng et al. 2015):

$$IM = \frac{R_{Dyn} - R_{stat}}{R_{stat}} \qquad (1-2)$$

Because the intended usage of *IM* is $(1 + IM)LL$, the dynamic effects can be represented using a dynamic amplification factor (*DAF*).

$$DAF = 1 + IM \qquad (1-3)$$

The *DAF* can be experimentally determined by dividing a structure's maximum dynamic response by its static response:

$$DAF = \frac{R_{Dyn}}{R_{stat}} \qquad (1-4)$$

This thesis defines dynamic amplification in terms of *DAF*.

In order to better understand the dynamic behavior of culverts, a literature review is conducted, followed by a parametric finite element study and field testing. The parametric finite element analysis is conducted examining five aspects of the soil-structure-pavement system:

- Fill depth
- Soil elastic modulus
- Span length
- Culvert slab thickness
- Asphalt pavement thickness

A field testing program subsequently investigates the influence of fill depth, span length, slab thickness and asphalt pavement thickness on in-service culverts.

1.5 Thesis Structure

This thesis is broken into six chapters: 1) introduction of research topic, 2) literature review of applicable research, 3) a description of the finite element models and results of the finite element analysis, 4) a description of the field testing program

and its results, 5) a comparison of finite element and field test results and 6) conclusions and recommendations. In the literature review, the theoretical single degree of freedom (SDOF) solution is introduced, which shows dynamic amplification to be a function of the load's duration (i.e. how long a load is applied for), shape (load magnitude over time) and a structure's natural period. Current research relevant to the *DAF* of conventional bridges and buried structures as well as codified specifications are also discussed, followed by a review of materials and material properties present in the soil-structure-pavement system.

The finite element modeling chapter discusses the parametric finite element analysis, the models' composition and the selection of load shape. Since the SDOF solution suggests that the load duration that causes the maximum *DAF* varies from culvert to culvert, a detailed discussion of the load duration selected for each individual model ensues. Finally, the influence of each parameter is discussed and results are compared to the SDOF system.

The experimental testing of five culverts in the state of Delaware is discussed in Chapter 4. Fully loaded dump trucks are driven across each culvert at vehicle speeds of 2.2, 8.9, 13.4 and 17.9 m/s and strain is measured. Strains observed during 2.2 m/s passes represent quasi-static (or "crawl") responses, while strains observed during 8.9, 13.4 and 17.9 m/s passes represent dynamic responses. Results for each culvert are first examined individually to better understand the behavior of individual culverts and then collectively to assess the influence of fill depth, span length, slab thickness and asphalt pavement thickness on the soil-structure-pavement system.

In Chapter 5, the results of the finite element analysis and field testing study are compared. One of the main findings is that the finite element model and field

testing results show often times contradictory and even opposite results. This finding is discussed in light of the literature review, which shows *DAF* to be extremely complex in nature.

Finally, the conclusion summarizes findings and gives recommendations for the application of *DAF* in the load rating process. Furthermore, potential areas for future research are outlined.

Chapter 2

LITERATURE REVIEW

2.1 Introduction

The following sections examine the body of literature relevant to the dynamic amplification of culverts and relevant material properties. By no means is it intended to be exhaustive; however, it is meant to give a complete picture of past and current research on these topics. This chapter will review the theoretical solution to a single degree of freedom (SDOF) system subject to common dynamic load functions, research on the dynamic behavior of bridges, research specific to the *DAF* for culverts, codified specifications, soil behavior and material properties.

2.2 Theoretical Solutions to a Single Degree of Freedom System

Prior to examining the experimental research and codified formulas for *DAF* it is important to understand dynamic theory. In his book, Dynamics of Structures, Chopra (2012) formulates the solutions to an SDOF system subjected to various loading functions. Several of these solutions will be discussed here. As shown in Figure 2.1, the system is comprised of a lumped mass (m), with stiffness k and has a single, vertical degree of freedom, where down is in the positive x-direction. For an undamped system with no initial velocity or acceleration, the vertical position (x) of the mass at a given time (t) can be determined by solving Duhamel's Integral (Chopra 2012):

$$x(t) = \frac{T_n}{2\pi m}\int_0^t P(\tau)\sin\frac{2\pi(t-\tau)}{T_n}\,d\tau \qquad (2-1)$$

Where:

x = vertical displacement
t = time at which the displacement, x, occurs
T_n = natural period
m = mass
P(τ) = applied force
τ = increment of time

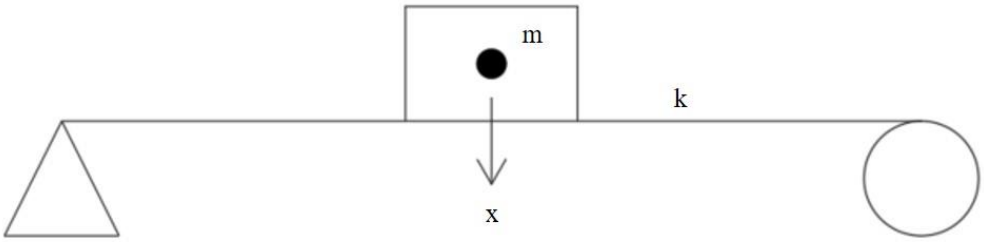

Figure 2.1 Diagram of Single Degree of Freedom System

The natural period is a measure of the number of harmonic oscillations the system makes per unit time. For an SDOF system it can be calculated using the equation:

$$T_n = 2\pi\sqrt{\frac{m}{k}} \qquad (2-2)$$

The applied force, P(τ), is broken into two parts: the static load (P_0), which is a constant, and a load function (f(τ)), which can vary with time.

$$P(\tau) = P_0 \times f(\tau) \qquad (2-3)$$

The load function is a scalar value that represents the magnitude of the total static load applied to the SDOF system at a given time, τ. Subsequent sections examine the

SDOF system's response to several load functions. The natural period used to calculate the displacement due to each load function is 0.1 seconds.

2.2.1 **Instantaneous Step Function**

A step function is the simplest dynamic load function that can be applied to a SDOF system. This function instantaneously applies the full magnitude of the static load and sustains it over the entire time interval.

$$f(t) = 1 \qquad (2-4)$$

Figure 2.2 shows the force magnitude with respect to time. As can be seen it immediately increases to one and remains constant.

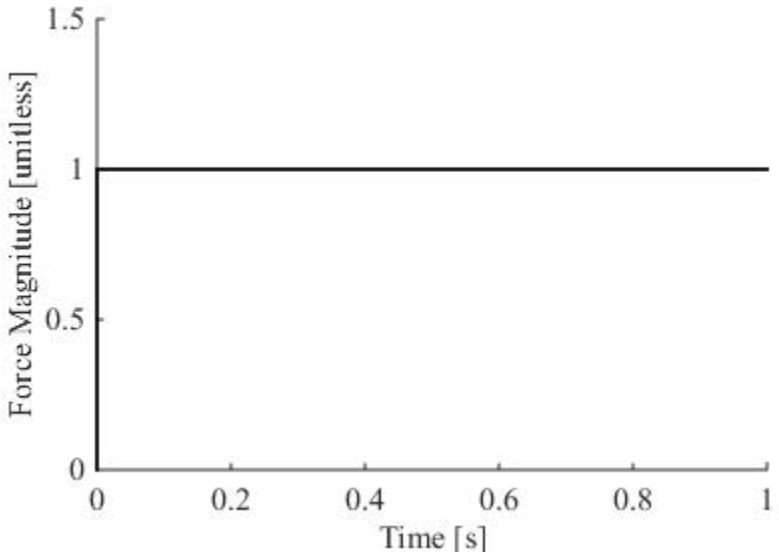

Figure 2.2 Step Function

The time history response of an SDOF system subjected to an instantaneous step function oscillates between zero and two times the static response. Consequently,

the *DAF* resulting from this function is always 2.0. As will be shown, this is not the case for other load functions. Figure 2.3 shows a sample displacement time history of a SDOF system subjected to an instantaneous step function that has been normalized with respect to the static response. As can be seen, the normalized static displacement is 1.0 and the maximum normalized dynamic displacement is 2.0.

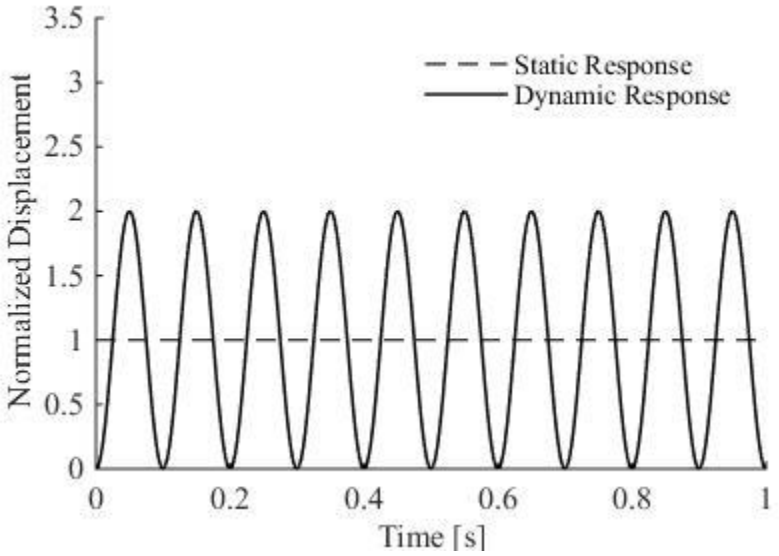

Figure 2.3 Sample Displacement Time History of a SDOF System Subjected to an Instantaneous Step Function

2.2.2 **Step Function with Finite Rise Time**

A step function with a finite rise time is similar to an instantaneous step function; however, instead of instantly applying the full magnitude of the static load, the load increases linearly over a defined period of time known as a ramp time (t_r).

$$f(t) = \begin{cases} \frac{t}{t_r} & t \leq t_r \\ 1 & t > t_r \end{cases} \qquad (2-5)$$

Figure 2.4 shows the magnitude of a generic step function with a finite rise time with respect to time (t_r = 0.25 seconds).

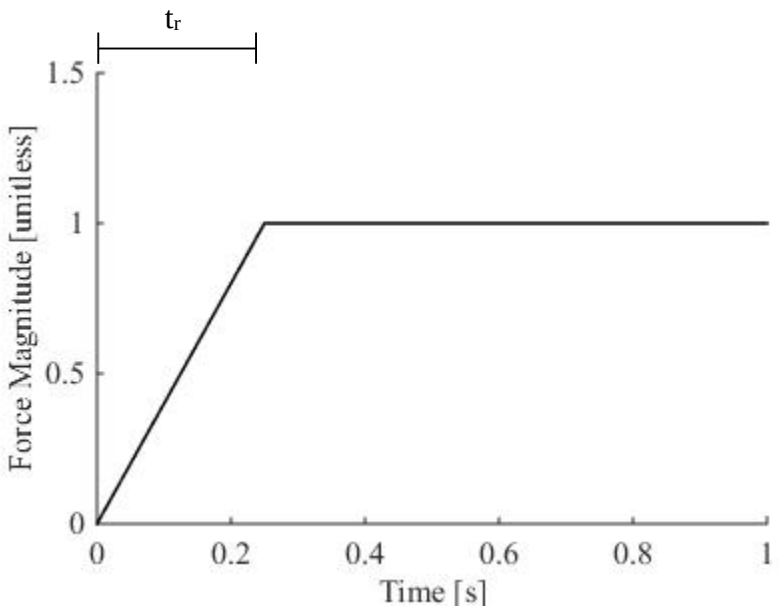

Figure 2.4 Generic Step Function with Finite Rise Time

The time history response of a SDOF system subjected to a step function with finite rise time oscillates about the value of the static response multiplied by the force magnitude. Figure 2.5 shows a sample displacement time history response normalized with respect to the static displacement. It should be noted that the peak dynamic response always occurs after the loading function has reached its full magnitude (Chopra 2012).

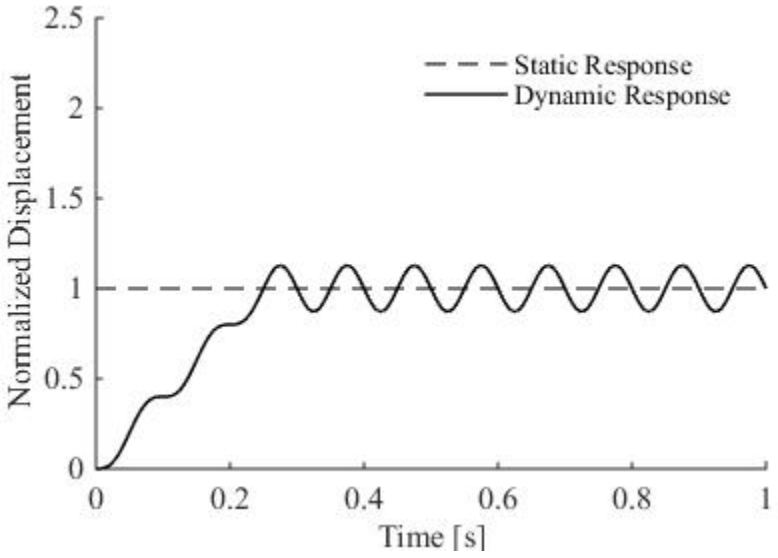

Figure 2.5 Sample Displacement Time History of a SDOF System Subjected to a Step Function with Finite Rise Time

Unlike an instantaneous step function, the dynamic amplification is not constant for every value of t_r. According to the theoretical solution, *DAF* is a function of the ratio between t_r and the system's natural period of vibration (T_n). Figure 2.6 shows the *DAF* as a function of this ratio. As can be seen, for small t_r/T_n ratios theoretical *DAF* values are close to 2.0, the solution to an instantaneous step function. However, as t_r/T_n increases *DAF* decreases to one. After reaching unity at t_r/T_n equal to 1.00, *DAF* increases again until it reaches a local maximum of 1.22 at a t_r/T_n ratio of 1.43. This pattern of increasing to a local maximum and then decreasing to one continues with the local maximum slightly decreasing as t_r/T_n increases. Intuitively this makes sense as one would imagine that a load applied over a very long period of time (i.e. for very large t_r) would induce a response similar to that of a static load,

while a load applied over an extremely short period of time would induce a response similar to an instantaneously applied load.

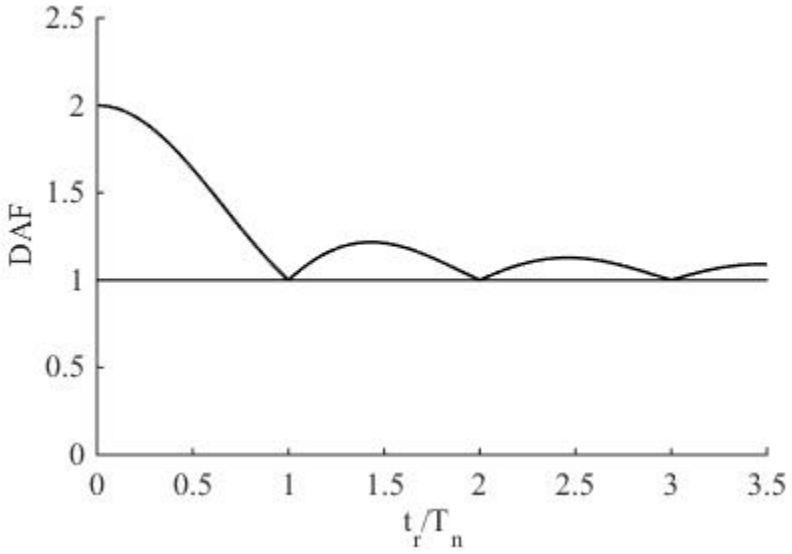

Figure 2.6 Normalized Peak Response of a SDOF System Subjected to a Step Function with Finite Rise Time

2.2.3 **Symmetric Triangular Load Pulse**

A symmetric triangular load pulse linearly increases in magnitude over a time t_r and then linearly decreases over the same duration of time. As a result, the total duration of the load pulse (t_d) is twice t_r.

$$t_d = 2t_r \qquad (2-6)$$

$$f(t) = \begin{cases} \dfrac{2t}{t_d} & t \le \dfrac{1}{2}t_d \\ 2\left(1 - \dfrac{t}{t_d}\right) & \dfrac{1}{2}t_d \le t \le t_d \\ 0 & t_d \le t \end{cases} \qquad (2-7)$$

Figure 2.7 shows a generic symmetric triangular load pulse.

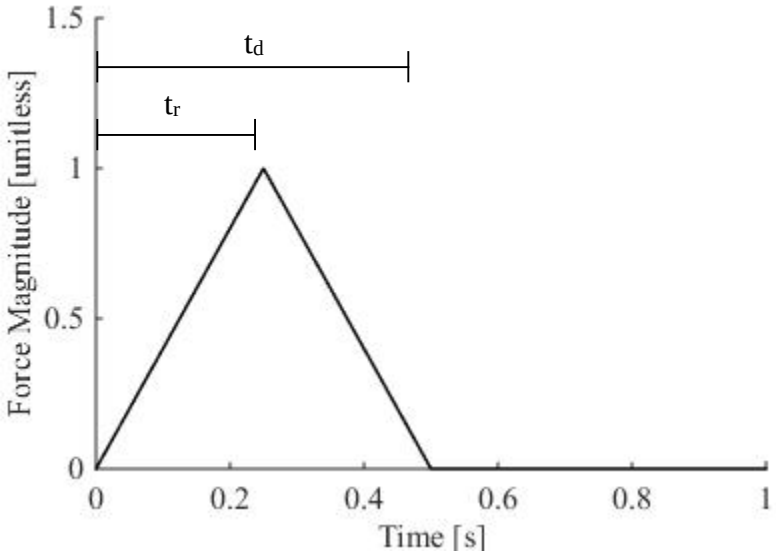

Figure 2.7 Generic Symmetric Triangular Pulse Force

Similar to a step function with finite rise time, the time history response oscillates about the static response multiplied by the magnitude of the triangular load pulse. After t_d (when the applied force equals zero) the response oscillates about zero. This can be seen in Figure 2.8. As with the step function with finite rise time, the peak response occurs after the loading function has reached its peak magnitude.

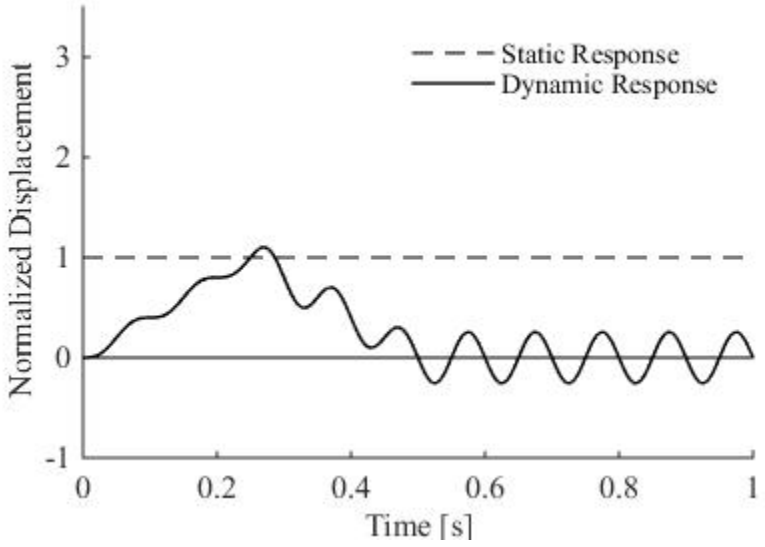

Figure 2.8 Sample Displacement Time History of a SDOF System Subjected to a Symmetric Triangular Load Pulse

Here too, *DAF* is a function of the ratio t_d/T_n ($2t_r/T_n$). While local maximum *DAF* values do decrease with t_d/T_n ratio, a fundamental difference exists between the step function with finite rise time and the symmetric triangular load pulse due to the fact that the peak response occurs after the maximum applied load in the triangular pulse. As a consequence, *DAF* starts at a value of zero for short pulse durations (rather than 2.0) and is always less than or equal to the value associated with a step function with a finite rise time.

Figure 2.9 shows *DAF* with respect to the t_d/T_n ratio for a system subject to a symmetric triangular load pulse. Here, three local maximums can be observed at t_d/T_n ratios equal to 0.9, 3.08, and 5.11 with *DAF*s equal to 1.52, 1.17, and 1.10, respectively. Additionally, *DAF* is less than one for some t_d/T_n ratios. Figure 2.9 only shows t_d/T_n ratios less than seven. If higher t_d/T_n ratios were displayed, more local

maximums would be seen. As with the step function with finite rise time, local maximums for *DAF* tend toward one as t_d/T_n increases.

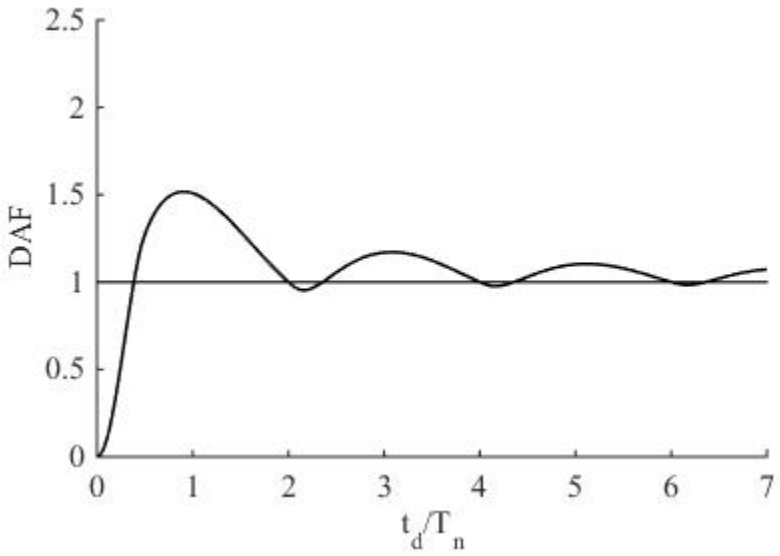

Figure 2.9 Normalized Peak Response of a SDOF System Subjected to a Symmetric, Triangular Pulse

2.2.4 **Half Sinusoidal Load Pulse**

A half sinusoidal load pulse takes the shape of a sine function from zero to π, where the function is at its maximum at t_r and returns to zero at t_d.

$$f(t) = \begin{cases} \sin\left(\frac{\pi t}{t_d}\right) & t \le t_d \\ 0 & t \ge t_d \end{cases} \qquad (2-8)$$

Figure 2.10 shows a generic half sinusoidal load pulse.

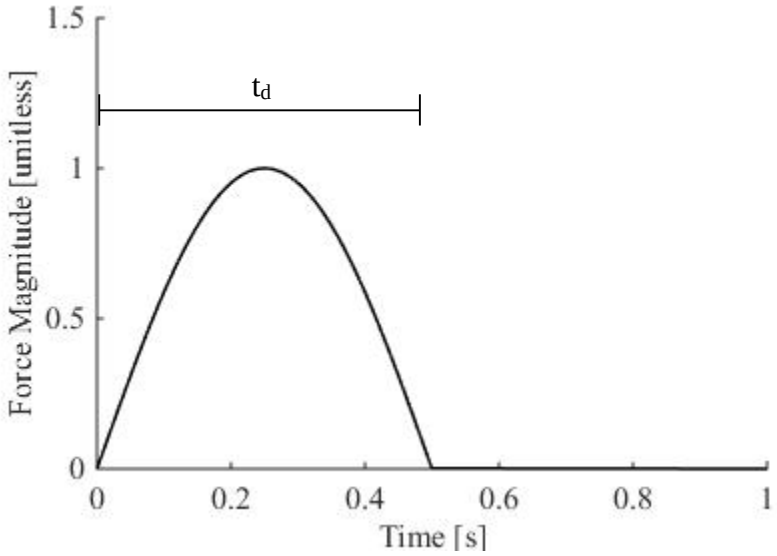

Figure 2.10 Generic Half Sinusoidal Pulse Function

Similar to the triangular load pulse, the time history response of a SDOF system subjected to a half sin load pulse oscillates about the static response multiplied by the magnitude of the load pulse during the pulse and then about zero afterwards. Figure 2.11 shows a sample displacement time history normalized with respect to the static displacement.

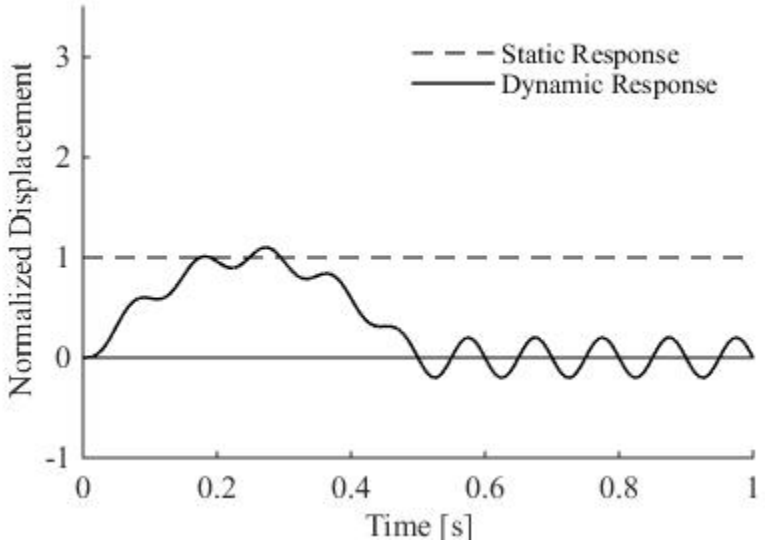

Figure 2.11 Sample Displacement Time History of a SDOF System Subjected to a Half Sinusoidal Load Pulse

Figure 2.12 shows the *DAF* for a step function with finite rise time, a symmetric triangular load pulse and a half sinusoidal load pulse. The ratio between t_d and T_n ranges between zero and 20. As can be seen, the half sinusoidal load pulse shows significantly less variation in *DAF* after the first peak than the other two load functions. For this reason, *DAF* is often slightly higher for a half sinusoidal load pulse. Like the step function with finite rise time and the symmetric triangular load pulse, the half sine function converges toward one as t_d/T_n increases. In general, it can be said that the local maximums of each load function are similar after the first peak.

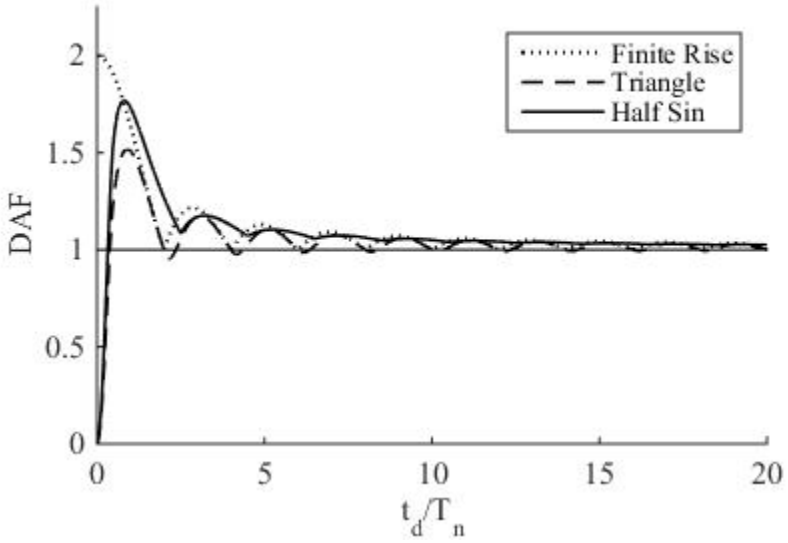

Figure 2.12 Theoretical Solution to a SDOF System Subjected to Three Pulse Forces of Equal Magnitude

2.3 *DAF* for Conventional Bridges

Over the past 150 years, the *DAF* for conventional, non-buried bridges has been studied in great detail. Much of the early work on the subject resulted from several railway bridge failures in Great Britain (Paultre et al. 1992). Subsequent to these failures, Wills (1849) examined the response of iron bars to moving loads. Later, other studies resulted from concerns with higher train speeds. In the United States, Robinson (1884) instrumented 13 bridges as a part of a Special Report to the Commissioner of Railroads and Telegraphs of Ohio. In 1911, Turneaure et al. (1911) led a comprehensive study on the topic for the American Railway Engineering Association (AREA). Results of this research suggested that *DAF* is a function of span length and were used to design railroad bridges through 1935 (Dhar et al. 1978).

In the 1920's it was recognized that the behavior of highway bridges was likely different from that of railway bridges and in 1927 the American Society of Civil

Engineers (ASCE 1931) reviewed the contemporary research on the dynamic amplification of highway bridges in order to give the profession guidance on this matter. Their findings concluded that the research at the time was insufficient to determine a relationship between *DAF* and span length. However, they observed that dynamic amplification decreased with increasing stress. Because stress is higher in longer span bridges it seemed reasonable to conclude that longer span bridges would yield lower dynamic load allowances.

Since the 1960's a considerable amount of research has contributed to this topic that has shown dynamic amplification to be extremely complex (McLean and Marsh 1998). Generally, the literature recognizes three parameters that influence the *DAF*: bridge natural frequency, the natural frequencies of the vehicle suspension system, and road surface roughness (AASHO 1962; Billing 1984; Hwang and Nowak 1991; Nowak 1999; Paultre et al. 1992; Tilly 1986; Wekezer et al. 2010). Tilly (1986) recorded the first bending frequencies (f_0) of 871 highway bridges and suggested that this frequency of vibration could be aptly described as a function of span length (L) according to the equation:

$$f_0 = 82L^{-0.9} \qquad (2-9)$$

Where L is in meters. However, he recognized that while natural frequency can be approximated using span length *DAF* cannot.

It has been recognized that trucks typically oscillate at two dominant frequencies, one between two and five hertz and another between 10 and 15 Hz (Cantieni 1984; Csagoly et al. 1972; Tilly 1986). As a result, increased dynamic effects are expected due to resonance when a bridge's natural frequency falls into one of those two ranges.

AASHO (1962) studied the dynamic response of 18 simply supported bridges. Among their results was the finding that *DAF* appeared to be a function of the speed parameter (α).

$$\alpha = \frac{v}{2f_B L} \qquad (2-10)$$

Where:

v = vehicle speed
f_B = bridge natural frequency
L = span length

By grouping terms, it can be seen that $v/2L$ is equal to t_r and $1/f_B$ is equal to T_n. Thus t_r/T_n is equivalent to $1/\alpha$. Additionally, it has been observed that *DAF* decreases with increasing truck weight (Hwang and Nowak 1991; Nowak 1999; Wekezer et al. 2010).

2.4 Research Specific to *DAF* of Buried Structures

Because of the relatively low hazard and risk of culvert failure as well as the relatively small cost of construction, little research has been conducted that examines dynamic loads on culverts. In 1988, Selig and Nash (1988) organized a workshop with leading engineers in the field of buried pipelines in order to outline research needs of the industry. Among their conclusions was the need to better understand loads on pipes, specifically indicating dynamic events. However, only a few studies have been conducted to date which seek to address this research need.

In 1926, Spangler et al. (1926) experimentally examined the effects of live load on small, circular culverts (exact dimensions not given) under static and dynamic conditions. In general, they found that Bousinesque theory could be used for live load distribution through soil, particularly noting that the theory developed for elastic solids seemed to apply for granular soils as well.

For dynamic tests, trucks were driven at speeds between 0 and 4.5 m/s and fill depths ranged between 0.6 and 3.7 m. During these tests, significant rutting was present due to the lack of pavement on roads at that time. Consequently, a *DAF* of 1.5 to 2.0 was recommended to account for rough road surfaces.

More recently, Manko and Beben (2008) dynamically tested a corrugated steel bridge in Sweden, examining the influence of vehicle speed, road surface roughness, and vehicle braking. The logarithmic decrement of damping was also recorded. The bridge had an effective span length of 12.3 m and the combined depth of fill and pavement was 1.0 m.

DAF calculated in the longitudinal direction of the bridge ranged between 1.05 and 1.31. The largest *DAF* was calculated for a vehicle speed of 10 km/h and the minimum *DAF* was calculated for a vehicle speed of 50 km/h. *DAF* values calculated for braking ranged between 1.18 and 1.20. To test the effects of road surface roughness, a plank (or threshold) was placed in the roadway to simulate a large surface deformation or discontinuity. *DAF* values calculated for threshold tests ranged between 1.15 and 1.20.

Values of the logarithmic decrement of damping ranged from 0.028 to 0.427, with an average of 0.14. Based on these results, damping can be calculated to range between 0.004 and 0.068, with an average of 0.023.

In 2012, Beben (2013) also conducted a series of experimental dynamic load tests on four corrugated steel culverts—two pipe culverts and two box (or arch) culverts. Culverts had varying span lengths and fill depths. During these tests culverts were instrumented at quarter points with both strain gauges and inductive gauges to measure vertical displacement. Static displacements were determined both by stopping

a loaded truck at critical points along the culvert and by filtering the dynamic test data. Dynamic tests were conducted at vehicle speeds of 10 km/h to 70 km/h in increments of 10 km/h.

Results showed good agreement between methods for determining the culverts' static response. Generally, the dynamic filtration method produced higher static loads (and thus lower *DAF* values), however differences were not greater than four percent. Vehicle speeds of 60 km/h produced the highest *DAF* in each test, ranging from 1.12 to 1.26 for displacements and 1.11 to 1.29 for strains.

It was also determined that *DAF* increased as span length increased. Additionally, *DAF* decreased as fill depth increased. Of the two parameters, fill depth was more influential on *DAF*. Beben also observed that the relationship between *DAF* and the ratio of fill depth to span length is approximately linear.

Chen and Harik (2012) used finite element modeling to examine the dynamic amplification of a buried concrete arch culvert due to truck loads. Parameters considered were vehicle speed, road surface roughness, concrete damping ratio, pavement type, and the ratio between truck suspension frequency and culvert frequency. All materials were considered to be linear elastic and damping was only applied to the concrete culvert.

Results showed that dynamic amplification as a function of truck velocity fluctuates considerably between velocities of 5 and 55 m/s. In some instances, *IM* fluctuates over 100 percent. A change in damping coefficient from 4 to 1 percent caused the maximum *IM* to increase from 0.10 to 0.34. Good agreement was observed between concrete and asphalt pavement models.

Road surface roughness had a considerable effect on *IM*. For roads in "perfect" condition an *IM* of 0.05 was observed for a truck traveling 20 m/s, while a road in extremely poor condition yielded an *IM* of 1.00. The influence of a truck's suspension was also tied to road surface conditions. For roads in "perfect" condition the ratio between the truck and culvert's natural frequencies had virtually no effect on *IM*. However, poor road conditions caused *IM* to vary from roughly 0.18 to 1.20 for ratios close to 1.0.

2.5 Codified Specifications

While it would be beneficial to experimentally determine the *DAF* for each bridge or culvert, it is not possible to do so for design and impractical for evaluation. As such, the *DAF* has been determined experimentally for a wide variety of bridges and empirical equations have been codified by various organizations around the world. As can be imagined, the equations for *DAF* vary considerably depending on the governing design code. Here the specifications used in the United States, New Zealand, Canada, and the Eurocode for non-buried and buried structures are discussed.

Deng et al. (2015) and McLean and Marsh (1998) serve as excellent resources for the history and formulations of *DAF* for non-buried bridges. They make reference to several additional specifications that could not be obtained for this thesis. Specifically, they discuss the Australian, Chinese and Japanese bridge design codes.

2.5.1 Non-Buried Bridges

In general, there are three approaches taken for specifying the *DAF* (or *IM*) for non-buried bridges. The first is to simply specify a single value of *DAF* for all bridges that represents the maximum expected *DAF* across all bridge types. This is the

approach taken in the United States where AASHTO (2012) defines *IM* for non-buried bridges as a constant 0.33. Similarly, the New Zealand Transportation Agency (NZTA) Bridge Code (2013) specifies the *DAF* (or *I*) as 1.30 for moment in cantilevers, deck slabs, reactions, and shear. In AASHTO (2012), *IM* is not required for wood components. Additionally, AASHTO (2011) allows for a reduction in *IM* to 0.20 and 0.10 for bridges with only minor surface deviations and smooth riding surfaces, respectively. However, these reductions can only be applied to longitudinal members over 12.2 m in length, during load rating.

Another approach allows for a reduction of *DAF* for span length (*L*). This is the case for moment in simple and continuous spans in NZTA (2013), which defines *DAF* (or *I*) as:

$$I = \begin{pmatrix} 1.30 & L \leq 12\,m \\ 1 + \dfrac{15}{L + 38} & L > 12\,m \end{pmatrix} \qquad (2-11)$$

Prior to the introduction of the AASHTO LRFD Bridge Design Specification, the Standard Specifications for Highway Bridges (AASHTO 2002) had a similar definition.

The Canadian Bridge Design Code (CHBDC) (CSA 2006) specifies *IM* in terms of the member type, number of truck axles, as well as construction material. For deck joints, *IM* is always 0.50. For all other components, an *IM* equal to 0.40 is used for single axle loads, 0.30 for two axle loads, and 0.25 for three axle loads. Additionally, the *IM* for wooden members can be multiplied by 0.70.

In Europe, the Eurocode (CEN 2002) does not specify a specific *IM* or *DAF* factor. Instead, it is built directly into the live load specification (Beben 2013). There

are some cases, such as the assessment of fatigue life, where obtaining *DAF* is necessary, however it is not typical.

2.5.2 Buried Bridge Structures

The obvious difference between buried bridge structures and conventional bridges is the presence of a soil layer between the roadway and bridge structure. Many codified specifications allow for reductions in *IM* or *DAF* based on the soil layer's thickness. The current AASHTO LRFD Bridge Design Specifications (AASHTO 2012) as well as its predecessor, the Standard Specifications for Highway Bridges (AASHTO 2002), both define *IM* for buried structures empirically in terms of fill depth. This is also the case in Canada as well as New Zealand.

According to AASHTO (2012), *IM* varies with fill depth (D_E) according to the equation:

$$IM = 33(1.0 - 0.125D_E) \geq 0\% \qquad (2-12)$$

Where D_E is in feet. In the commentary to AASHTO (2012), the decrement in *IM* is justified due to damping provided by the layer of soil. Damping is believed to increase with fill depth. (AASHTO 2002) defines *IM* (or *I*) as a step function:

$$I = \begin{pmatrix} 30\% & 0' \leq D_E \leq 1' \\ 20\% & 1'1" < D_E \leq 2' \\ 10\% & 2'1" < D_E \leq 3' \end{pmatrix} \qquad (2-13)$$

Where *I* equals zero after three feet of fill.

Similar to AASHTO (2002; 2012), NZTA (2013) linearly varies *DAF* according to fill depth. At zero meters of fill *DAF* equals 1.30 and at 1.0 meters of fill *DAF* is equal to 1.00.

The CHBDC (CSA 2006) specifies different values for *IM* based on vehicle type that range from 0.175 to 0.50 as discussed. For box-type buried structures the specified *IM* can be reduced by (1-0.5D_E), however the final value of *IM* must not to be less than 0.10. For arch-type buried structures, *IM* is specified as 0.4(1-0.5D_E) regardless of vehicle type.

2.6 Soil Behavior

2.6.1 Soil-Structure Interaction

In structural engineering it is not common to consider soil as a structural component in the same manner as one would consider concrete or steel. However, for culvert design and evaluation a soil's material properties have a significant impact on the loading condition.

Interplay between soil and structural behavior is known as soil-structure interaction (Lawson et al. 2010). This phenomenon occurs as a result of slab bending under applied loads. When this happens, the soil near the center of the span will naturally deflect more than the soil towards the culvert walls. Consequently, interparticle friction develops an arch-type structure within the soil layer, distributing the load away from the center of the span. This mechanism is akin to stress flow in an elastic continuum, however the stress only acts in compression because soil is anisotropic.

Soil-structure interaction is accounted for in AASHTO (2012) by distributing the HL-93 tire patch width according to fill depth. However, this method is known to produce conservative and sometimes overconservative results (McGrath et al. 1996; McGrath et al. 2005; Orton et al. 2015).

2.6.2 Soil Damping

In addition to distributing loads, soil also has the ability to dissipate vibrations through damping. Several researchers (Lo Presti et al. 1997; Menq 2003; Seed et al. 1986; Senetakis et al. 2012; Senetakis and Madhusudhan 2015) have studied damping in soils and found it to be a function of shear strain. Menq (2003) specifically examined the dynamic properties of soil at small shear strains. Results showed that damping ratios are less than 4 percent for shear strains below $1x10^{-3}$. This is consistent with other researchers' projections (Seed et al. 1986).

2.7 Materials

2.7.1 Material Properties

The choice of material properties can meaningfully influence a structural analysis. However, this is can be difficult for some materials due to inherent variability within the acceptable limits for construction. Material properties of particular importance to this research are elastic modulus and Poisson's ratio. Table 2.1 shows the properties of asphalt, concrete, and soil as suggested from an aggregate of sources in the literature.

Table 2.1 Material Properties from the Literature

Material	Elastic (or Resilient) Modulus (MPa)	Poison's Ratio	Source
Asphalt	3100	0.3	Janoo et al. (2003)
Asphalt	2096 – 2644	-	Loulizi et al. (2006)
Asphalt (Unaged 25°)	2472	-	Idham et al. (2013)
Asphalt (Aged 25°)	2739	-	Idham et al. (2013)
Asphalt (Unaged 40°)	811	-	Idham et al. (2013)
Asphalt (Aged 40°)	914	-	Idham et al. (2013)
Soil	30 and 80	0.3	Moore and Brachman (1994)
Soil (Base)	410	0.4	Janoo et al. (2003)
Soil (Base)	120 – 600	-	Muhunthan and Jennings (1994)
Soil (Subgrade)	83	0.4	Janoo et al. (2003)
Soil (Subgrade)	412	-	Muhunthan and Jennings (1994)
Soil (Gravels & Sand-Gravel Mixtures)	70 – 700+ Typical: 250	0.3	Lawson et al. (2009)
Soil (Well Graded Sand, 85% Compaction)	9-23	0.19 – 0.26	Petersen et al. (2010)
Concrete	$E_c = 0.043 K_1 {\gamma_c}^{1.5} \sqrt{f'_c}$	-	AASHTO (2012)

Asphalt Pavement

Due to the time dependent nature of asphalt compaction, the elastic modulus can be difficult to obtain. However, after several loading cycles the elastic behavior of asphalt concrete becomes linear and can be aptly described by the resilient modulus (Mamlouk and Sarofim 1988). Factors influencing the properties of asphalt pavement are binder oxidation and temperature. Over the course of asphalt's life, oxidation causes the asphalt binder to harden, increasing the stiffness of the asphalt-aggregate mixture (Idham et al. 2013). Additionally, asphalt behavior changes drastically with respect to temperature. Idham et al. (2013) studied both of these effects' influence on modulus of resilience. They showed a small change in stiffness due to oxidation, however almost a 66 percent reduction occurred in stiffness from 25 to 40 °C, depending on aggregate grain size. Aged asphalt with maximum aggregate size of 10 mm and 28 mm reduced from roughly 3000 MPa to 1200 MPa and 2700 MPa to 1000 MPa, respectively. Additionally, Loulizi et al. (2006) tested three different specimens and reported resilient moduli of 2644, 2096, and 2275 MPa at 40 ℃. Uddin (1998) estimated an asphalt modulus of 2000 MPa based on in-situ testing.

Whitmoyer and Kim (1994) examined the properties of asphalt concrete using the impact resonant method. This method applies an impact load to a cylindrical sample and uses the sample's resonant vibrational response to determine material properties. For temperatures around 30 °C it was observed that damping ratio was roughly 0.1, and Poisson's ratio was roughly 0.4. At 40 °C the damping ratio was measured to be 0.15.

Soil Fill

Granular soils are typically used as fill in construction. Soil stiffness varies as a function of confining pressure, strain amplitude and void ratio, which can change significantly depending on the job site and in situ conditions (Seed et al. 1986; Selig 1990). Based on research conducted by Selig (1990), Moore and Brachman (1994) performed a finite element study of culverts using 30 and 80 MPa soil. However, Muhunthan and Jennings (1994) conducted a finite element study of a rehabilitated roadway and used 410 MPa for soil subgrade and a possible range of 120 to 600 MPa for base course material. Janoo et al. (2003) used finite element modeling to study roadway rutting and used a soil elastic modulus of 410 MPa for base material and 83 MPa for subgrade.

Lawson et al. (2009) provides an in depth guide for load rating culverts using finite element analysis. For sands and sandy-gravels with moderate amounts of silts and organics they recommend elastic moduli ranging from 35 to 350 MPa, with a typical value of 140 MPa. For gravels and sandy-gravels with low fines they recommend elastic moduli between 70 and 700 MPa, with a typical value of 250 MPa. Petersen et al. (2010) suggest that soil fill elastic modulus values range from nine to 23 MPa and also suggest using a stress-dependent modulus of elasticity.

Similar variability exists for Poisson's ratio. Janoo et al. (2003) suggest a Poisson's ratio of 0.4 while Petersen et al. (2010) suggest ratios as low as 0.19. While Lawson et al. (2009) recognize a possible range of Poisson's ratios between 0.1 and 0.5, they indicate that 0.3 is a typically accepted value.

Concrete

In reinforced concrete design, it is typically assumed that concrete behaves linear-plastically. According to the LRFD bridge design code , the elastic modulus of concrete (E_c) can be determined using the equation (AASHTO 2012):

$$E_c = 0.043 K_1 \gamma_c{}^{1.5} \sqrt{f'_c} \qquad (2-14)$$

Where:

K_1 = correction factor for source of aggregate to be taken as 1.0 unless determined by physical test
γ_c = density of concrete in kg/m^3
f'_c = concrete compressive yield stress in MPa

AASHTO (2012) also allows for 2 percent damping in concrete.

2.7.2 **Material Models**

Due to the large variability in soil properties, Jayawickrama et al. (2012) suggest that a linear elastic soil modulus definition is sufficient. Additionally, a linear elastic material model aids in computational efficiency (Moore and Brachman 1994). Janoo et al. (2003) and Dancygier and Karinski (1999) similarly use this assumption.

Chapter 3

PARAMENTRIC FINITE ELEMENT ANALYSIS

3.1 Outline of Parametric Study

3.1.1 Purpose

While many of the prominent design codes from around the world specify a different *DAF* (or *IM*) for non-buried structures than for buried structures, at this time it is unclear on what research, if any, the *DAF* for buried structures is based. For that reason, and to better understand the soil-structure-pavement system's behavior as a whole, the present parametric study is undertaken.

3.1.2 Procedure

This study uses Abaqus/CAE (a commercial finite element software) to create and analyze finite element models of the soil-structure-pavement system which is subjected to dynamic loads when a vehicle crosses a culvert. Given the high potential for variability in geometric and material properties from one culvert to another, five parameters are varied:

- Fill depth (D_E),
- Soil elastic modulus (E_E),
- Span length (L),
- Culvert slab thickness (t_s),
- And asphalt pavement thickness (t_a)

Three values are chosen for each parameter that represent the range of variation expected in typical culvert designs. Additionally, the system is analyzed with no asphalt as pavement is not present during most stages of construction. Values for each

parameter can be seen in Table 3.1. In total, 324 unique model configurations are analyzed. A general schematic of the models can be seen in Figure 3.1. Only half of the soil-structure-pavement system is modeled because the real culvert system is considered to be symmetric. The load is represented by the variable q.

Table 3.1 Parameters Varied and Their Values

Fill Depth (D_E) [m]	Soil Elastic Modulus (E_E) [MPa]	Span Length (L) [m]	Culvert Slab Thickness (t_s) [m]	Pavement Thickness (t_a) [m]
0.61	70	2.44	0.254	0
1.22	320	3.66	0.356	0.076
1.83	570	4.88	0.457	0.152
-	-	-	-	0.229

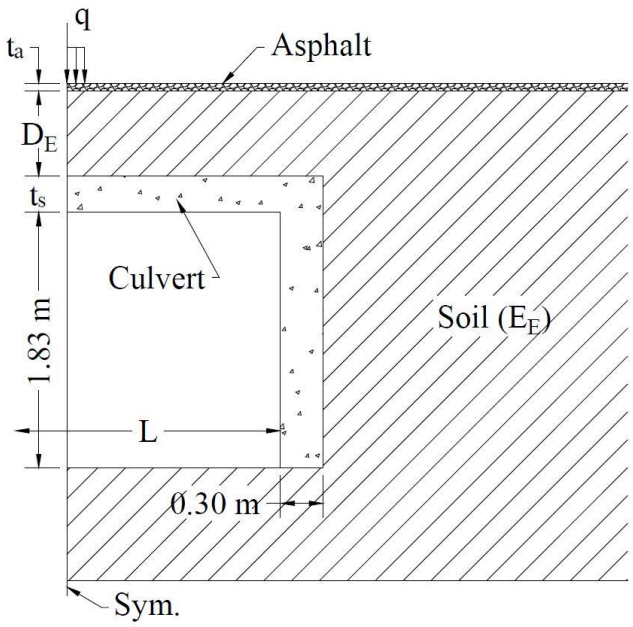

Figure 3.1 Schematic of Culvert Model

For each individual configuration, a model of the dynamic loading condition is created along with a model of the static loading condition. The *DAF* is determined by dividing the maximum computed dynamic displacement at center span ($\delta_{dyn,max}$) by the computed static displacement at center span (δ_{stat}).

$$DAF = \frac{\delta_{dyn,max}}{\delta_{stat}} \qquad (3-1)$$

Since the dynamic displacement is inherently a function of time, the maximum dynamic displacement is selected from the time history response, an example of which is shown in Figure 3.2.

In the literature it is often discussed whether displacement or stress more accurately captures the behavior of the structure during field testing. For finite element analyses, displacement should be used because it is a primary dependent variable. Stress is a secondary dependent variable. Thus, stress is calculated as a derivative of displacement and is therefore less accurate (Kaliakin 2002).

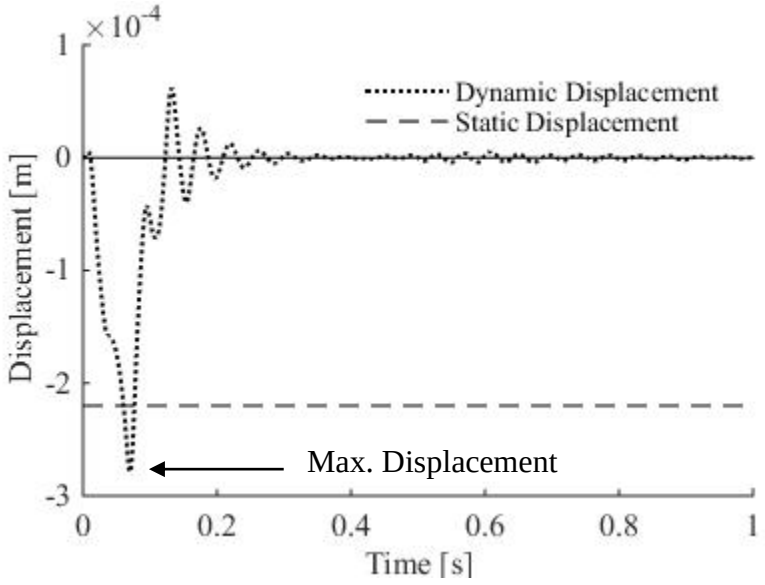

Figure 3.2 Sample Time History Response

3.2 Model Description

The models developed in this research represent three-sided box sections subjected to static and dynamic loads. Taking advantage of symmetry, only half of the culverts is modeled. As such, each of the models consists of a 0.30 m thick concrete leg and half of the culvert's slab, covered by a layer of soil fill and in many cases pavement. Additionally, soil is extended away from the concrete box section and below it.

The models are constructed using eight node, plane-strain, continuous elements (Abaqus element type CPE8). The primary reason for using a plane-strain model as opposed to a three dimensional model is to increase computational efficiency. While it is recognized that live load attenuation occurs both in and out of the plane, the author believes that the two-dimensional simplification will affect the static and

dynamic conditions equally. Thus, inaccuracies caused by fixing out of plane degrees of freedom are minimized.

The entire soil-structure-pavement system is modeled as a composite section, sharing nodes along the boundaries where the different materials are in contact. Consequently, no separation is allowed between the pavement, soil, and concrete. While in reality a small amount of separation does occur between the culvert and soil, a sensitivity analysis was a conducted as a part of this study that revealed these effects to be limited for the range of parameters and magnitude of loads used in this investigation. McGrath and Mastroianni (2002) also indicate that it is reasonable to assume that all portions of the model act in unison.

3.2.1 Boundary Conditions and Mesh

In any model, the mesh size as well as the type and location of boundary conditions are critical for obtaining accurate results. Particular to the dynamic analysis, the extents of the soil layer should be set such that boundary conditions do not overconstrain the model and must allow the load to properly propagate through the structure. Consequently, a sensitivity analysis was conducted to determine the appropriate mesh size and location of boundary conditions. Based on the results, the approximate mesh sizes near and far from the culvert are 0.116 and 0.5 m, respectively. It was also found that the soil (and pavement) must be extended 30 m horizontally from the culvert structure and 8.78 m below the footing. The automatic mesh generation tool is used in Abaqus to generate the mesh for each model. A typical mesh and boundary conditions can be seen in Figure 3.3.

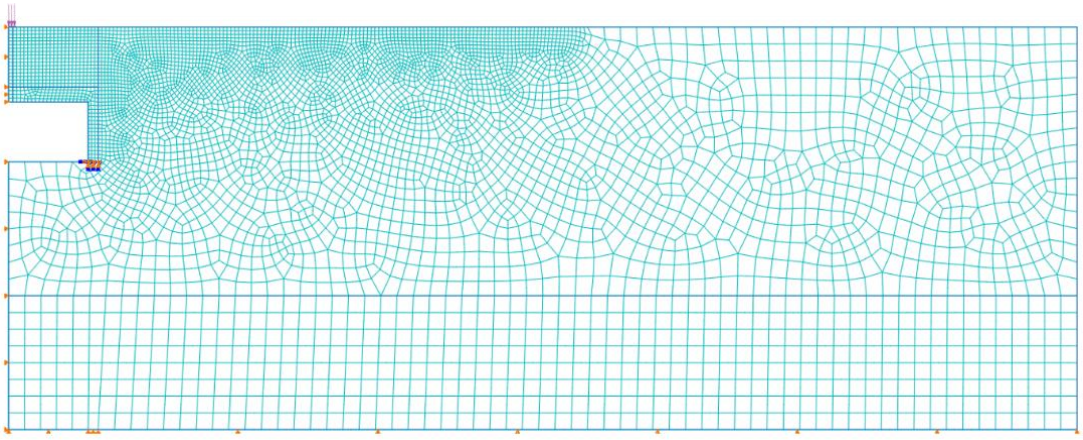

Figure 3.3 Typical Model Mesh, Boundary Conditions and Loading

As a general rule, restraints are minimized wherever possible. Consequently, the bottom boundary of the model is only restrained in the vertical direction and the horizontal direction is free. The model is horizontally restrained along the line of symmetry and fixed in both directions at the base of the culvert. The top and right edges are completely free and unrestrained.

3.2.2 **Materials**

All material definitions are linear elastic. As a result, the only material properties necessary for this analysis are elastic modulus, Poisson's ratio, density, and damping. Values are all selected based on information found in the literature and can be seen in Table 3.2.

Two percent damping is applied to all materials. This is a typically specified value for concrete and believed to be conservative for soils as well, i.e. soils will generally provide higher levels of damping than is used here. Given the findings of Manko and Beben (2008), two percent damping is reasonably conservative. For these

models, the critical damping formulation is used in Abaqus. For critical damping, the damping ratio is input as a percentage of the critical damping ratio and applied at the model level rather than the material level (Abaqus 2013).

Table 3.2 Selected Material Properties

Material	Elastic Modulus (MPa)	Poisson's Ratio	Density (kg/m^3)	Damping (%)
Asphalt	1000	0.40	2350	2
Concrete	24100	0.15	2370	2
Soil	*Varies*	0.30	1922	2

3.3 Applied Loads

Two models are created for each of the 324 parameter configurations: one static model and one dynamic model. The construction of these models are the same; the only difference lies in the load application. A general, static load is applied for the static models and modal dynamics is used in the dynamic models. In both instances, the magnitude of applied loads are equivalent to an AASHTO (2012) HL-93 rear axle load (142.3 kN or 32 kips) applied to a 0.25 m (10 in.) tire patch width on the pavement surface at center span. If no pavement is present in the model the load is applied to the surface of the soil. The distributed pressure applied to the tire patch is 557,600 Pa (81 psi).

3.3.1 Dynamic Load Function

Over the course of this research, many dynamic load functions were considered (instantaneous step function, step function with finite rise time, triangular, sinusoidal, etc.). After examining the properties of each, it was determined that a

symmetric, triangular load pulse applied at midspan best represents a truck traveling across the structure while remaining simple in nature. This determination was made primarily because the peak response takes place after the maximum load is applied. In order to obtain a realistic result, the load function must decrease after reaching its maximum value. Figure 3.4 diagrams the general form of this function. Here pulse duration (t_d) signifies the time it takes for a truck (or one axle of a truck) to cross a culvert.

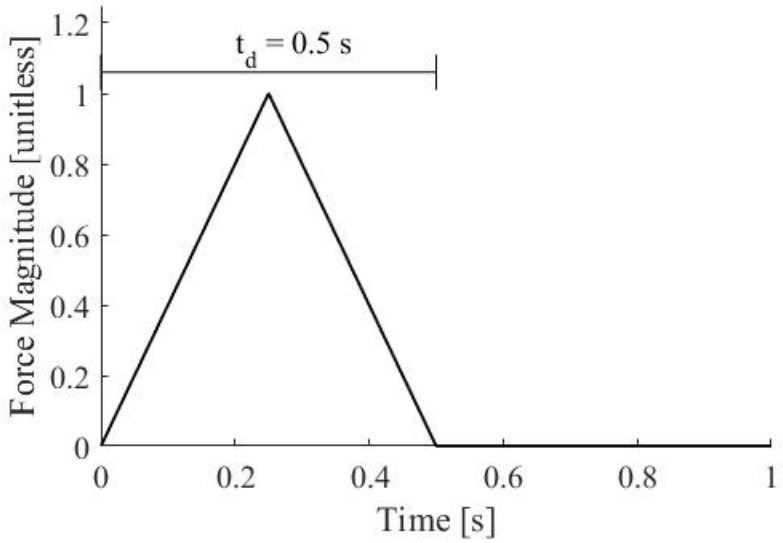

Figure 3.4 Symmetric Triangular Pulse Force

3.3.2 **Method for Determining Appropriate Pulse Duration**

Pulse Duration Input

There are several ways to input a load function into finite element modeling software. This study employs a tabular definition, meaning that amplitude values are

specified at certain times in a table and the amplitude is linearly interpolated between those points. Table 3.3 shows the input table for the load function shown in Figure 3.4.

Table 3.3 Sample Load Amplitude Input

Time (s)	Amplitude (unitless)
0	0
0.25	1
0.5	0
1	0

Discussion of Vehicle Speed

When a vehicle crosses a culvert its pulse duration (t_d) is a function of the span length (L) and the vehicle speed (v).

$$t_d = \frac{L}{v} \qquad (3-2)$$

Likewise, the pulse duration input into finite element modeling software is representative of a vehicle traveling over the length of the culvert's span at a certain speed. By rearranging terms, the representative vehicle speed can be calculated by the equation:

$$v = \frac{L}{t_d} \qquad (3-3)$$

According to the theoretical solution to a SDOF system subjected to a symmetric, triangular load pulse, the dynamic amplification is a function of the ratio between pulse duration and the natural period of the structure (T_n) (Chopra 2012). This suggests that for any culvert model the *DAF* is dependent on the vehicle speed

represented by the pulse duration. Indeed, the theory suggests that any *DAF* on the theoretical curve (Chopra (2012)) in Figure 3.5 could be obtained for a single structure by simply varying the representative rate of travel. Subsequently, if a modeled structure's natural period and span length are known, as well as the applied load's pulse duration, one should be able to predict the *DAF*. Using this logic, load pulses are selected in order to produce the maximum dynamic amplification within reasonable limits placed on vehicle speed. In this study, a "reasonable" vehicle speed is one that is less than or equal to 40.5 m/s (90 mph).

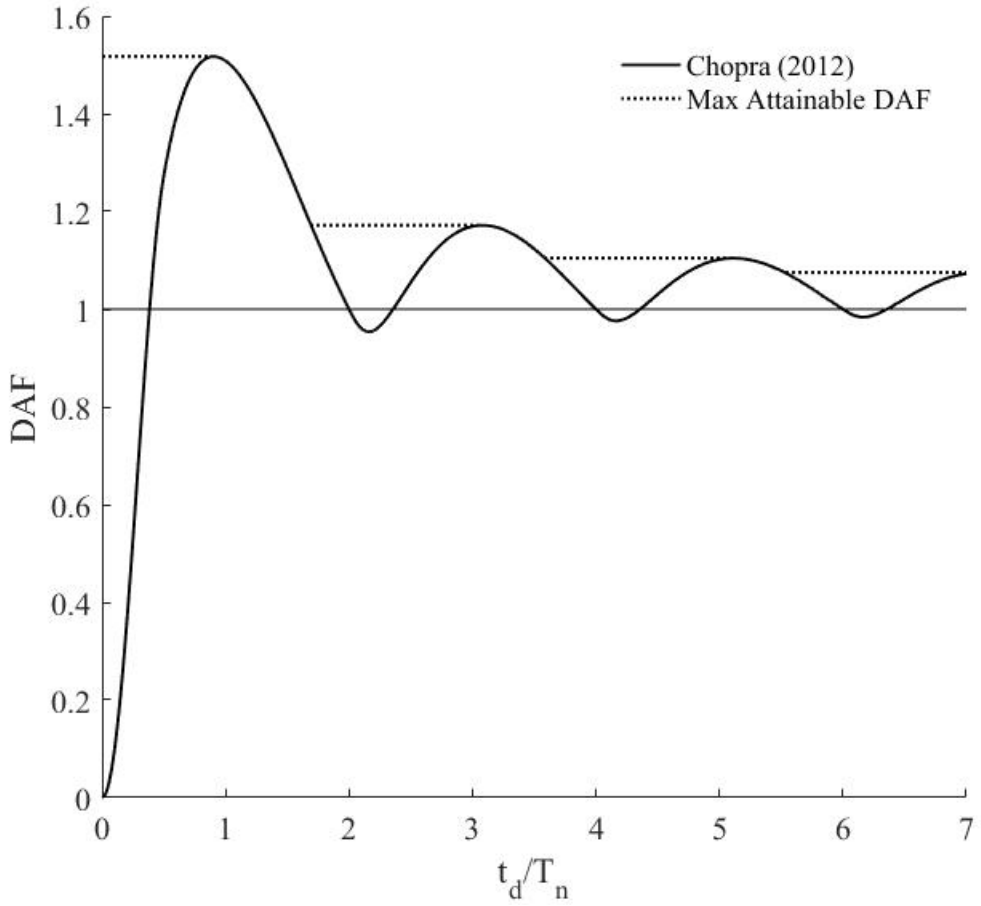

Figure 3.5 Maximum *DAF* Attainable According to the Theoretical Solution to a SDOF System Subjected to a Symmetric, Triangular Pulse

When applying Equation 3-2 to the theoretical curve (Chopra (2012)) in Figure 3.5 it can be understood that the t_d/T_n ratio decreases as vehicle speed increases. Conversely, t_d/T_n increases as vehicle speed decreases. Thus, if a 40.5 m/s representative vehicle speed causes a structure's t_d/T_n ratio to be equal to 2.0 and it is possible for vehicles to travel slower than 40.5 m/s, then it is also possible for the structure to experience all *DAFs* resulting from t_d/T_n ratios greater than 2.0 on the curve in Figure 3.5. Because this study is interested in determining the maximum possible *DAF* for each model configuration, selecting the appropriate load pulse is critical to obtaining realistic and conservative results.

Method of Selection

Since pulse duration is a model input and natural period is unique to a model's geometric and material properties, a "target" t_d/T_n ratio can be selected to produce the maximum theoretical result if the natural period is known. In this study, natural periods range between 0.013 and 0.074. This was determined according to an analysis that will be discussed in a later section. Based on these periods and the restriction placed on vehicle speed (less than or equal to 40.5 m/s), the maximum dynamic amplification for each model configuration is expected to occur between t_d/T_n ratios of 3.08 (the second local maximum in Figure 3.5) and 5.11 (the third local maximum in Figure 3.5).

When examining Figure 3.5 one can see that the maximum attainable *DAF* decreases to the right of 3.08 and is constant from 3.58 to 5.11. As a result, 3.08 is the target t_d/T_n ratio when vehicle speeds will allow it. In those cases, the pulse duration input into the finite element model is determined using the equation:

$$t_d = 3.08T_n \qquad (3-4)$$

However, if vehicle speeds necessary to obtain a t_d/T_n ratio of 3.08 are in excess of 40.5 m/s, a target t_d/T_n ratio is selected based on the following criteria:

$$t_d = \begin{cases} \dfrac{\mathrm{L}}{40.5\ m/s}, & \dfrac{L}{3.58T_n} < 40.5\ m/s \\ 5.11T_n, & \dfrac{L}{3.58T_n} \geq 40.5\ m/s \end{cases} \qquad (3-5)$$

For cases where $L/(3.58T_n)$ is less than 40.5 m/s, specified values of t_d cause t_d/T_n ratios fall between 3.08 and 3.58 on the curve in Figure 3.5. For cases where $L/(3.58T_n)$ is greater than or equal to 40.5 m/s, specified values of t_d cause a t_d/T_n ratio of 5.11 (the third local maximum in Figure 3.5). The reason why no target t_d/T_n ratios fall between 3.58 and 5.11 is because a hypothetical vehicle can always drive slower and attain a higher *DAF* at a t_d/T_n ratio of 5.11. Figure 3.6 diagrams the process of selecting the load pulse that will deliver the maximum *DAF* according to the theoretical SDOF solution.

Because the finite element models are multi degree of freedom systems and therefore are not expected to conform exactly to the SDOF solution, a check is conducted for configurations having target t_d/T_n ratios of 3.08 and 5.11 (a non-limited vehicle speed) to make sure that these ratios do in fact deliver the maximum dynamic load. For many cases 3.08 and 5.11 proved to be correct, however some required a slight adjustment in t_d. As a result, some t_d/T_n ratios used in this study are greater than or less than 3.08 and 5.11. A check is not conducted for t_d/T_n ratios between 3.08 and 3.58 because the pulse duration is restricted by vehicle speed and thus cannot increase.

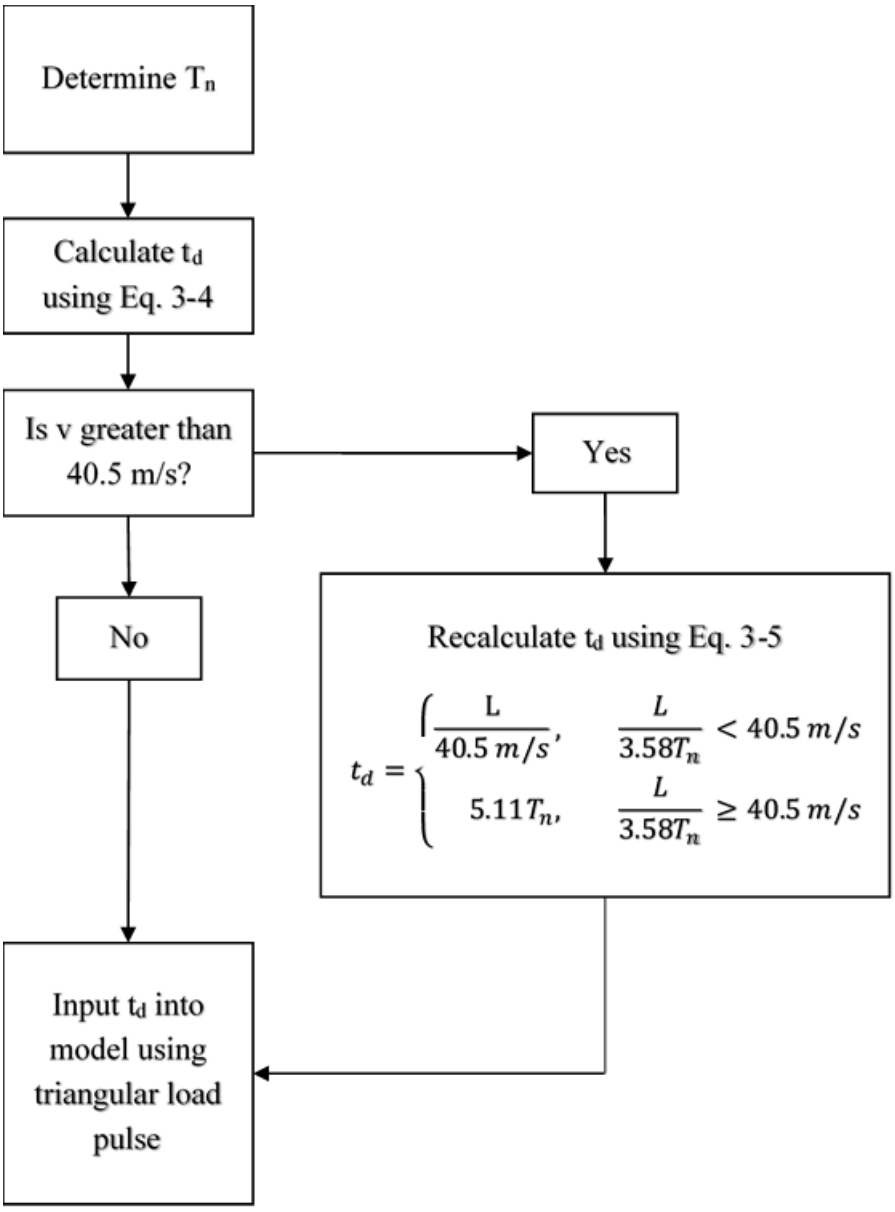

Figure 3.6 Determination of Pulse Duration

Determination of Natural Period

Because the load pulse duration is determined as a function of each structure's natural period, it is necessary to determine the natural period prior to analyzing the structure's response to a triangular load pulse. This is accomplished by subjecting each of the 324 model configurations to an instantaneous step function (the simplest load function) and post-processing the time history data with respect to displacement at mid-span of the culvert. Because the natural period of vibration can be defined as the number of oscillations per unit time, the natural period of each structure is determined by dividing a period of time (*t*) by the number of oscillations (*n*) occurring in that time:

$$T_n = \frac{t}{n} \qquad (3-6)$$

Figure 3.7 gives a general example of this process. Table 3.4 shows the maximum minimum, average, and standard deviation of natural periods determined from the analyses and the resulting pulse durations used in this study.

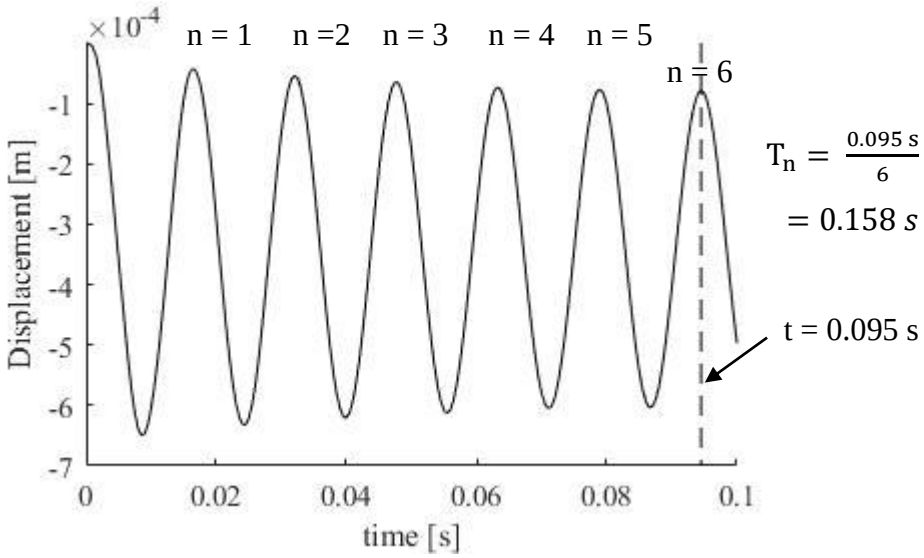

Figure 3.7 Determination of Natural Period

Table 3.4 Natural Period and Pulse Duration Information

	Maximum	Minimum	Average	Standard Deviation
Natural Period (T_n) [s]	0.013	0.074	0.028	0.068
Pulse Duration (t_d) [s]	0.228	0.060	0.109	0.037

3.3.3 **Number of Modes Analyzed**

When performing a dynamic modal analysis, each mode shape is isolated and the result is determined by superimposing the solutions for each mode. In any such analysis, the engineer can decide the number of mode shapes he or she would like to use. In many commercially available software packages, users are given the option to select specific modes or a range of modes to analyze. For this thesis, a sensitivity analysis was conducted examining the number of modes necessary to give accurate results while remaining as efficient as possible. Results of this analysis indicate that

3000 modes should be used for the dynamic analysis. The smallest model analyzed during this study has 24802 possible modes and the largest model has 38098 possible modes. Thus the number of modes analyzed is between eight and 12 percent of all possible modes. A typical run time on the University of Delaware's cluster computer is 10 minutes.

3.4 Model Results

3.4.1 Introduction of Results

Over the course of this study 324 individual model configurations are created by varying five model parameters: soil fill depth, soil elastic modulus, span length, slab thickness, and asphalt pavement thickness. Fundamentally, this parametric study is most concerned with better understanding which geometric and material properties most influence the dynamic amplification of culverts. Subsequently, it is interested in corroborating the current AASHTO (2012) *IM* definition and possibly identifying parameters that could further refine AASHTO (2011; 2012) specifications.

The following sections first examine the influence of individual parameters on *DAF* and compare results to the theoretical SDOF solution given by Chopra (2012). The influence of each parameter on the system's natural period is then examined and results of previous sections are then discussed in light of the SDOF theory. Figure 3.8 shows a flow chart diagraming the method of obtaining the *DAF* for each model configuration.

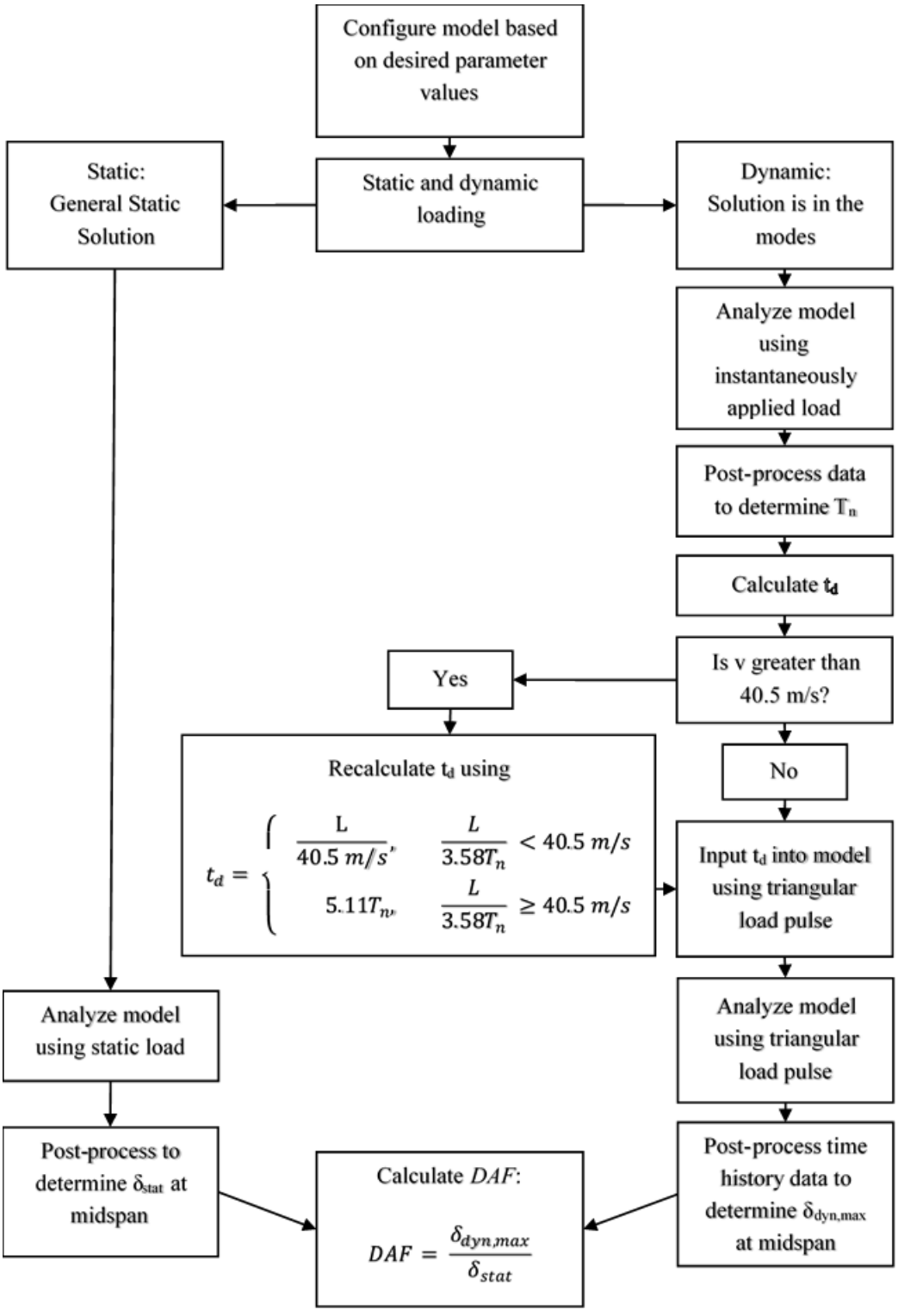

Figure 3.8 Determination of *DAF* Flow Chart

3.4.2 **Influence of Individual Parameters on *DAF***

Fill Depth

Figure 3.9 shows *DAF* as a function of fill depth. Based on the linear fit, *DAF* tends to increase as fill depth increases. The slope of the linear fit trend is 0.042 1/m. For a 1.22 m increase in fill depth *DAF* increases by 0.051 on average. Table 3.5 shows the maximum, minimum, range, average and standard deviation of results at each fill depth. It is interesting that while the minimum and average *DAF* at each fill depth increases as fill depth increases, the maximum does not. Instead the maximum computed *DAF* occurs at 1.22 m of fill depth. The fill depth recording the largest range and standard deviation of *DAF* values is also 1.22 m.

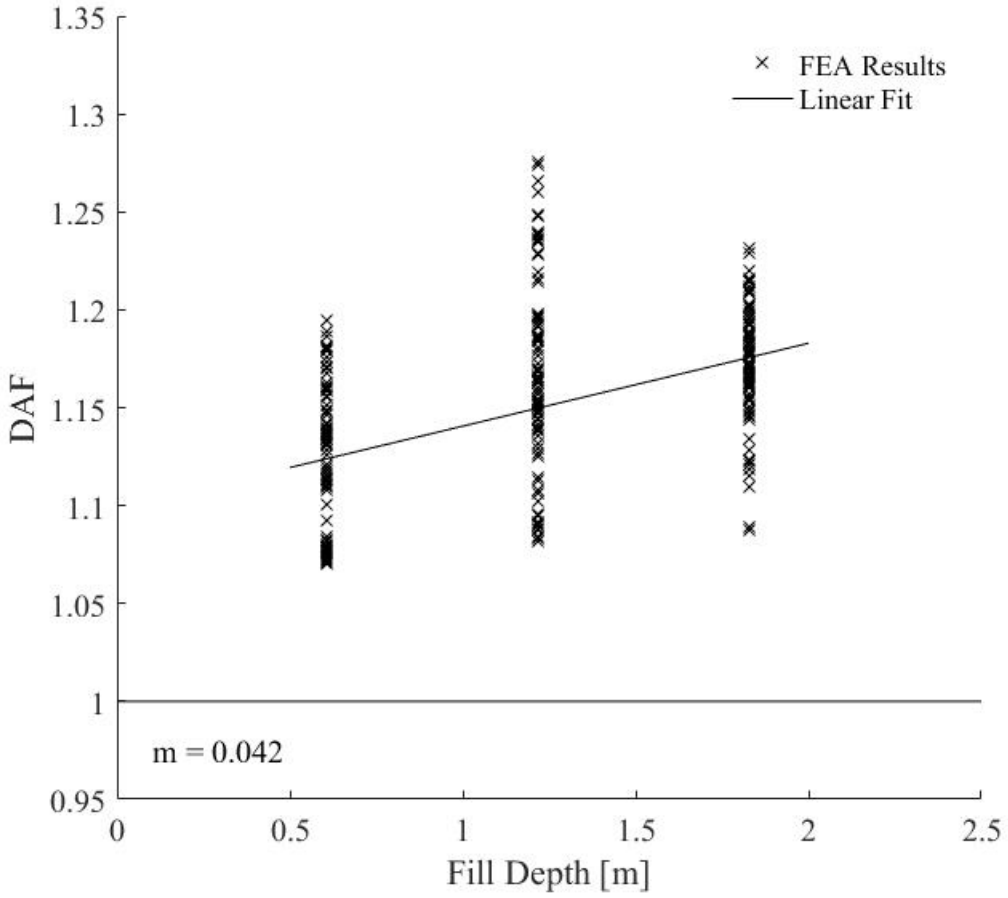

Figure 3.9 *DAF* as a Function of Fill Depth

Table 3.5 Minimum, Maximum, Range, Average and Standard Deviation of *DAF* at Each Fill Depth

Fill Depth (m)	Minimum	Maximum	Range	Average	Standard Deviation
0.61	1.07	1.19	0.12	1.12	0.037
1.22	1.08	1.28	0.20	1.16	0.048
1.83	1.09	1.23	0.14	1.17	0.028

Results of this study contradict provisions put forward by AASHTO (2002; 2012), which suggest that *DAF* decreases as fill depth increases. While the maximum *DAF* computed during the finite element study is 1.28, below the maximum of 1.33 suggested by AASHTO, the slope of AASHTO (2012) provisions is -0.14 1/m. Over a 1.22 m increase in fill depth AASHTO allows for a 0.17 decrease in *DAF*.

Figure 3.10 compares finite element results to AASHTO specifications. It can be seen that all *DAF* values computed for a fill depth of 1.83 m are larger than the specified *DAF* of 1.08. Additionally, 40 percent of results at 1.22 m of fill are larger than the specified *DAF* of 1.17. No *DAF* values at 0.61 m of fill are larger than the specified *DAF* of 1.25. This suggests that AASHTO specifications are overconservative at low fill depths and underconservative at high fill depths.

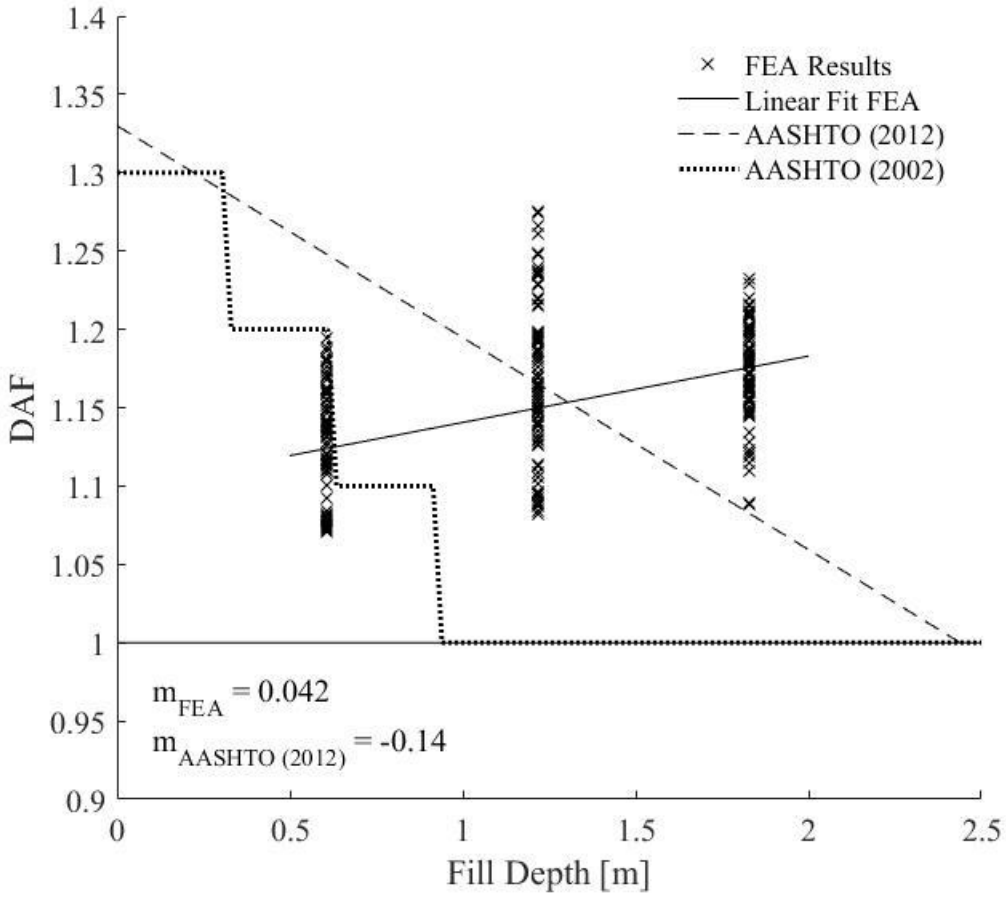

Figure 3.10 Finite Element Results compared to AASHTO (2002; 2012)

Soil Elastic Modulus

Figure 3.11 shows *DAF* as a function of soil elastic modulus. Based on the linear fit, *DAF* tends to decrease as soil elastic modulus increases. The slope of the linear fit trend is -0.00014 1/MPa. Over the largest range of soil elastic moduli studied, 500 MPa, the *DAF* is expected to decrease by 0.07 on average. Table 3.6 gives the minimum, maximum, range, average and standard deviation of results at each elastic modulus. The minimum *DAF* decreases between 70 and 320 MPa, while it remains constant between 320 and 570 MPa. The maximum and average *DAF* decreases as elastic modulus increases. It is interesting to note that the range and standard deviation of computed *DAF* values decreases as soil elastic modulus increases. As a result, the variability in results decreases as soil elastic modulus increases.

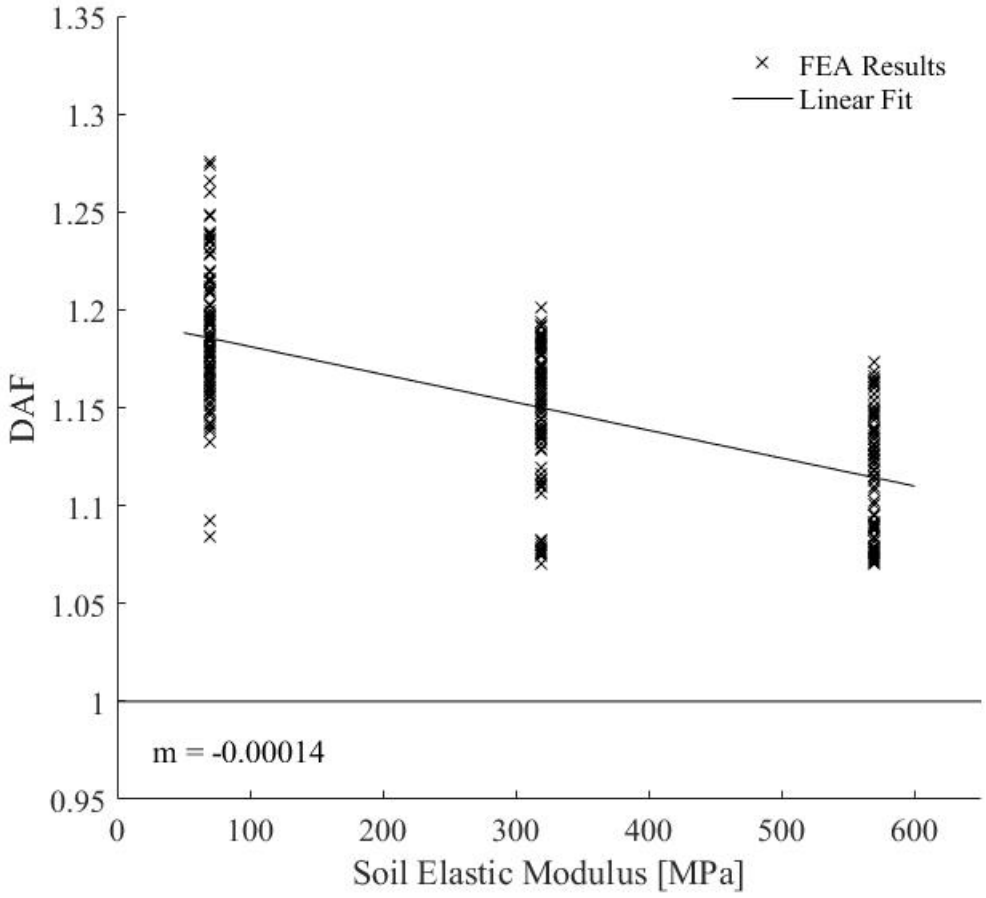

Figure 3.11 *DAF* as a Function of Soil Elastic Modulus

Table 3.6 Minimum, Maximum, Range, Average and Standard Deviation of *DAF* at Each Soil Elastic Modulus

Soil Elastic Modulus (MPa)	Minimum	Maximum	Range	Average	Standard Deviation
70	1.08	1.28	0.20	1.19	0.035
320	1.07	1.20	0.13	1.15	0.033
570	1.07	1.17	0.10	1.12	0.032

Span Length

Figure 3.12 shows the computed *DAF* as a function of span length. Based on the linear fit, *DAF* tends to slightly decrease as span length increases. The slope of the linear fit trend is -0.0026 1/m. For an increase in span length of 2.44 m the *DAF* is expected to decrease by 0.006 on average. Table 3.7 gives the minimum, maximum, range, average and standard deviation of results at each span length. The minimum and average *DAF* computed at each span length remain relatively constant as span length increases, while the maximum *DAF* decreases. As a result, the range and standard deviation of *DAF* at each fill depth decrease as well. Likewise, the variability of results decreases as span length increases.

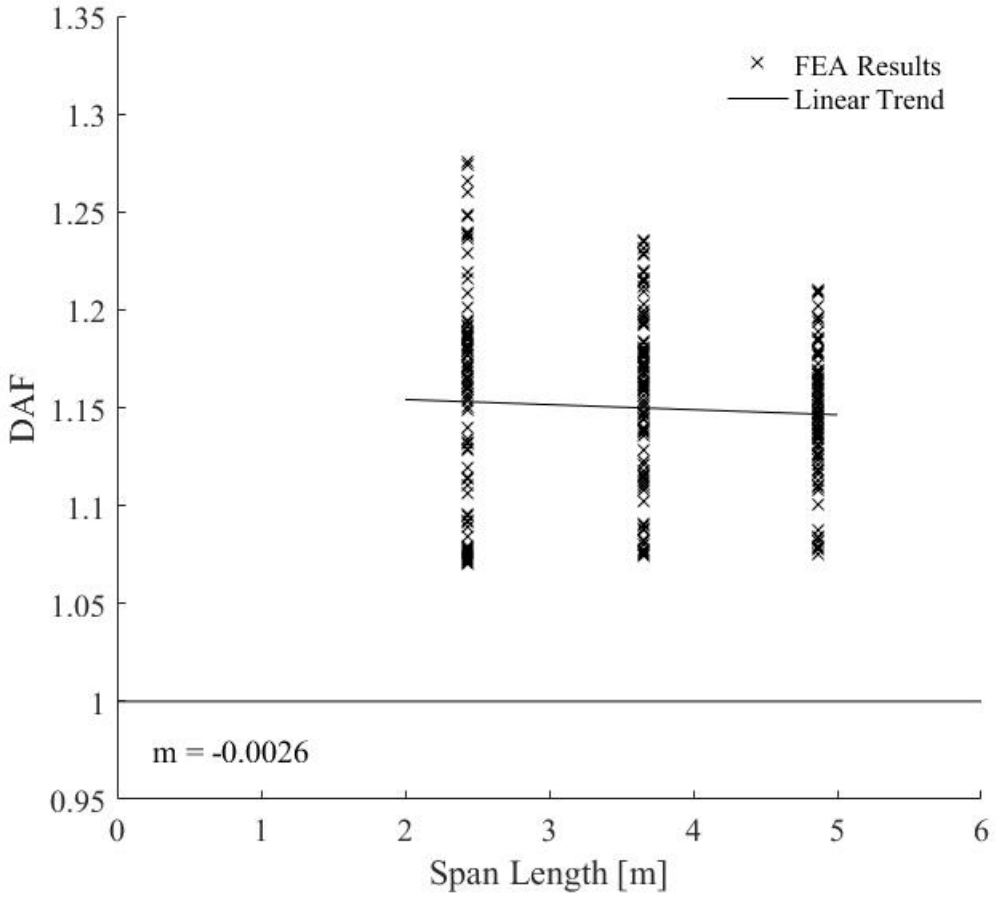

Figure 3.12 *DAF* as a Function of Span Length

Table 3.7 Minimum, Maximum, Range, Average and Standard Deviation of *DAF* at Each Span Length

Span Length (m)	Minimum	Maximum	Range	Average	Standard Deviation
2.44	1.07	1.28	0.21	1.15	0.055
3.66	1.07	1.23	0.16	1.15	0.044
4.88	1.08	1.21	0.13	1.15	0.030

Slab Thickness

Figure 3.13 shows the *DAF* as a function of slab thickness. Based on the linear fit, *DAF* tends to decrease as slab thickness increases. The slope of the linear fit trend is -0.072 1/m. Over the maximum increase in slab thickness studied, 0.203 m, the *DAF* is expected to decrease by 0.015 on average. Table 3.8 gives the minimum, maximum, range, average and standard deviation of results at each slab thickness. In keeping with the linear fit, the minimum and average *DAF* decreases slightly as slab thickness increases. However, counter to the linear fit trend, the maximum *DAF* at each slab thickness slightly increases as slab thickness increases. Additionally, both the range and standard deviation increases as slab thickness increases.

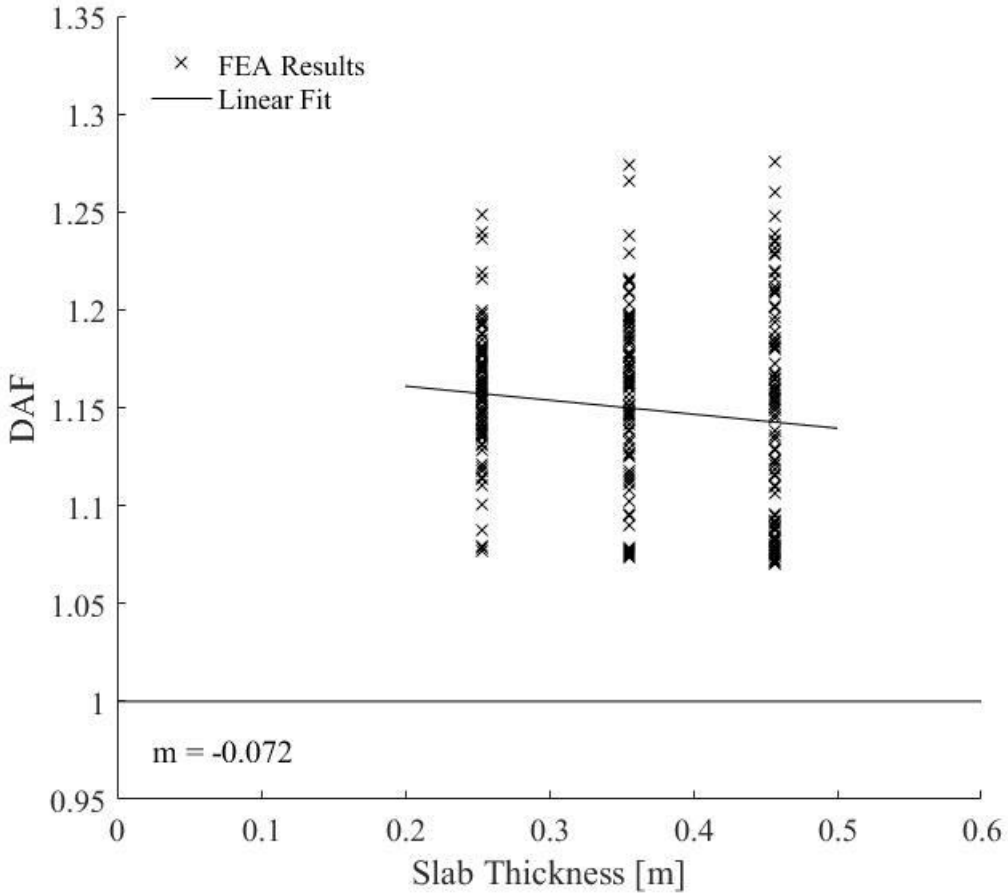

Figure 3.13 *DAF* as a Function of Slab Thickness

Table 3.8 Minimum, Maximum, Range, Average and Standard Deviation of *DAF* at Each Slab Thickness

Slab Thickness (m)	Minimum	Maximum	Range	Average	Standard Deviation
0.254	1.08	1.25	0.17	1.16	0.031
0.356	1.07	1.27	0.20	1.15	0.044
0.457	1.07	1.28	0.21	1.14	0.054

Pavement Thickness

Figure 3.14 shows the computed *DAF* as a function of asphalt pavement thickness. Based on the linear fit, *DAF* increases slightly as pavement thickness increases. The slope of the linear fit trend is 0.014 1/m. For an increase in pavement thickness of 0.229 the *DAF* is expected to increase by 0.003 on average. Table 3.9 gives the minimum, maximum, range, average and standard deviation of results for each pavement thickness. As can be seen, the minimum and average *DAF* at each pavement thickness are relatively constant. However, the maximum *DAF* decreases as pavement thickness increases. As a consequence, the range decreases as well. The standard deviation changes little as pavement thickness increases.

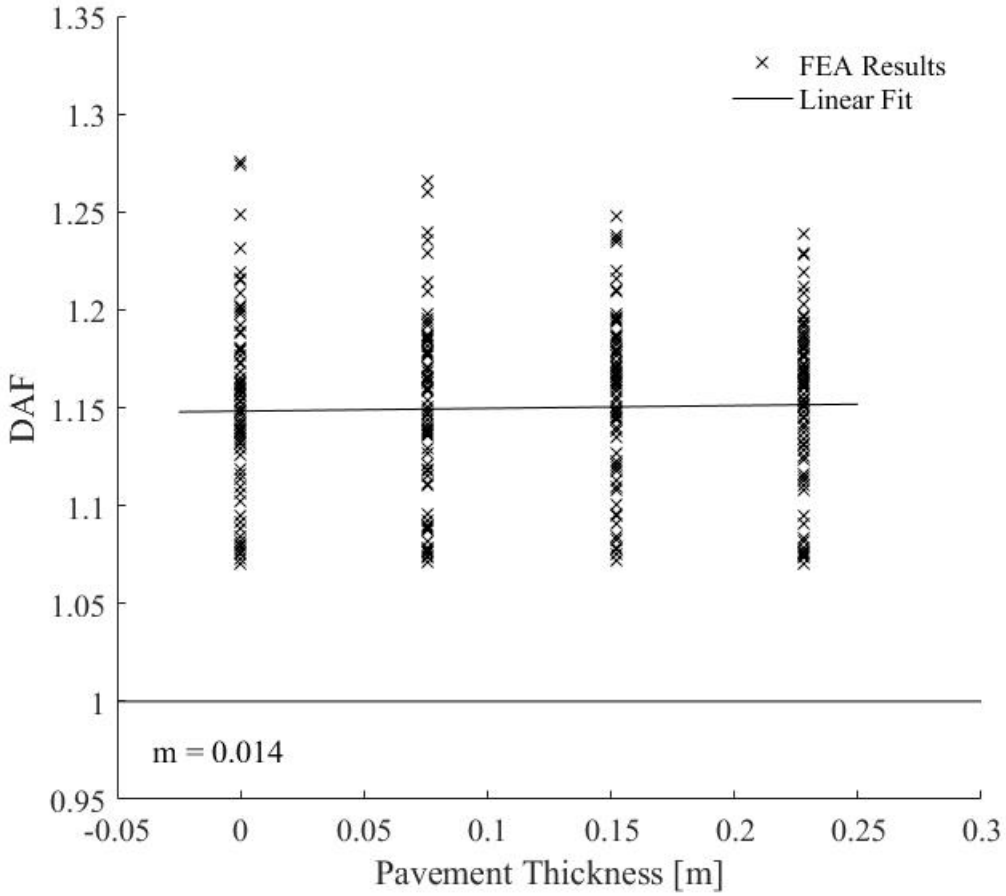

Figure 3.14 *DAF* as a Function of Pavement Thickness

Table 3.9 Minimum, Maximum, Range, Average and Standard Deviation of *DAF* at Each Pavement Thickness

Pavement Thickness (m)	Minimum	Maximum	Range	Average	Standard Deviation
0	1.07	1.28	0.21	1.15	0.046
0.076	1.07	1.27	0.20	1.15	0.046
0.152	1.07	1.25	0.18	1.15	0.043
0.229	1.07	1.24	0.17	1.15	0.041

Comparison of Parameters

Table 3.10 gives the slope of linear fit, difference between extreme parameter values, average expected change in *DAF* between minimum and maximum parameter values (slope of linear fit times the difference between extrema) and the standard deviation from the linear fit for each parameter studied. In general, fill depth and pavement thickness have a positive correlation to *DAF* while soil elastic modulus, span length and slab thickness have a negative correlation to *DAF*.

Using the average change in *DAF* as an indication of a parameter's influence on the system, it can be seen that soil elastic modulus has the greatest influence on *DAF* followed by fill depth. Comparatively, span length, slab thickness and asphalt pavement thickness have little influence on *DAF*.

Table 3.10 Comparison of Individual Parameters' Influence on *DAF*

Parameter	Slope of Linear Fit	Difference Between Extrema	Average Change in DAF	Standard Deviation from Linear Fit
Fill Depth	0.042 /m	1.22 m	0.051	0.039
Soil Elastic Modulus	-0.00014 /MPa	500 MPa	-0.070	0.033
Span Length	-0.0026 /m	2.44 m	-0.006	0.044
Slab Thickness	-0.072 /m	0.203 m	-0.015	0.044
Pavement Thickness	0.014 /m	0.229 m	0.003	0.044

It should also be noted that fill depth and soil elastic modulus are the only two parameters where the average change in *DAF* between extreme parameter values is greater than or equal to one standard deviation from the linear fit; and soil elastic modulus is the only parameter where the average change in *DAF* between extreme

parameter values is greater than two standard deviations from the linear fit. This indicates a high amount of variability for fill depth, span length, slab thickness and pavement thickness. A large factor in this variability is that individual parameters appear to have a different influence on the system depending on the value of other parameters.

Figure 3.15 shows a plot of fill depth for the three values of soil elastic modulus while holding span length, slab thickness, and pavement thickness constant. Values of span length, slab thickness and pavement thickness are 2.44, 0.457 and 0.0 m, respectively. As can be seen, an increase in fill depth influences the behavior of a 70 MPa soil model much differently than a 320 MPa or 570 MPa soil model. At a low fill depth, all models have a similar *DAF*, while at a middle fill depth the smallest soil elastic modulus has a much higher *DAF* than the other two values. Moreover, the 70 MPa soil model decreases between fill depths of 1.22 and 1.83 m where *DAF* values of the higher soil elastic moduli always increase as fill depths increase. This behavior, where an increase in parameter value affects the system's behavior much differently in one area of the parameter space than in another, is common for each of the five parameters.

Figure 3.16 shows a plot of span length for the three values of soil elastic modulus, while holding fill depth, slab thickness, and pavement thickness constant. Values of fill depth, slab thickness and pavement thickness are 0.61, 0.254 and 0.229 m, respectively. Similar to the way the 70 MPa soil in Figure 3.15 influenced the system differently than the other two values of soil modulus, here all three soil elastic moduli show different behavior. As can be seen, the *DAF* for configurations with 70 MPa soil decreases with increasing span length, while the *DAF* for configurations with

320 MPa soil is influenced little by span length, and the *DAF* for configurations with 570 MPa soil increases with increasing span length. This shows that the soil-structure-pavement system is extremely complex in nature.

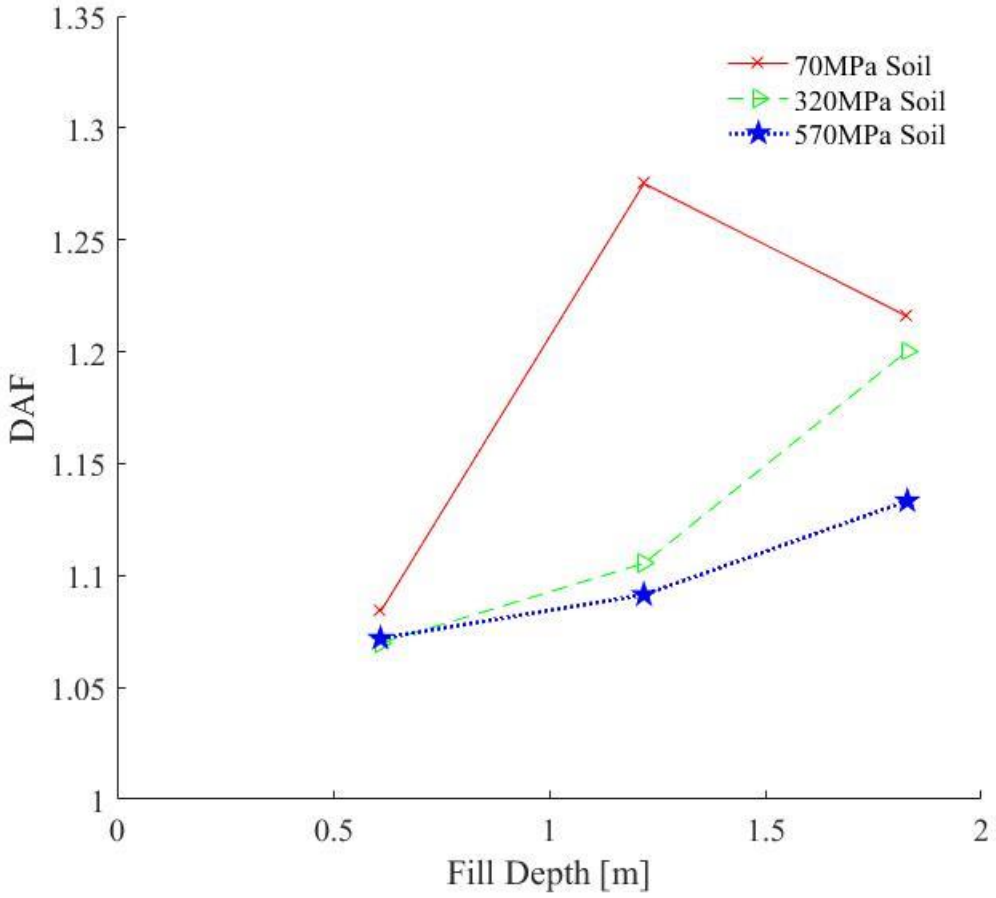

Figure 3.15 Influence of Fill Depth on *DAF* for Three Values of Soil Elastic Modulus

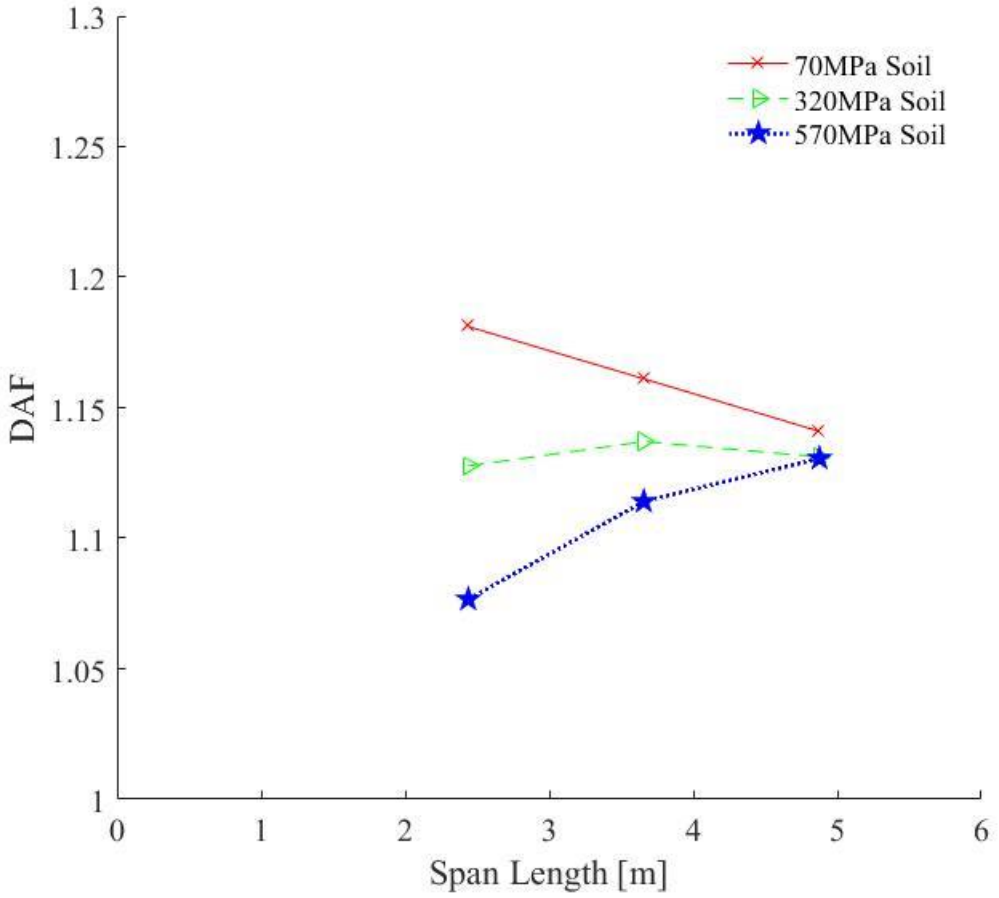

Figure 3.16 Influence of Span Length on *DAF* for Three Values of Soil Elastic Modulus

3.4.3 Theory Comparison

At the outset of this analysis it was determined that a symmetric, triangular load pulse applied at center span adequately approximates the load applied by a moving tuck. As a consequence, the t_d/T_n ratio is chosen to maximize the dynamic amplification within reason (vehicle speeds no higher than 40.5 m/s) with an anticipated maximum *DAF* of 1.17, according to the SDOF solution (Chopra 2012). From the target t_d/T_n ratio of 3.08 the *DAF* is expected to decrease to 1.10 as the t_d/T_n ratio approaches 3.58. If a t_d/T_n ratio between 3.58 and 5.11 is required due to a limiting vehicle speed the theory suggests that a ratio of 5.11 will give the maximum possible *DAF* for that model configuration. For models with target t_d/T_n ratios of 5.11 *DAF* values are expected to be 1.10.

Fundamentally, the increase in t_d/T_n ratio is a result of the restriction placed on vehicle speed. Of the 324 model configurations, 142 (44 percent) have higher target t_d/T_n ratios than 3.08 and 55 (17 percent) have target t_d/T_n ratios of 5.11. Figure 3.17 compares the finite element results obtained in this research to those suggested by the SDOF solution (Chopra 2012). The results of a single analysis are shown by an "x" sign in the figure. As can be seen, the SDOF solution captures the general behavior of the system quite well. Results are higher at t_d/T_n ratios around 3.08 and decrease as t_d/T_n increases. Results are also approximately 1.10 at t_d/T_n ratios around 5.11. On average the *DAF* obtained during the finite element analysis is 0.002 less than the *DAF* calculated using the SDOF solution.

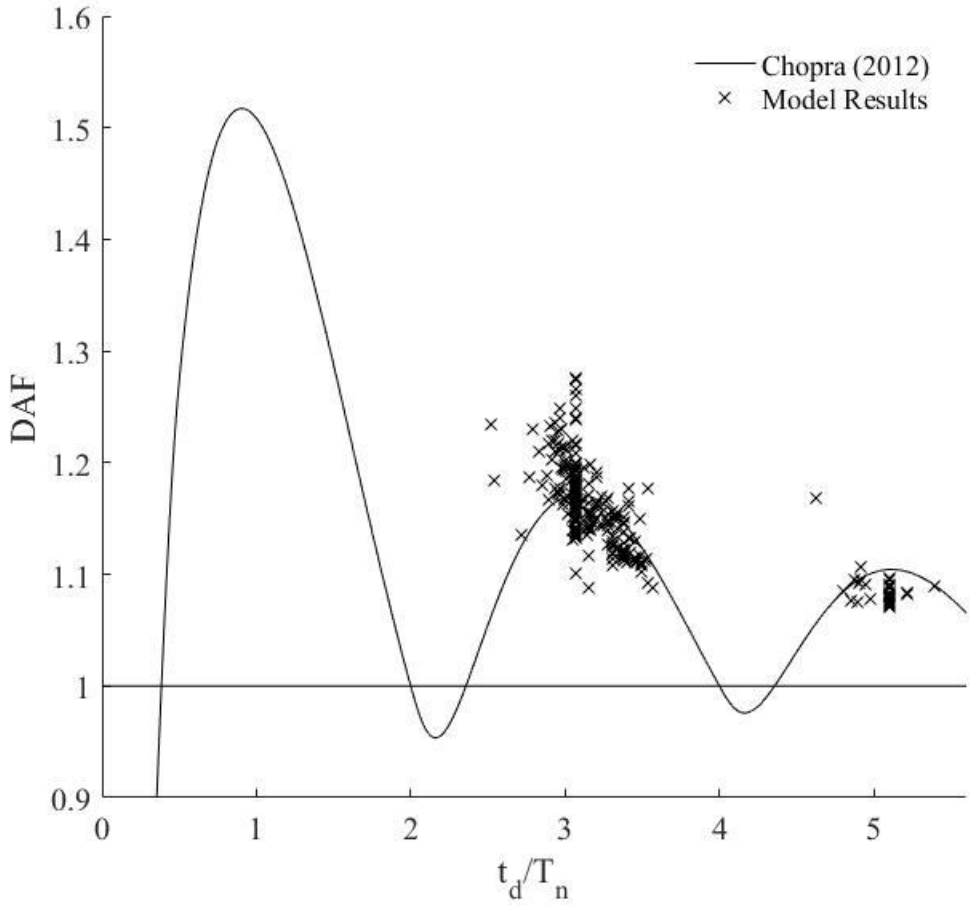

Figure 3.17 Comparison of Finite Element Results to SDOF Solution

Nonetheless, differences exist between the results of this study and the SDOF solution. The maximum modeled *DAF* is 1.28, 0.11 higher than the maximum anticipated *DAF* from the SDOF solution. Several model configurations have *DAFs* approximately the same value. Additionally, several configurations have *DAFs* more than 0.05 below the SDOF solution. As a consequence, the standard deviation of results from the theoretical SDOF solution is 0.032. This variability is primarily due to the fact that the finite element models employed in this study are a multi-degree of freedom systems. As a result, some disagreement is expected.

3.4.4 **Influence of Parameters on Natural Period**

Figures 3.18 to 3.22 show the natural period of each model configuration as a function of the five parameters studied and displays the slopes of the linear fit lines. Based on the linear fit, it can be seen that natural period tends to increase as fill depth, span length and asphalt pavement thickness increase and tends to decrease as soil elastic modulus and slab thickness increase. It also can be seen that a fair amount of variability exists in results.

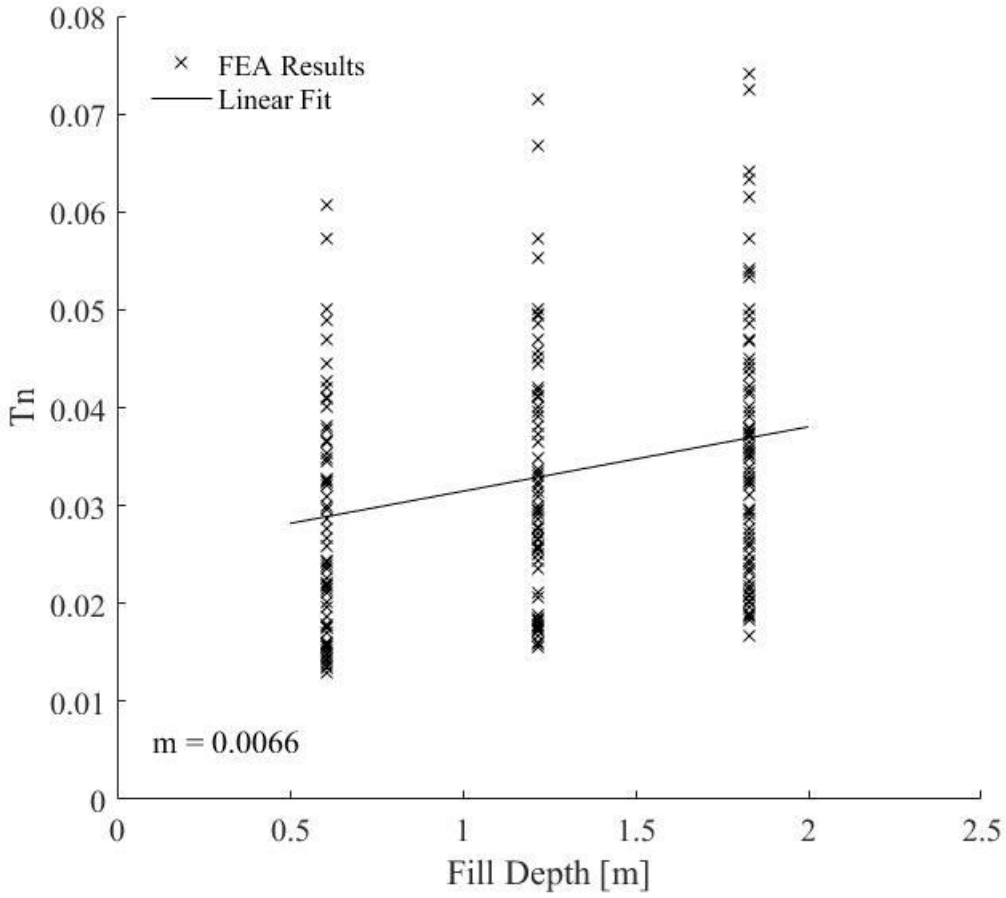

Figure 3.18 Influence of Fill Depth on Natural Period

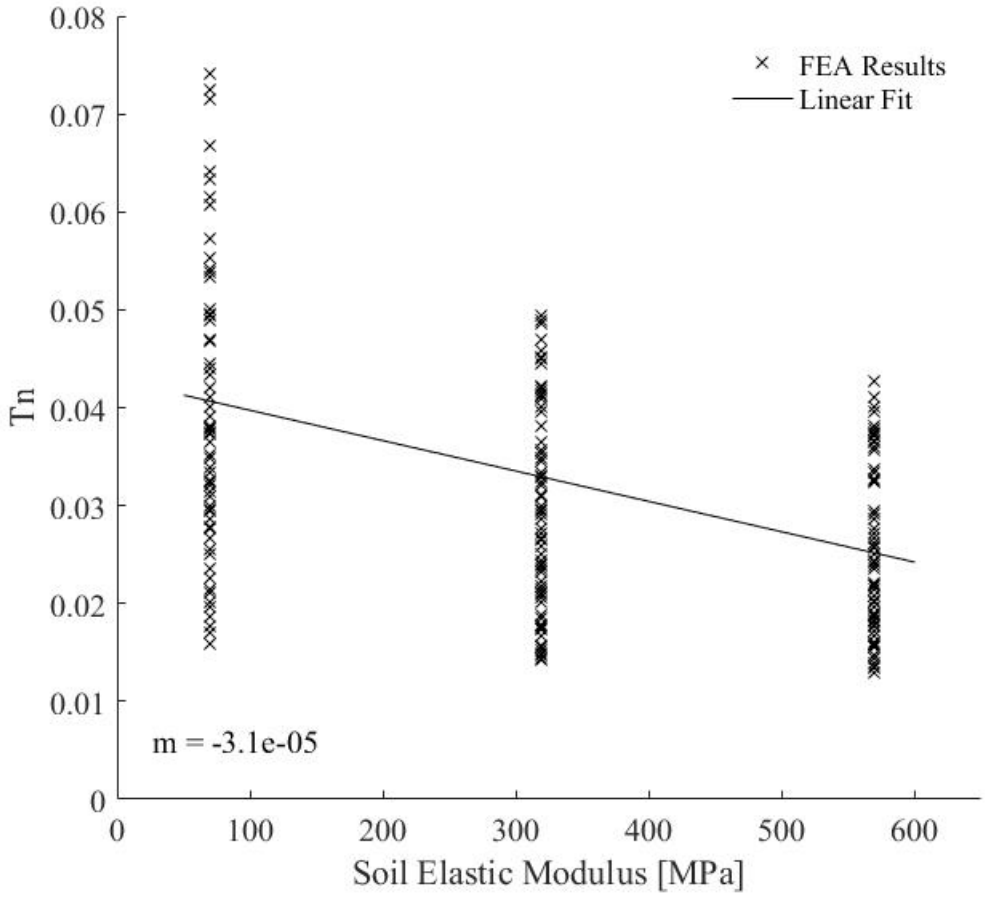

Figure 3.19 Influence of Soil Elastic Modulus on Natural Period

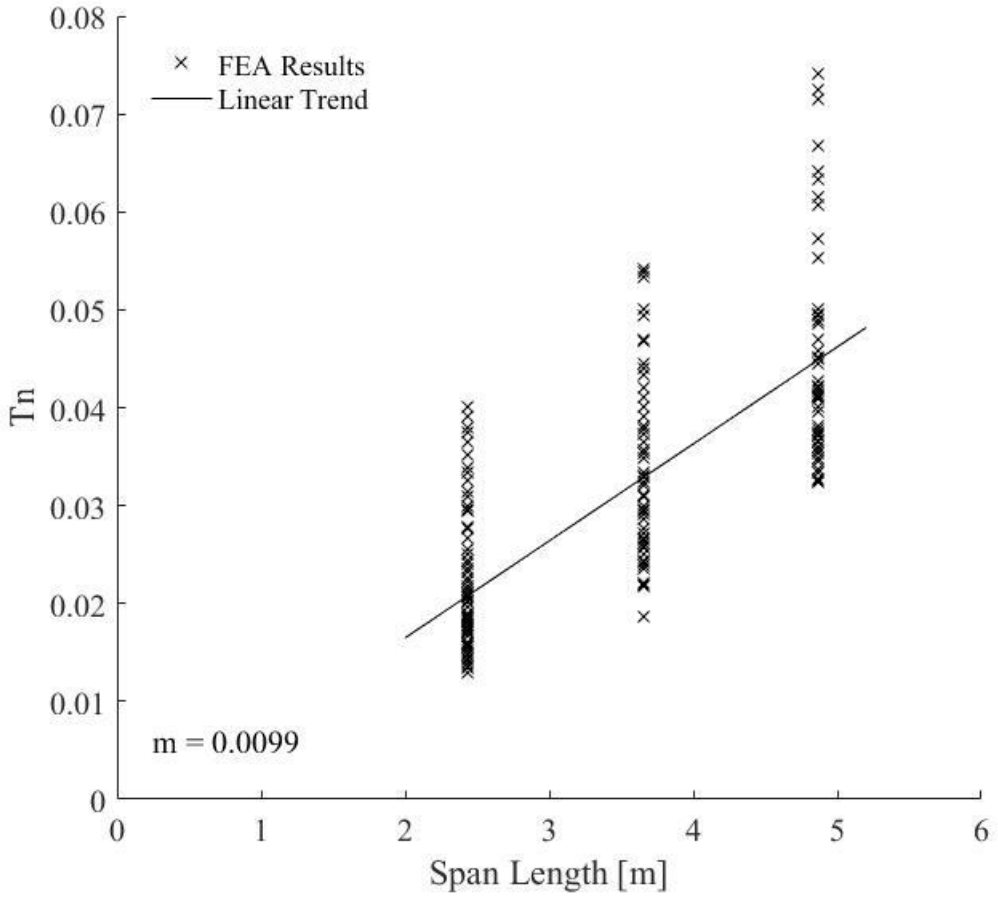

Figure 3.20 Influence of Span Length on Natural Period

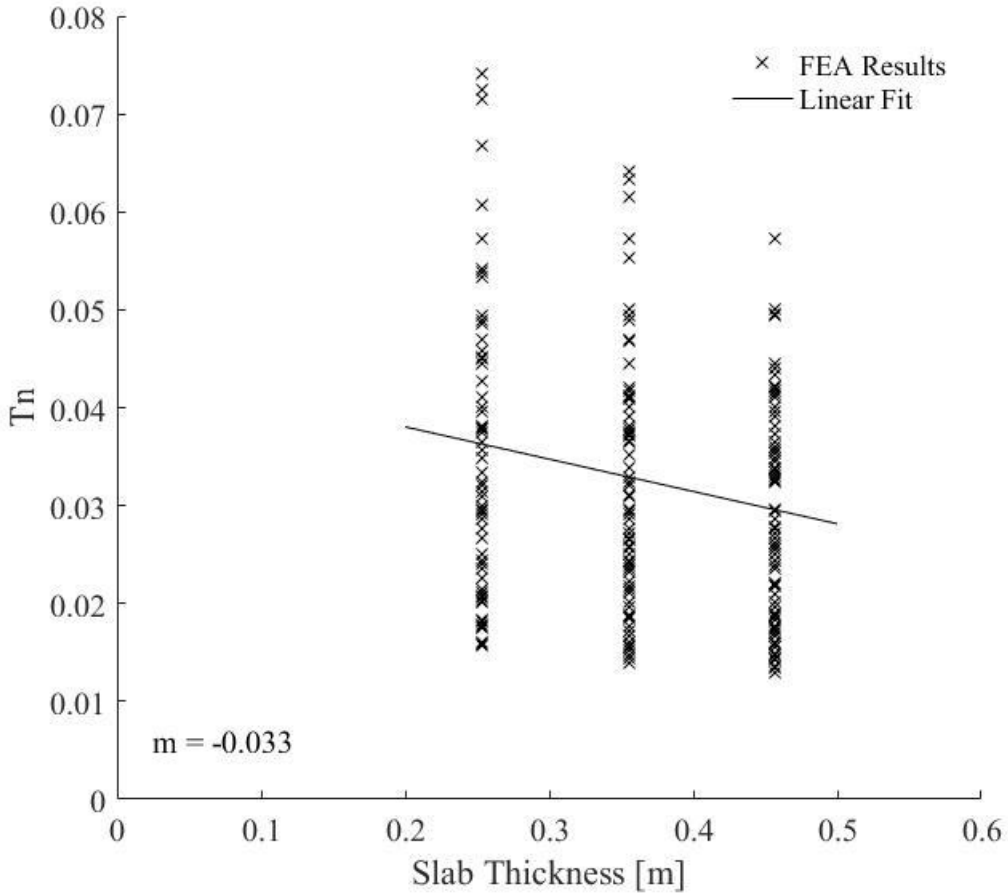

Figure 3.21 Influence of Slab Thickness on Natural Period

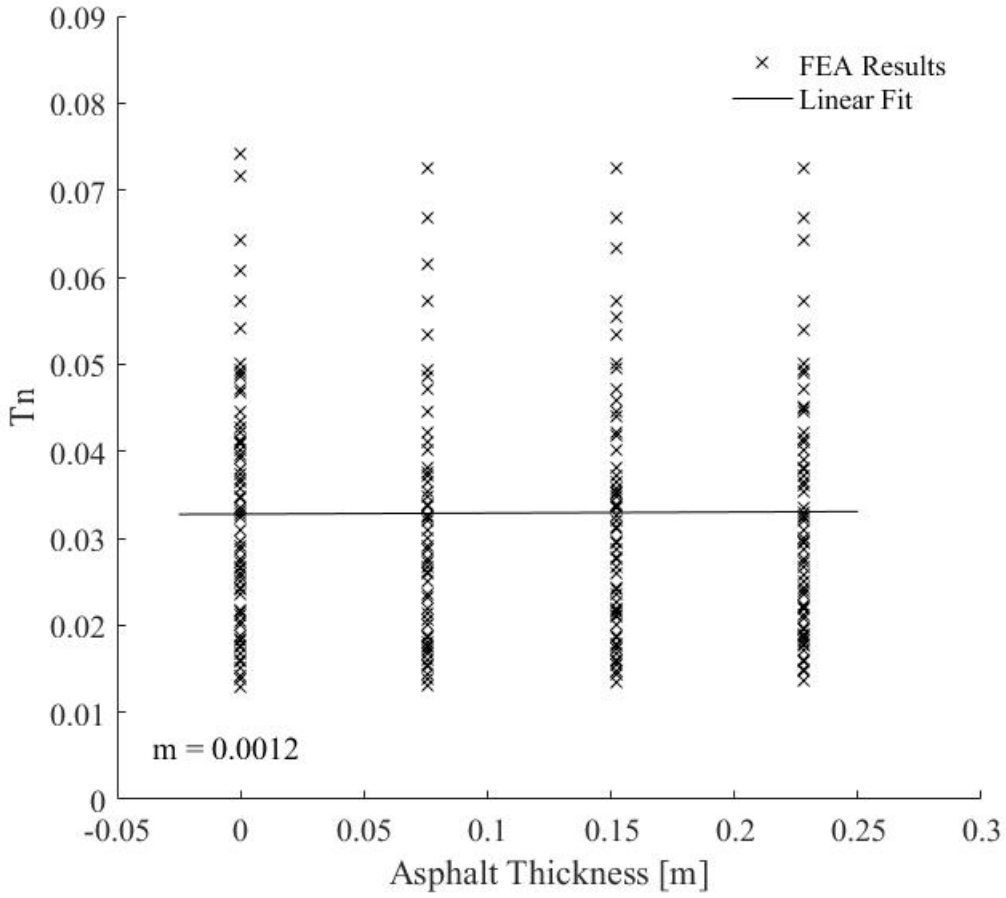

Figure 3.22 Influence of Pavement Thickness on Natural Period

Table 3.11 gives the slope of the linear fit, the difference between extreme parameter values, average expected change in natural period between extreme parameter values (slope of linear fit times the difference between extrema), the average change in T_n as a percent of the average T_n and the standard deviation from the linear fit. Span length influences the natural period more than any other parameter. Not only is the average change in natural period between extreme parameter values of the greatest magnitude, but the standard deviation from the linear fit is the lowest as well. This indicates that the natural period is expected to change the most for a change in span length and that the variability associated with that change is the least.

Soil elastic modulus is the next most influential parameter on natural period as the average change in natural period between extreme parameter values is approximately double that of fill depth and slab thickness, and approximately 50 times that of pavement thickness. The variability of natural period as a function of soil elastic modulus is also slightly less than fill depth, slab thickness and pavement thickness.

When comparing the average change in natural period between extreme parameter values to the standard deviation from the linear fit, it is difficult to say that fill depth, slab thickness and pavement thickness have a meaningful influence on natural period. This is because the average change between the minimum and maximum parameter values does not exceed one standard deviation from the linear fit. Pavement thickness in particular has very little influence as the standard deviation is approximately 40 times larger than the average change in natural period.

Table 3.11 Comparison of Individual Parameters' Influence on Natural Period

Parameter	Slope of Linear Fit	Difference Between Extrema	Average Change in T_n Between Extrema	Average Change Relative to the Average T_n	Standard Deviation from Linear Fit
Fill Depth	0.0066 1/m	1.22 m	0.008	29%	0.0127
Soil Elastic Modulus	-0.000031 1/MPa	500 MPa	-0.016	57%	0.0115
Span Length	0.0099 1/m	2.44 m	0.024	86%	0.0087
Slab Thickness	-0.033	0.203 m	-0.007	25%	0.0129
Pavement Thickness	0.0012	0.229	0.0003	1%	0.0131

3.4.5 **Discussion of Individual Parameters In-Light of Theory**

Fill Depth

Possibly the most obvious difference between buried bridge structures and conventional bridges is the presence of soil between the structure's slab and the roadway. While soil has a similar density to concrete, its stiffness is two to three orders of magnitude less. Consequently, the natural period of a buried structure is expected to be higher than that of a similar structure without fill or with less fill. In previous sections it was shown that *DAF* can be reasonably approximated by a SDOF solution and that natural period tends to increase as fill depth increases. Moreover, it was discussed that as natural period increases, the vehicle speed required to attain the same t_d/T_n ratio decreases. Because a vehicle speed is less likely to be limited and the t_d/T_n ratio is decreasing, an increase in natural period is generally expected to increase the *DAF*. This trend was observed for fill depth.

Table 3.12 gives the average t_d/T_n ratio, standard deviation of t_d/T_n ratio, the maximum theoretical *DAF* at the average t_d/T_n ratio (as determined using Figure 3.5) and the average computed *DAF* from finite element results for each fill depth studied. As can be seen, the t_d/T_n ratio tends to decrease as fill depth and subsequently natural period increases. Furthermore, the theoretical maximum and average computed *DAF* increase as average t_d/T_n ratio decreases.

However, while the average trends follow those suggested by the SDOF solution, results are much too variable on an aggregate level to predict t_d/T_n ratio or *DAF*. This is particularly true for fill depths of 0.61 m as the standard deviation of t_d/T_n ratios is 0.909. Figure 3.23 shows the results of this study broken down by fill depth and compares them to the SDOF theory. As can be seen, model configurations having each fill depth occur throughout the entire range of t_d/T_n ratios.

Table 3.12 Average t_d/T_n Ratio, Standard Deviation of t_d/T_n Ratio, Maximum Theoretical *DAF* at Average t_d/T_n Ratio and Average *DAF* for Each Value of Fill Depth

Fill Depth (m)	Average t_d/T_n	Standard Deviation of t_d/T_n	Maximum Theoretical *DAF* at Average t_d/T_n	Average Finite Element *DAF*
0.61	3.84	0.909	1.10	1.12
1.22	3.43	0.705	1.14	1.16
1.83	3.13	0.304	1.17	1.17

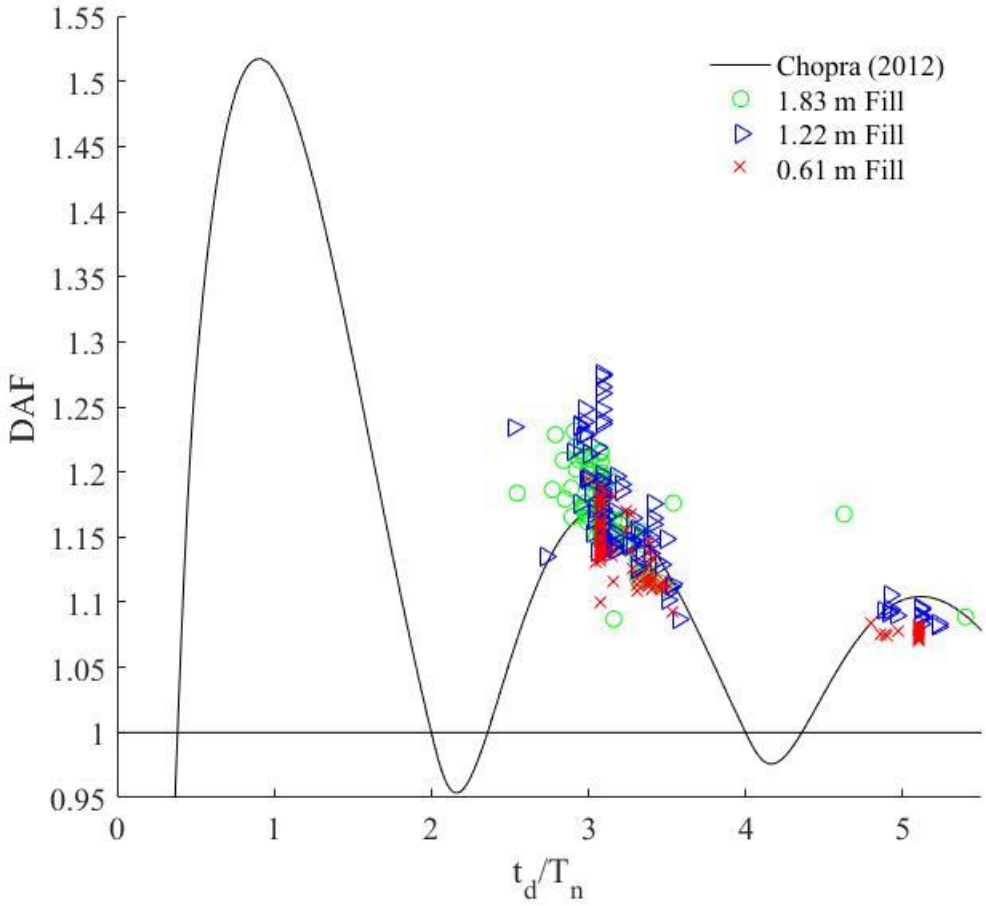

Figure 3.23 Influence of Fill Depth Compared to SDOF Theory

Soil Elastic Modulus

Soil elastic modulus directly influences the stiffness of the system. An increase in soil elastic modulus is expected to decrease the natural period and thus increase t_d/T_n ratio. Table 3.13 gives the average t_d/T_n ratio, standard deviation of t_d/T_n ratio, the maximum theoretical *DAF* at the average t_d/T_n ratio (as determined using Figure 3.5) and the average computed *DAF* from finite element results for each soil elastic modulus studied. Results show that increasing soil elastic modulus tends to increase t_d/T_n ratio and decrease the average computed *DAF* from finite element results.

While the standard deviation of t_d/T_n ratio is only 0.208 at 70 MPa, it is 0.905 at 570 MPa. As a result, it is difficult to say that soil elastic modulus is predictive of *DAF*. As can be seen in Figure 3.24, 70 MPa soil modulus values tend to have lower t_d/T_n ratios, however model configuration with 320 MPa and 570 MPa soil moduli have a wide range of t_d/T_n ratios.

Table 3.13 Average t_d/T_n Ratio, Standard Deviation of t_d/T_n Ratio, Maximum Theoretical *DAF* at Average t_d/T_n Ratio and Average *DAF* for Each Value of Soil Elastic Modulus

Soil Elastic Modulus (MPa)	Average t_d/T_n	Standard Deviation of t_d/T_n	Maximum Theoretical *DAF* at Average t_d/T_n	Average Finite Element *DAF*
70	3.08	0.208	1.17	1.19
320	3.37	0.643	1.15	1.15
570	3.95	0.905	1.10	1.12

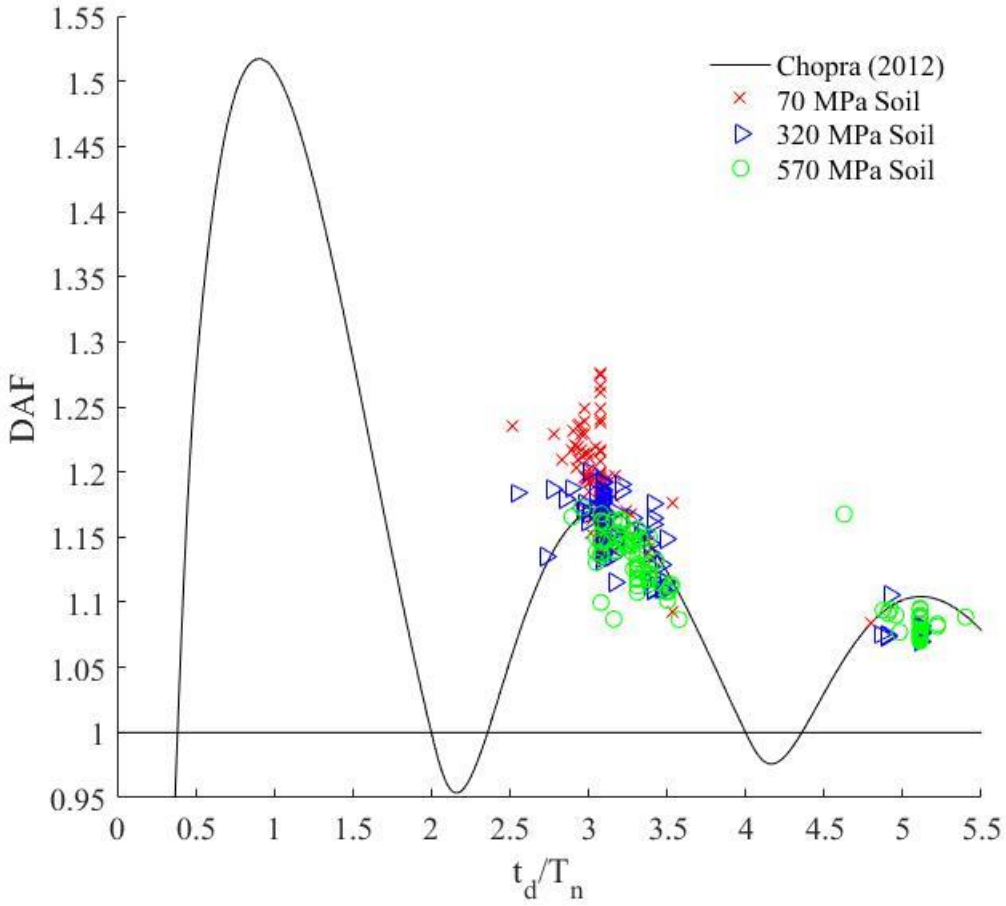

Figure 3.24 Influence of Soil Elastic Modulus Compared to SDOF Theory

Span Length

Span length is unique among the parameters examined in this study because it influences both the pulse duration and the structure's natural period. As span length increases the stiffness of the asphalt-soil-structure system decreases, thus increasing T_n. However, pulse duration is the ratio of the span length to vehicle speed. As a result, span length also increases pulse duration. Consequently, span length's relationship to the t_d/T_n ratio and subsequently *DAF* is more complex than other parameters.

Of all the parameters examined in this study, span length has the largest influence on the natural period. On average, the maximum increase in span length between extreme parameter values causes a 0.024 s increase in natural period (86 percent of the average natural period). However, the influence of natural period appears to be somewhat minimized by the pulse duration. Table 3.14 gives the average t_d/T_n ratio, standard deviation of t_d/T_n ratio, the maximum theoretical *DAF* at the average t_d/T_n ratio (as determined using Figure 3.5) and the average computed *DAF* from finite element results for each span length studied. The average *DAF* computed during the finite element analysis does not change with increasing span length. This is in contrast to the theory, which suggests an increase in *DAF* based on an increasing t_d/T_n ratio. One explanation for this is that lower span lengths tend to have slightly higher *DAF* values at similar t_d/T_n ratios as higher span lengths; while at the same time, higher span lengths tend to have higher t_d/T_n ratios.

Table 3.14 Average t_d/T_n Ratio, Standard Deviation of t_d/T_n Ratio, Maximum Theoretical *DAF* at Average t_d/T_n Ratio and Average *DAF* for Each Value of Span Length

Span Length (m)	Average t_d/T_n	Standard Deviation of t_d/T_n	Maximum Theoretical *DAF* at Average t_d/T_n	Average Finite Element *DAF*
2.44	3.68	0.876	1.10	1.15
3.66	3.46	0.747	1.13	1.15
4.88	3.27	0.511	1.16	1.15

Figure 3.25 shows the results of this study broken down by span length and compared to the SDOF theory. As can be seen, more configurations with span lengths of 2.44 and 3.66 m have t_d/T_n ratios of approximately 5.11, yet they also tend to have the highest *DAF* values at t_d/T_n ratios of approximately 3.08. It should also be noted that the standard deviation of t_d/T_n ratios for each is high for span length. This may also be a contributing factor.

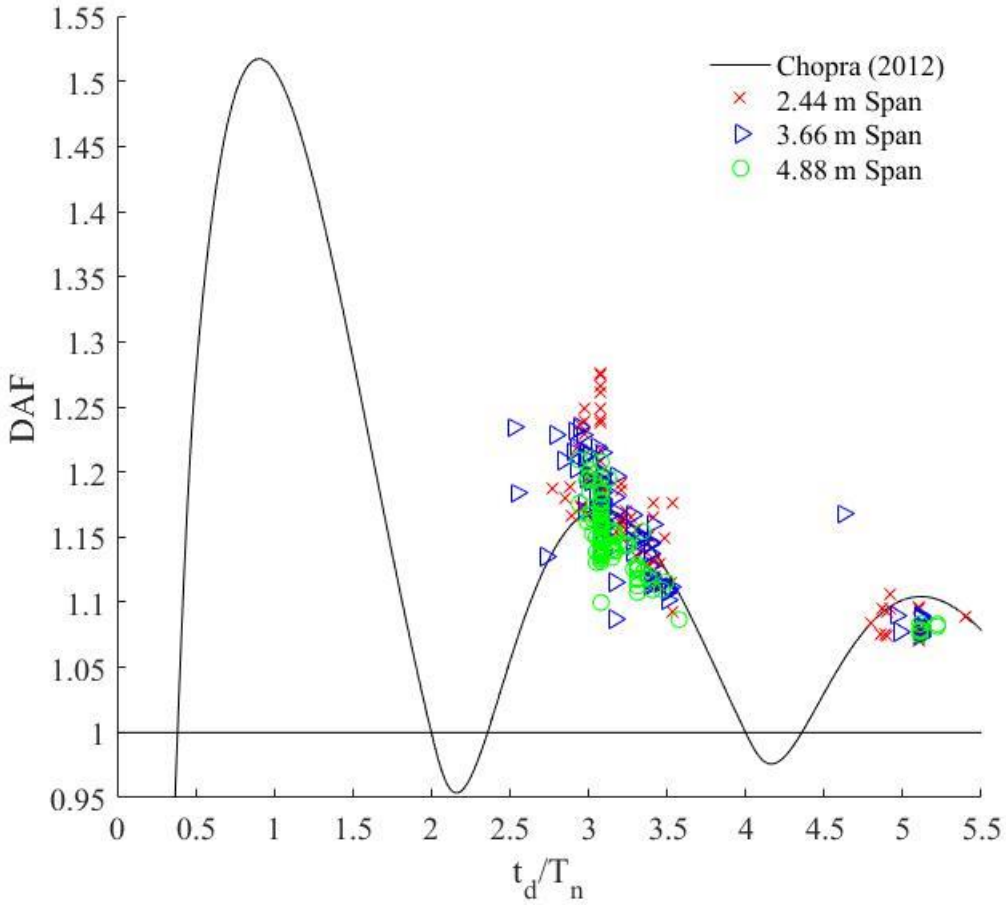

Figure 3.25 Influence of Span Length Compared to SDOF Theory

Slab Thickness

While an increase in slab thickness does increase the mass of the system, it has a larger effect on the structure's stiffness. On average, natural period decreases by 0.007 s (25 percent of the average natural period) between extreme parameter values. Table 3.15 gives the average t_d/T_n ratio, standard deviation of t_d/T_n ratio, the maximum theoretical *DAF* at the average t_d/T_n ratio (as determined using Figure 3.5) and the average computed *DAF* from finite element results for each slab thickness studied. As can be seen, the average t_d/T_n ratio increases as slab thickness increases. Conversely, the average computed *DAF* from finite element results increases. While it is true that the average *DAF* generally follows expected trends, the variability in t_d/T_n ratio for each parameter value is high. Figure 3.26 shows a similar range of t_d/T_n ratios for all slab thicknesses. As a result, slab thickness is not predictive of t_d/T_n ratio.

Table 3.15 Average t_d/T_n Ratio, Standard Deviation of t_d/T_n Ratio, Maximum Theoretical *DAF* at Average t_d/T_n Ratio and Average *DAF* for Each Value of Slab Thickness

Slab Thickness (m)	Average t_d/T_n	Standard Deviation of t_d/T_n	Maximum Theoretical *DAF* at Average t_d/T_n	Average Finite Element *DAF*
0.254	3.19	0.398	1.17	1.16
0.356	3.45	0.714	1.13	1.15
0.457	3.76	0.918	1.10	1.14

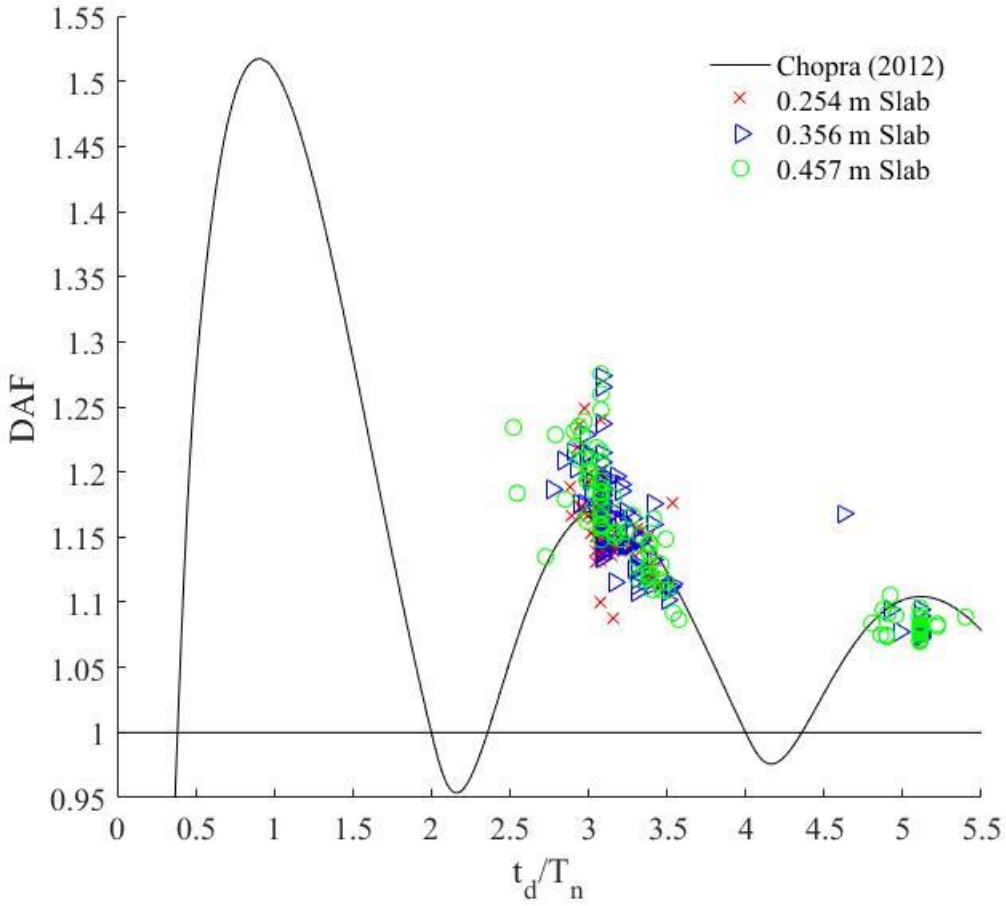

Figure 3.26 Influence of Slab Thickness Compared to SDOF Theory

Asphalt Pavement Thickness

Asphalt pavement thickness has been shown to have little effect on natural period. As a result, the t_d/T_n ratio is expected to change little for a change in asphalt pavement thickness. Table 3.16 gives the average t_d/T_n ratio, standard deviation of t_d/T_n ratio, the maximum theoretical *DAF* at the average t_d/T_n ratio (as determined using Figure 3.5) and the average computed *DAF* from finite element results for each pavement thickness studied. As can be seen the values for each field change little, if any, from thickness to thickness. Additionally, the standard deviations of t_d/T_n ratios are large. As a result, pavement thickness is not predictive of t_d/T_n ratio or *DAF*. As can be seen in Figure 3.27, models of all asphalt thicknesses have similar t_d/T_n ratios and *DAF* values. Given the lack of influence on natural period, these results should be expected.

Table 3.16 Average t_d/T_n Ratio, Standard Deviation of t_d/T_n Ratio, Maximum Theoretical *DAF* at Average t_d/T_n Ratio and Average *DAF* for Each Value of Pavement Thickness

Span Length (m)	Average t_d/T_n	Standard Deviation of t_d/T_n	Maximum Theoretical *DAF* at Average t_d/T_n	Average Finite Element *DAF*
0	3.49	0.768	1.13	1.15
0.076	3.49	0.769	1.13	1.15
0.152	3.45	0.733	1.13	1.15
0.229	3.44	0.718	1.15	1.15

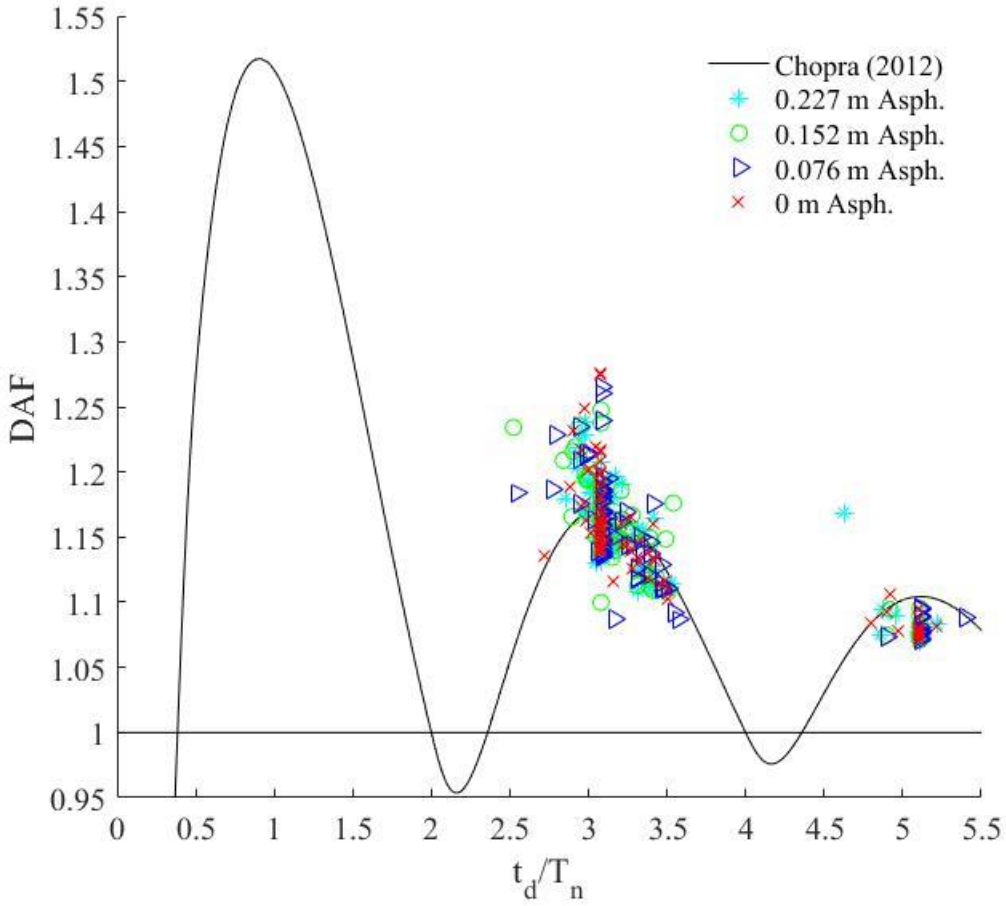

Figure 3.27 Influence of Pavement Thickness Compared to SDOF Theory

Chapter 4

FIELD TESTING

4.1 Outline of Field Testing

4.1.1 Introduction

To date, only a hand full of studies have experimentally examined the dynamic behavior of culverts. Moreover, none could be found that studied the dynamic amplification of reinforced concrete box culverts. In order to fill this gap in experimental research tests are conducted as a part of this thesis that examine the dynamic behavior of five culverts in the state of Delaware. In each test, the static and dynamic response of the culvert is determined due to fully loaded dump trucks. Culverts are chosen with varying geometric properties and fill depths—the intent being to capture the response of culverts that are a representative sample of Delaware's state inventory. Tables 4.1 and 4.2 summarize the culverts' construction type, roadway information and geometric properties (note that fill depths and pavement thicknesses are only estimates based on a review of existing drawings, field inspection reports and other documentation).

Table 4.1 Culvert Construction and Roadway Information

Culvert No.	Construction Type	No. of Marked Lanes	Pavement Type	Roadway Condition
1	Cast-in-place, four-sided box	2	Asphalt	Good
2	Precast, four-sided box	2	Asphalt	Good
3	Cast-in-place, three-sided box	4	Asphalt	Good
4	Precast, three-sided box	2	Asphalt	Good
5	Precast, three-sided box	2	Asphalt	Good

Table 4.2 Culvert Geometric Properties

Culvert No.	Fill Depth (m)	Span Length (m)	Slab Thickness (m)	Pavement Thickness (m)
1	0.38	3	0.3	0.23
2	0.5	4.3	0.3	0.15
3	0.41	5.5	0.51	0.2
4	0	7.7	0.38	0.44
5	0	6.4	0.76 (including parapet)	0.07

4.1.2 **Instrumentation**

This research uses a Bridge Diagnostics Inc. (BDI), Structural Testing System (STS), which includes quick mount strain transducers, data acquisition system, and software. The STS, as set up during the testing of Culvert 2, can be seen in Figure 4.1. The BDI strain transducers have a 76 mm (3 in.) gauge length. In many instances 229 mm (9 in.) steel extensions were placed on the sensors to increase the gauge length to 305 mm (12 in.). This is recommended when testing concrete. The transducer/extension apparatus had steel feet at both ends that were used to mount the sensor to the culvert. Transducers were affixed to the culvert using high viscosity, rubber toughened cyanoacrylate glue applied with an accelerant. Prior to mounting the sensors, the surface was prepared using a wire brush. Several tests attempted to use string potentiometers to measure displacement, however deflections were so small that results could not be distinguished from ambient noise. For that reason, only strain is reported.

Figure 4.1 BDI Structural Testing System Setup for Culvert 2

For each test, the road is divided into three test lanes: one in each marked lane of travel and one directly over the marked centerline. Five strain transducers were placed on the underside of the top slab, along the centerline of the culvert, at locations corresponding to the fog lines, center of each marked lane and center line of the roadway. Thus, sensors were located at the center and offset to the edges of each tested lane. In some instances, surface roughness and surface cracks in the concrete did not allow for sensors to be placed exactly along the centerline of the culvert. For those few cases, sensors are located approximately 0.3 m away from the centerline. Additionally, there was some concern that culverts constructed of precast sections may show different behavior towards the edges of the sections than at the sections' center. As a result, additional sensors were placed at the center of individual precast sections when the layout called for sensors to be placed near a section's edge. Figure 4.2 shows the test layout for Culvert 1.

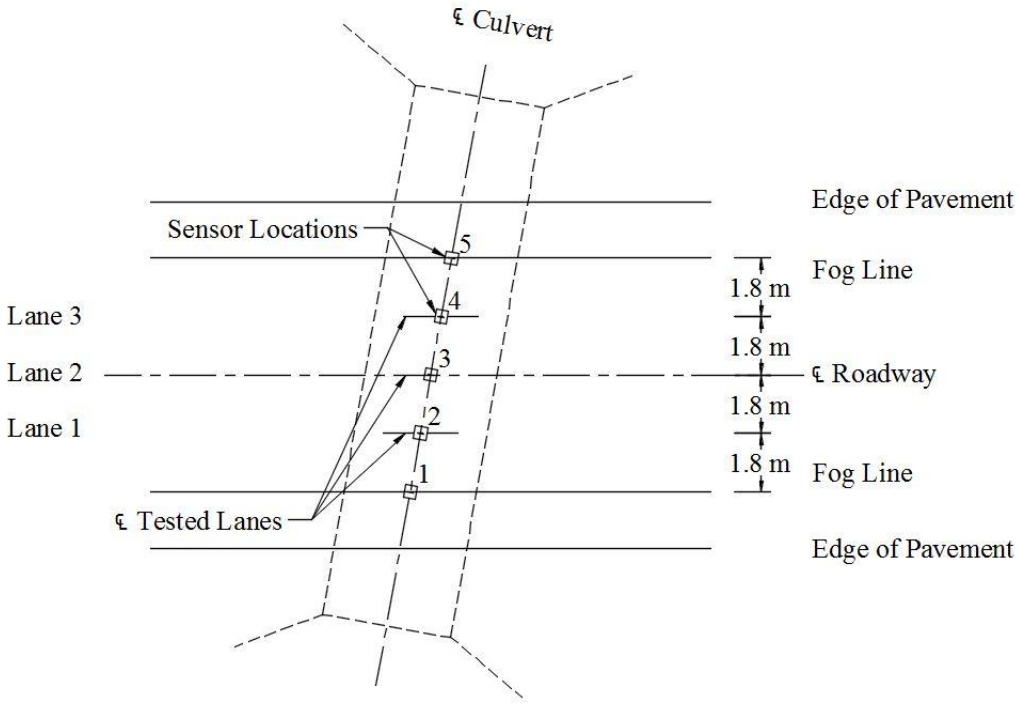

Figure 4.2 Culvert 1 Test Layout

4.1.3 **Trucks**

In each pass, two fully loaded dump trucks are driven across the culvert. trucks are spaced at approximately six truck lengths so that their respective load pulses do not interfere with one another. Figure 4.3 shows the truck spacing during the testing of Culvert 2.

Trucks used were all the same make and model. Figure 4.4 diagrams the wheel and axle spacing for the trucks used during testing.

Figure 4.3 Trucks During Load Test

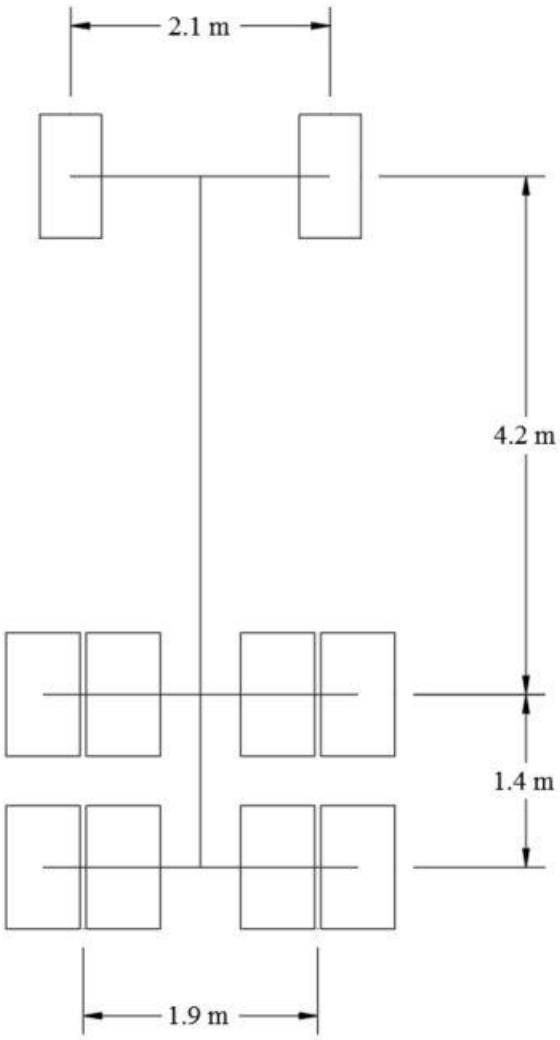

Figure 4.4 Truck Wheel and Axle Spacing

After testing, each truck was weighed in order to obtain the static load applied by each truck. Two scales were used to determine the weight of each wheel (or wheel pair) one axle at a time. Figure 4.5 shows a picture of a loaded scale. The individual wheel loads were then combined to form a total truck weight. The weights of the two trucks used for each test can be seen in Table 4.3.

Figure 4.5 Truck on Scale

Table 4.3 Truck Weights

Culvert	Truck 1 (kN)	Truck 2 (kN)
1	283	282
2	304	295
3	252	274
4	258	251
5	235	242

4.1.4 **Organization of Tests**

Table 4.4 gives the test plan for each culvert and shows the number of passes planned for every test in each lane. One pass accounts for the crossing of both trucks. It should be noted that both trucks did not complete every pass in Table 4.4. One truck broke down during the testing of one culvert and faulty data was discovered during one pass of another culvert. Those issues will be discussed in a later section; this is simply a representation of what was planned. It should also be noted that exact truck speeds were not recorded during testing. Rather, truck drivers were requested to drive the speeds outlined in Table 4.4 and inform the author when they did not reasonably meet the target speed. Once informed that targets were not met, the author directed that passes be repeated.

Table 4.4 Number, Speed and Location of Passes Planned for the Testing of Each Culvert

Culvert No.	Speed (m/s)	Number of Truck Passes		
		Lane 1	Lane 2	Lane 3
Culvert 1	2.2	2	2	2
	8.9	-	1	-
	13.4	1	1	1
	17.9	-	1	-
Culverts 2-5	2.2	2	2	2
	8.9	2	2	2
	13.4	2	2	2
	17.9	2	2	2

4.1.5 **Determination of *DAF***

The goal for each of the load tests is to determine a *DAF* for each culvert. While the exact method is not the same for every test, general procedures remain consistent. As discussed, the *DAF* is calculated as the ratio between a structure's

dynamic and static responses (R_{Dyn} and R_{Stat}, respectively). For this study the response measured is strain. Thus, *DAF* is calculated as the ratio of the dynamic strain to the static strain.

To represent a static load, trucks are driven across the culvert at a quasi-static or "crawl" speed (about 2.2 m/s). Figure 4.6 shows a sample strain time history response for one crawl speed pass. In this plot the passes made by Truck 1 and Truck 2 are superimposed. As discussed, during testing trucks were spaced such that the culvert responded to each load individually. For each truck, two distinct loads can be seen crossing the culvert. The front axle crosses first and the two rear axles appear as one load, crossing second.

As indicated in Table 4.4, two crawl speed passes are made by both trucks in each lane during all tests. The static strain for Truck 1 at each sensor location is determined by averaging the maximum strain response during the two crawl passes made by Truck 1 at speeds of 2.2 m/s. Similarly, for Truck 2 the static strain at each sensor location is determined by averaging the maximum strains caused during the two crawl passes made by Truck 2 at speeds of 2.2 m/s.

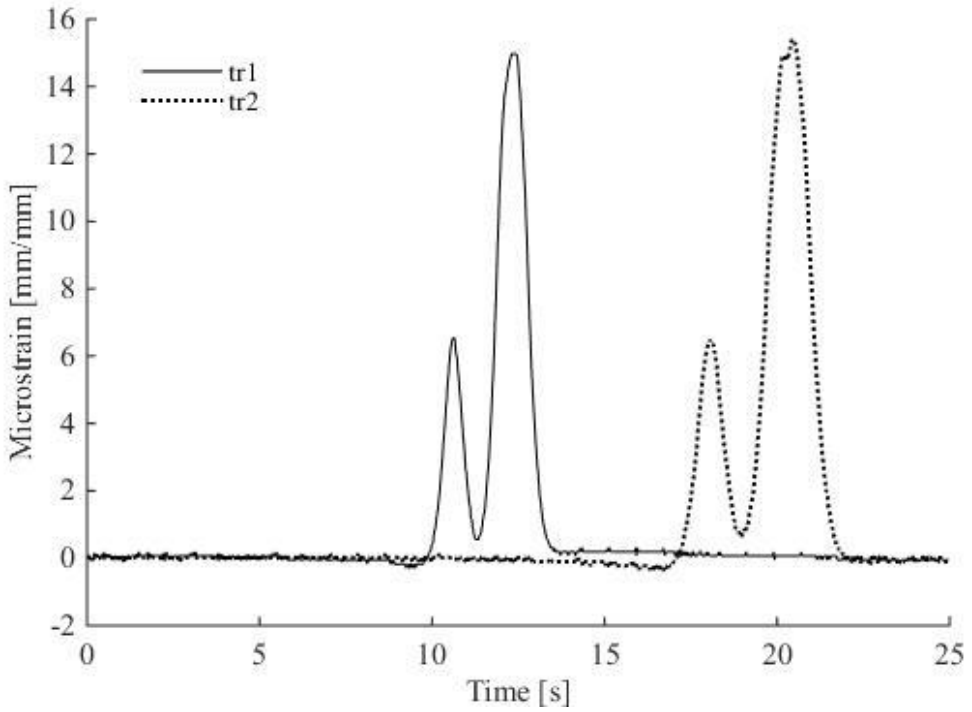

Figure 4.6 Measured Response of Culvert Due to a Quasi-Static Load

For dynamic passes, the trucks are driven across the culvert at typical vehicle speeds, ranging from 8.9 m/s to 17.9 m/s. Culvert strain responses to trucks traveling at typical vehicle speeds are similar to those of a crawl pass, with two clearly distinguishable loads. Additionally, the dynamic strain for each pass is determined by taking the maximum strain.

Figure 4.7 shows a sample strain time history response taken from the same sensor shown in Figure 4.6, however trucks are traveling at approximately 13.4 m/s. As with Figure 4.6, the passes made by Truck 1 and Truck 2 in Figure 4.7 are superimposed. During testing trucks were spaced such that the culvert responded to each load individually. For the purposes of calculating the *DAF*, each individual

dynamic truck pass is considered separately from the other dynamic passes. This differs from quasi-static passes where the two maximum static strains are averaged to form the static strain.

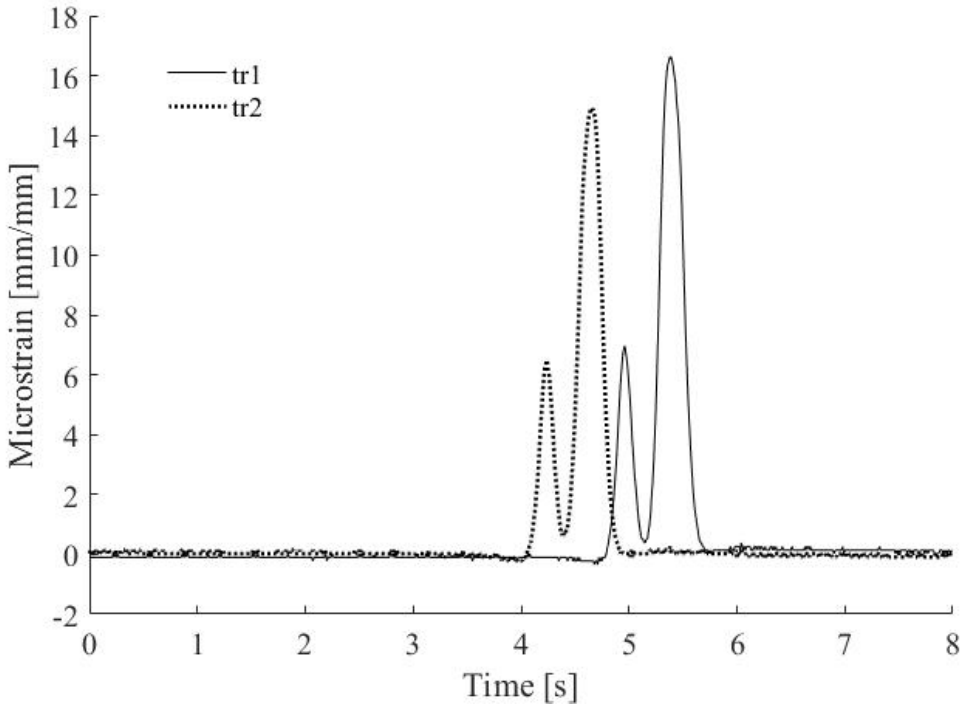

Figure 4.7 Measured Response of Culvert Due to a Dynamic Load

Figure 4.8 shows the maximum strain recorded at each sensor location for a truck driven in lane 1 of Culvert 3 for all speeds tested. The x-axis in the plot corresponds to the sensor's distance from the centerline of the roadway: lane 1 is in the negative direction and lane 3 is in the positive direction. As shown in Equation 4-1, the *DAF* is calculated for truck passes at each sensor location using the ratio of maximum dynamic strain ($\varepsilon_{Dyn,Max}$) to the static strain (ε_{Stat}).

$$DAF = \frac{\varepsilon_{Dyn,Max}}{\varepsilon_{Stat}} \qquad (4-1)$$

It should be noted that the dynamic strains recorded due to Truck 1 are only compared to the static strains due to Truck 1. Similarly, Truck 2 dynamic strains are only compared to Truck 2 static strains.

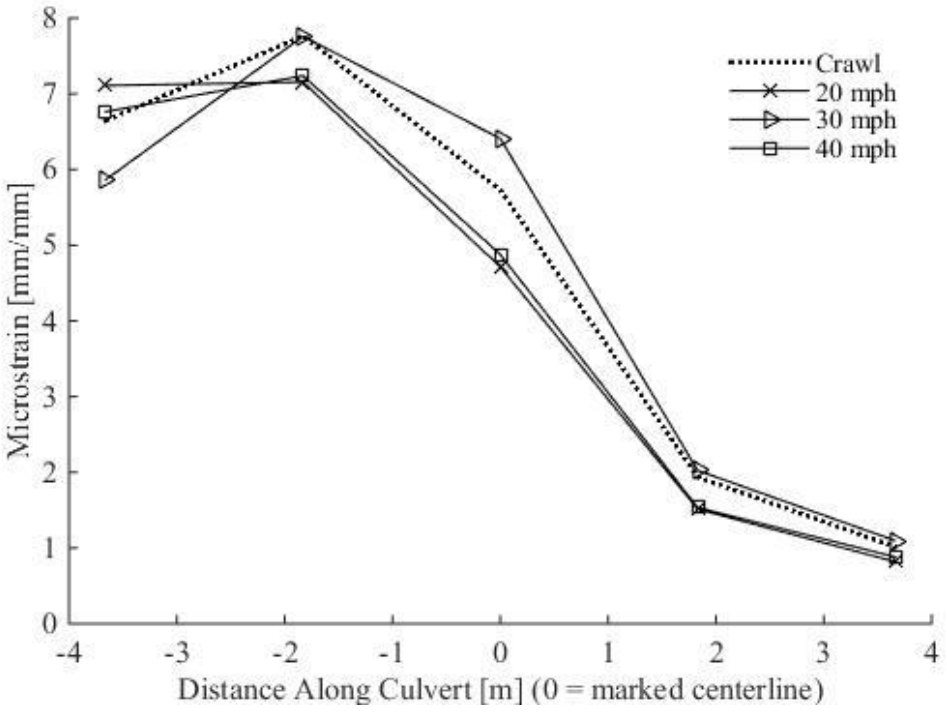

Figure 4.8 Strain Across the Culvert due to a Truck in Lane 1

4.2 Individual Field Tests

4.2.1 Culvert 1

Culvert Description

Culvert 1 carries a well-traveled local road with two lanes of traffic, one in both directions, over a small creek. The culvert is of cast-in-place construction and is skewed 10 degrees. The section is a four sided box. Figure 4.9 shows an elevation view of Culvert 1. The span is 3 m in length and 0.38 m of soil fill is present between the culvert and pavement. The pavement layer is 0.23 m thick.

Figure 4.9 Culvert 1 Elevation

Due to its cast in place construction, Culvert 1 only required sensors to be located at the center and edges of each tested lane. Since the centerline of the road serves as the center of lane 2, the right edge of lane 1 and the left edge of lane 3, five sensors are placed on the culvert. Figure 4.10 diagrams the sensor layout for Culvert 1.

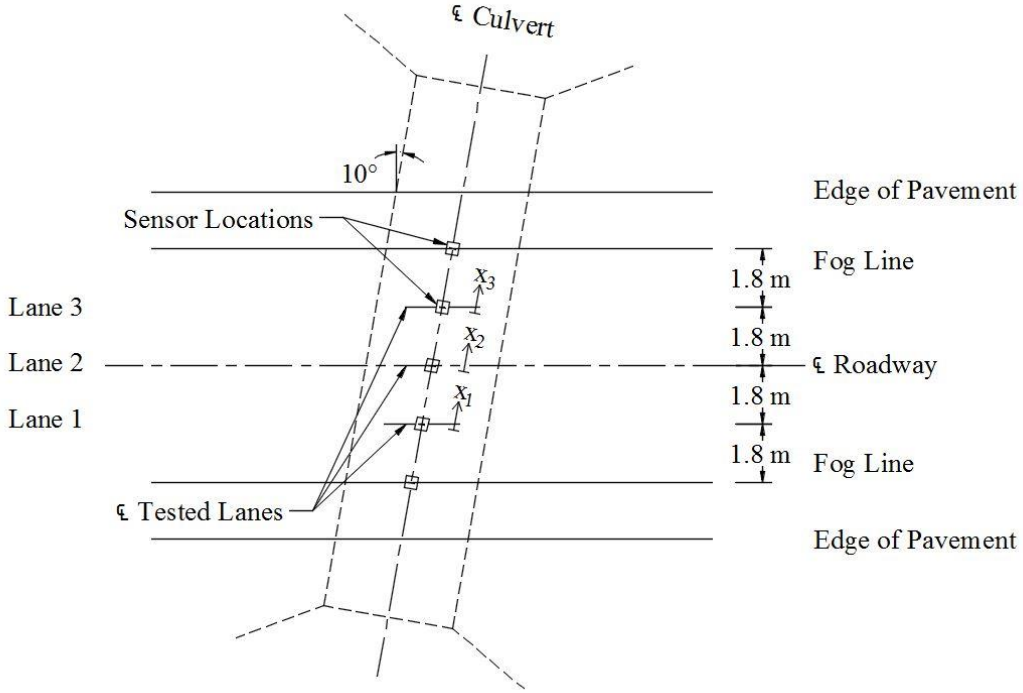

Figure 4.10 Culvert 1 Sensor Layout

Test Procedure

Culvert 1 was tested first. Two static passes were conducted in each tested lane and one dynamic pass was made in each lane at a vehicle speed of 13.4 m/s. Two

additional passes were made in lane 2, one at 8.9 m/s and another at 17.9 m/s. Thus, five dynamic passes were completed by each truck.

Test Results

As a result of the five passes made by each truck (10 passes combined) and the five sensors placed on the culvert, 50 different *DAF* values were calculated during the testing of Culvert 1. The *DAF* has been calculated for all readings, regardless of the strain magnitude. The maximum *DAF* calculated for all three tested lanes is 1.37, the average *DAF* is 0.97 and the standard deviation of results is 0.14. Figure 4.11 shows *DAF* values observed at all sensors used during testing. Sensor locations are reported relative to the center of the roadway, using x_2 in Figure 4.10 as the origin. Therefore, the center of lane 1 is located at -1.8 m, the center of lane 2 is located at 0 m, and the center of lane 3 is the located at 1.8 m. All but three *DAF* values (six percent) fall within two standard deviations of the average and all *DAF* values are within three standard deviations. Additionally, 68 percent of *DAF* values are less than one.

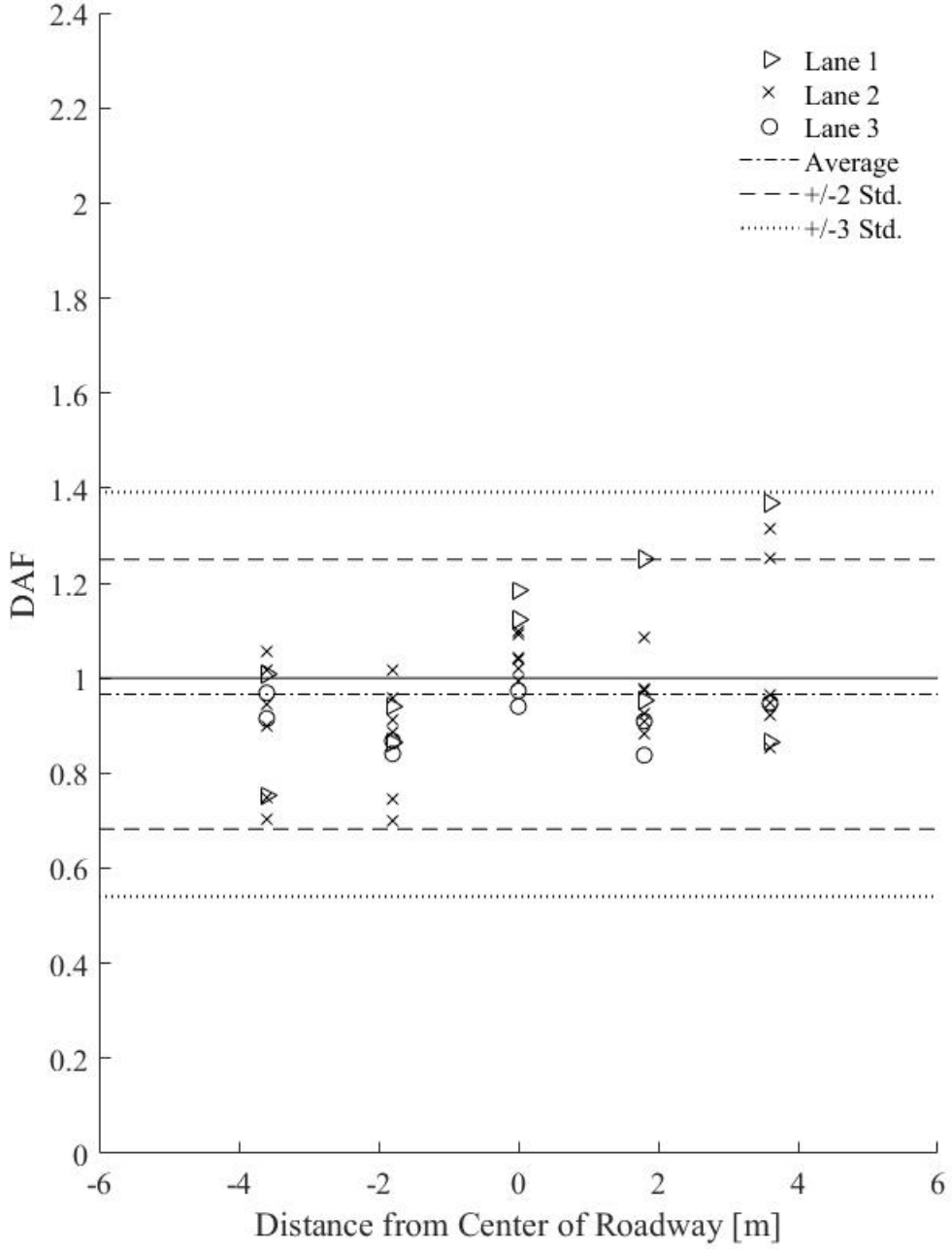

Figure 4.11 Culvert 1 Results Reported Relative to the Center of the Roadway (Center of Lane 2)

Figure 4.12 shows the *DAF* calculated at each sensor location, where the sensor's position is reported in relation to the center of the tested lane. The positive x-direction is shown for each lane in Figure 4.10; x_1 is the origin for lane 1, x_2 is the origin for lane 2 and x_3 is the origin for lane 3. When examining the results for Truck 2 at 8.9 and 17.9 m/s it can be seen that *DAF* is larger in the positive direction and lower in the negative direction. This may be the result the truck driving slightly right of center in the tested lane. If a truck is located slightly to the right or left of center, the dynamic strain will be increased in the direction of the shift and decreased in the opposite direction. Subsequently, *DAF* will be larger in the direction of the shift and lower in the opposite direction.

Additionally, these affects have a much greater impact on sensors that initially record low strains because the increase or decrease in strain magnitude is a larger percentage of the static strain. It can be seen that *DAF* values towards the center of the tested lane generally show less variability and are closer to the average. The fact that sensors toward the center of the tested lane record higher static strains is likely the reason for this disparity in *DAF* values. After testing Culvert 1, it was determined that more passes should be performed in each lane and that more passes should be conducted at higher and lower vehicle speeds.

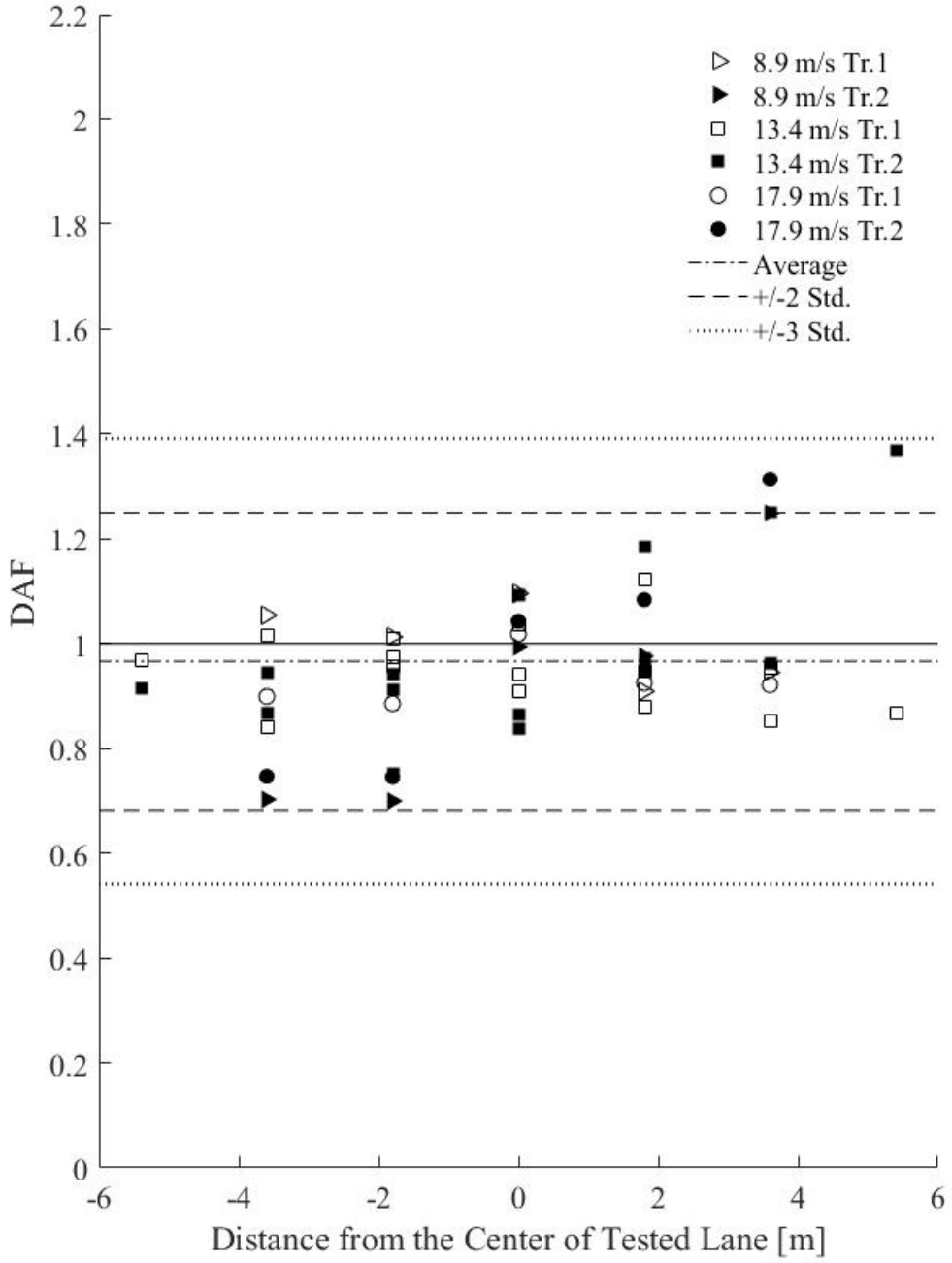

Figure 4.12 Culvert 1 Results Reported Relative to the Center of the Tested Lane

4.2.2 **Culvert 2**

Culvert Description

Culvert 2 carries a local road with two lanes of traffic, one in both directions, over a golf cart path. The culvert is constructed of 8 precast box sections that range in width from 1.22 m to 1.83 m. The sections are post-tensioned together using an effective force of 68.9 kPa across the culvert cross section. Figure 4.13 shows an elevation view of Culvert 2. The span is 4.25 m long and has 0.8 m of soil fill cover. The pavement layer is 0.15 m thick. It is also worth noting that the roadway is slightly curved over the culvert.

Figure 4.13 Culvert 2 Elevation

Similar to Culvert 1, sensors were located at the center and edges of each tested lane. Because Culvert 2 is constructed of precast box sections additional sensors were required. As shown in Figure 4.14, additional sensors are offset 0.5 m from the sensors at the center of lane 1, lane 2, and lane 3. This was done because those three sensors were near the edge of box sections. In total, eight sensors were used to test Culvert 2.

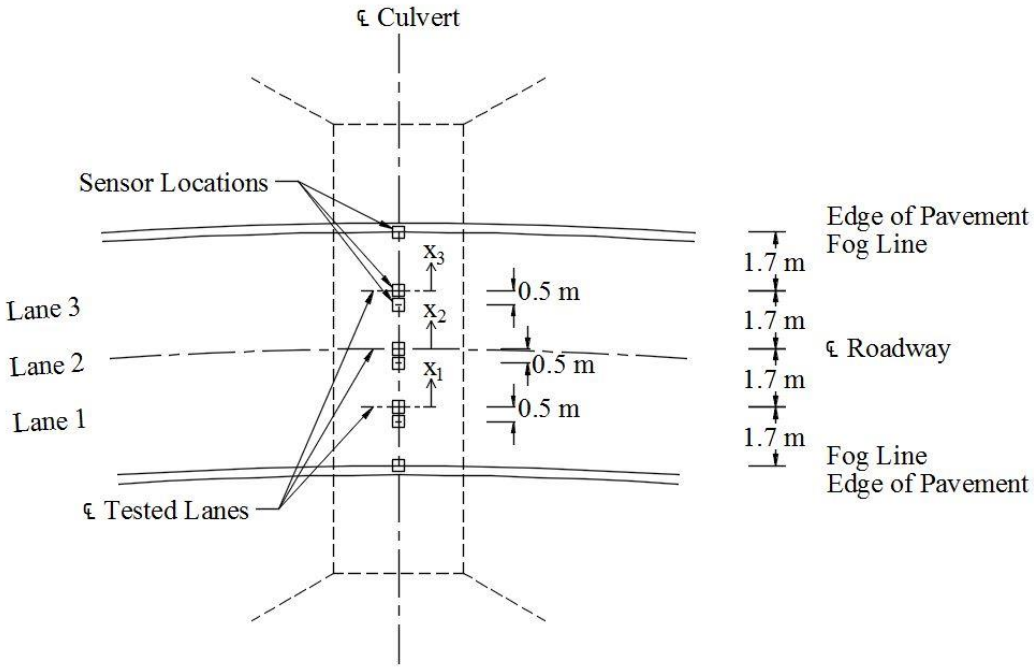

Figure 4.14 Culvert 2 Sensor Layout

Test Procedure

When testing Culvert 2, two static passes were made in each tested lane. Additionally, six dynamic passes were made in each lane. Dynamic passes include

two passes at 8.9 m/s, two passes at 13.4 m/s and two passes at 17.9 m/s. Truck 2 broke down during testing and could not complete one pass in lane 3 at 17.9 m/s and did not complete any passes at 8.9 m/s. As a result, Truck 1 completed 18 passes and Truck 2 only completed 11.

Test Results

Due to the 29 combined truck passes and eight sensors, 232 *DAF* values were calculated for Culvert 2. The *DAF* has been calculated for all readings, regardless of the strain magnitude. The maximum *DAF* calculated for all three tested lanes is 2.13, the average *DAF* is 0.99 and the standard deviation of results is 0.22. Figure 4.15 shows *DAF* values observed at all sensors used during testing. Sensor locations are reported relative to the center of the roadway, using x_2 in Figure 4.14 as the origin. Therefore, the center of lane 1 is located at -1.7 m, the center of lane 2 is located at 0 m, and the center of lane 3 is the located at 1.7 m. Four percent of values are greater than two standard deviations from the average and two percent of values are greater than three standard deviations from the average. Some of this variability may be due to incomplete load transfer between precast box sections. However, it is possible that the curvature in the road is significantly affecting results. As the truck approaches the culvert, angular momentum may cause the truck load to shift from the center of the axles towards the outside of the curve. Since centripetal force is a function of the squared velocity, it would make sense that dynamic strains are influenced more by this effect than static strains, thus altering the *DAF*.

With the exception of the sensor located at -3.4 m (the fog line of lane 1) *DAF* appears to be larger in the positive direction than in the negative direction. If the load were more dramatically shifted from the center of the axles towards the outside of the

curve during dynamic passes, higher dynamic strains would occur in sensors towards the outside of the curve (in the positive direction) and lower dynamic strains would occur in sensors towards the inside of the curve (in the negative direction). Though these affects may be small, they would have a much greater impact on sensors that initially record low strains (i.e. farther from the load application) because the increase or decrease in strain is a larger percentage of the static strain. In Figure 4.15, it can be seen that the highest *DAF* values are recorded at sensors farthest in the positive direction while the trucks are in lane 1. Additionally, some of the lowest *DAF* values are recorded at sensors in the negative direction for trucks in lane 3. These results support this hypothesis.

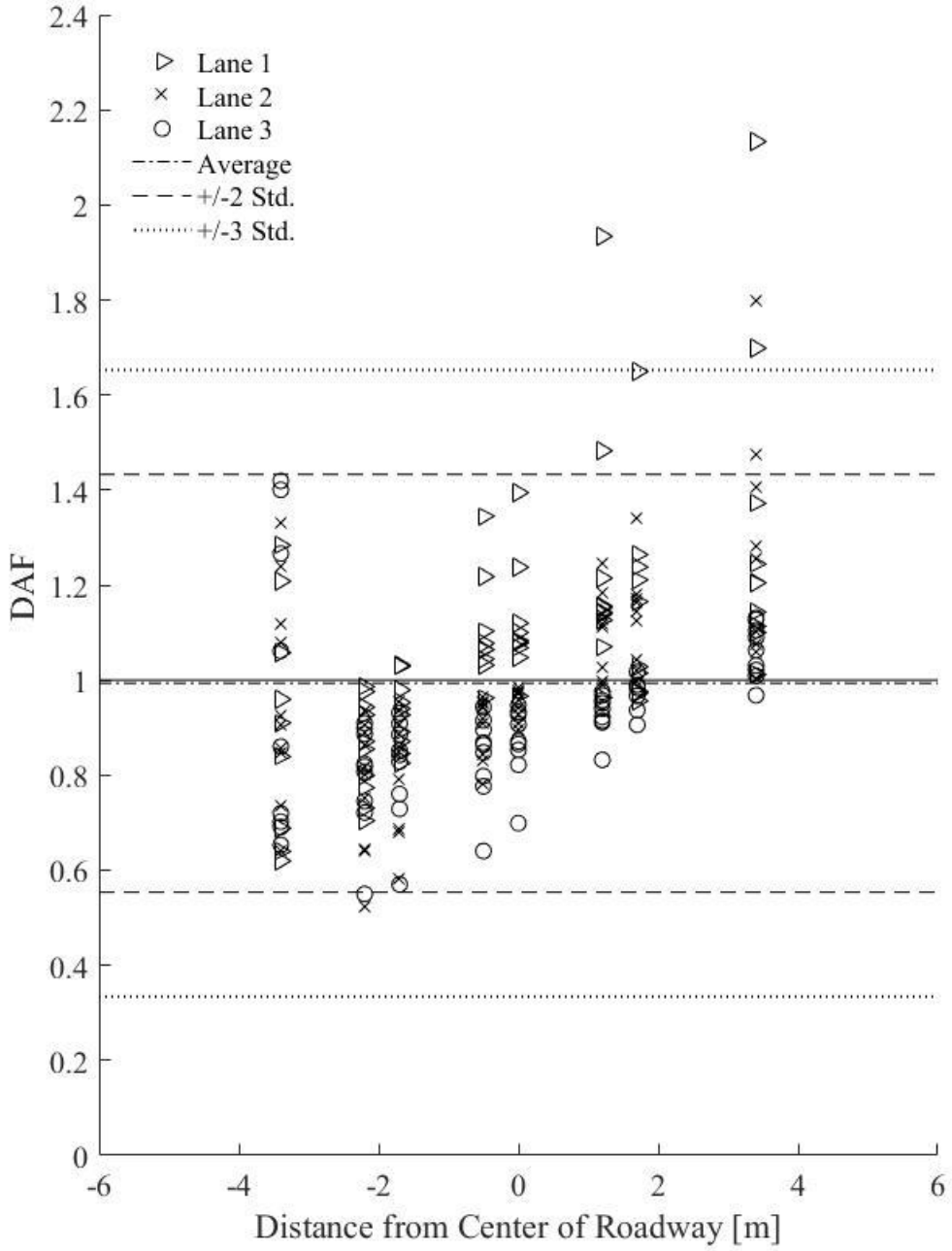

Figure 4.15 Culvert 2 Results Reported Relative to the Center of the Roadway (Center of Lane 2)

Figure 4.16 shows the *DAF* calculated at each sensor location, where the sensor's position is reported in relation to the center of the tested lane. The positive x-direction for each lane is shown in Figure 4.14; x_1 is the origin for lane 1, x_2 is the origin for lane 2 and x_3 is the origin for lane 3. As can be seen in both Figure 4.15 and Figure 4.16, a significant amount of variability exists in the results for this test. Particularly, the range of *DAF* values is 1.61, which is larger than the average *DAF*. However, it should be recognized that values calculated at the center of the tested lane and at -0.5 m generally have *DAF* values between approximately the average and one standard deviation below the average. Results at these locations also show significantly less variability than other locations.

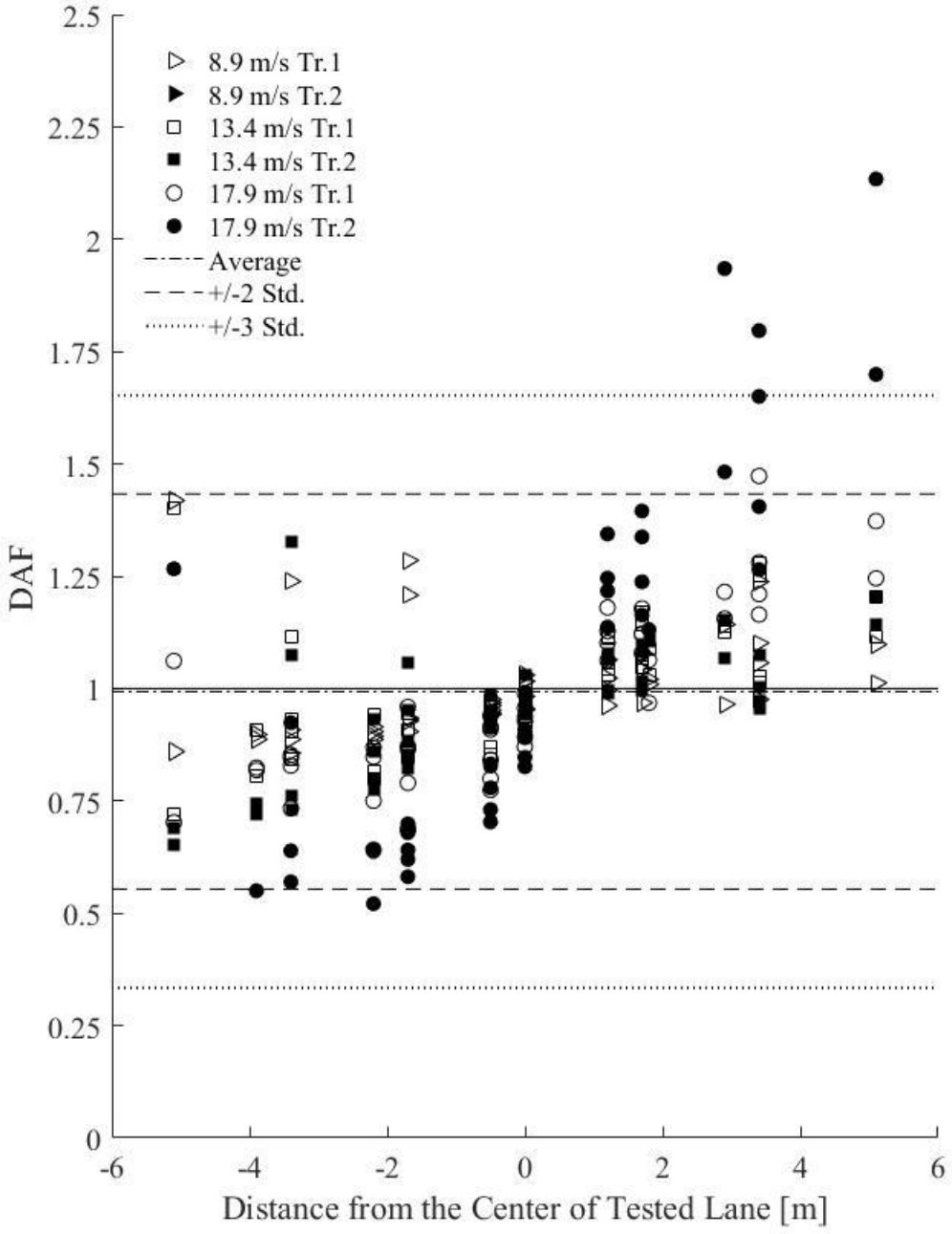

Figure 4.16 Culvert 2 Results Reported Relative to the Center of the Tested Lane

4.2.3 **Culvert 3**

Culvert Description

Culvert 3 carries a highly traveled state route with four lanes of travel, two in both directions, separated by a 5.5 m median. The culvert crosses a creek that is 5.5 m wide. Only lanes in one direction are tested. Figure 4.17 shows an elevation view of Culvert 3. The culvert is a cast-in-place, three-sided box section with a span length of 5.5 m. A layer soil fill 0.41 m thick is present between the culvert slab and bottom of pavement. The pavement layer is 0.2 m thick.

Due to its cast in place construction, Culvert 3 only required sensors to be located at the center and edges of each tested lane. As such only five strain transducers were used. Figure 4.18 shows the sensor layout for Culvert 3.

Figure 4.17 Culvert 3 Elevation

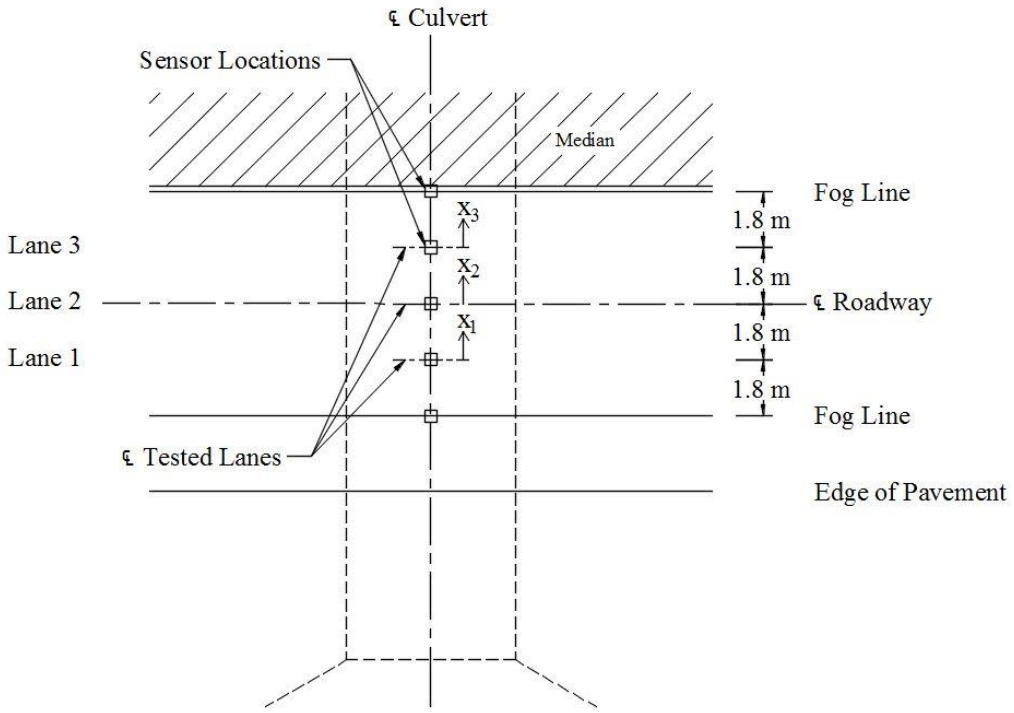

Figure 4.18 Culvert 3 Sensor Layout

Test Procedure

When testing Culvert 3, two static passes and six dynamic passes were made in each tested lane. Dynamic passes include two passes at 8.9 m/s, two passes at 13.4 m/s and two passes at 17.9 m/s. In total, 18 dynamic passes were completed by each truck for Culvert 3.

Test Results

As a result of the 18 passes made by each truck and the five sensors used, 180 individual values of *DAF* were calculated for Culvert 3. The *DAF* has been calculated for all readings, regardless of the strain magnitude. The maximum *DAF* calculated for all three tested lanes was 1.24, the average was 0.94, and the standard deviation was

0.12. Figure 4.19 shows *DAF* values observed at all sensors used during testing. Sensor locations are reported relative to the center of the roadway, using x_2 in Figure 4.18 as the origin. Therefore, the center of lane 1 is located at -1.8 m, the center of lane 2 is located at 0 m, and the center of lane 3 is the located at 1.8 m. Of the 180 *DAF* values calculated, one percent are greater than three standard deviations from the average and six percent are more than two standard deviations from the average.

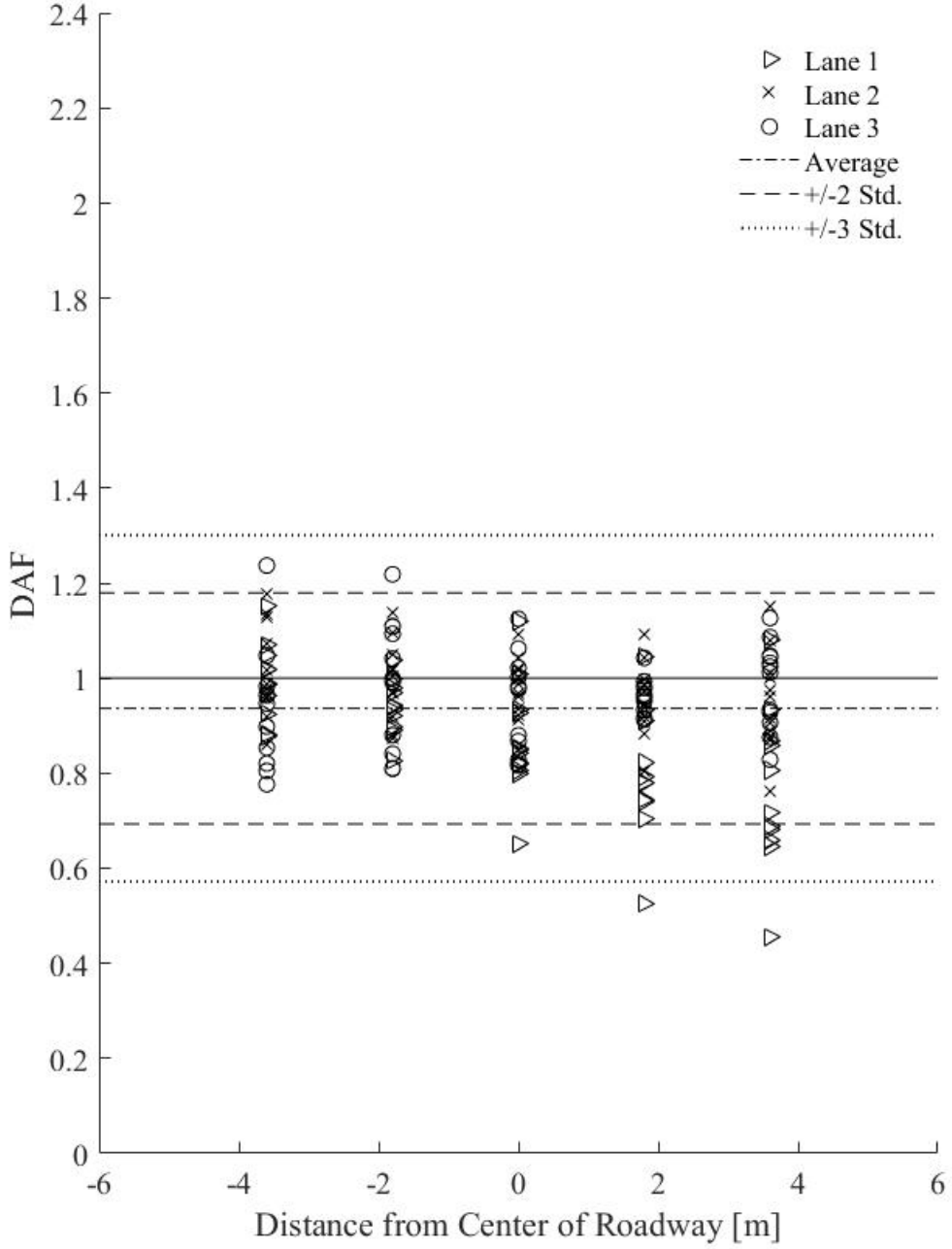

Figure 4.19 Culvert 3 Results Reported Relative to the Center of the Roadway (Center of Lane 2)

Figure 4.20 shows the *DAF* calculated at each sensor location, where the sensor's position is reported in relation to the center of the tested lane. The positive x-direction for each lane is shown in Figure 4.18; x_1 is the origin for lane 1, x_2 is the origin for lane 2 and x_3 is the origin for lane 3. It can be seen that sensors in the positive direction report several low *DAF* values for Truck 1 at 17.9 m/s and sensors to the left report several high *DAF* values for Truck 1 at 17.9 m/s. This may be the result of the truck being located slightly in the negative direction. As with other culverts, the least amount of variability occurs at the center of the tested lane.

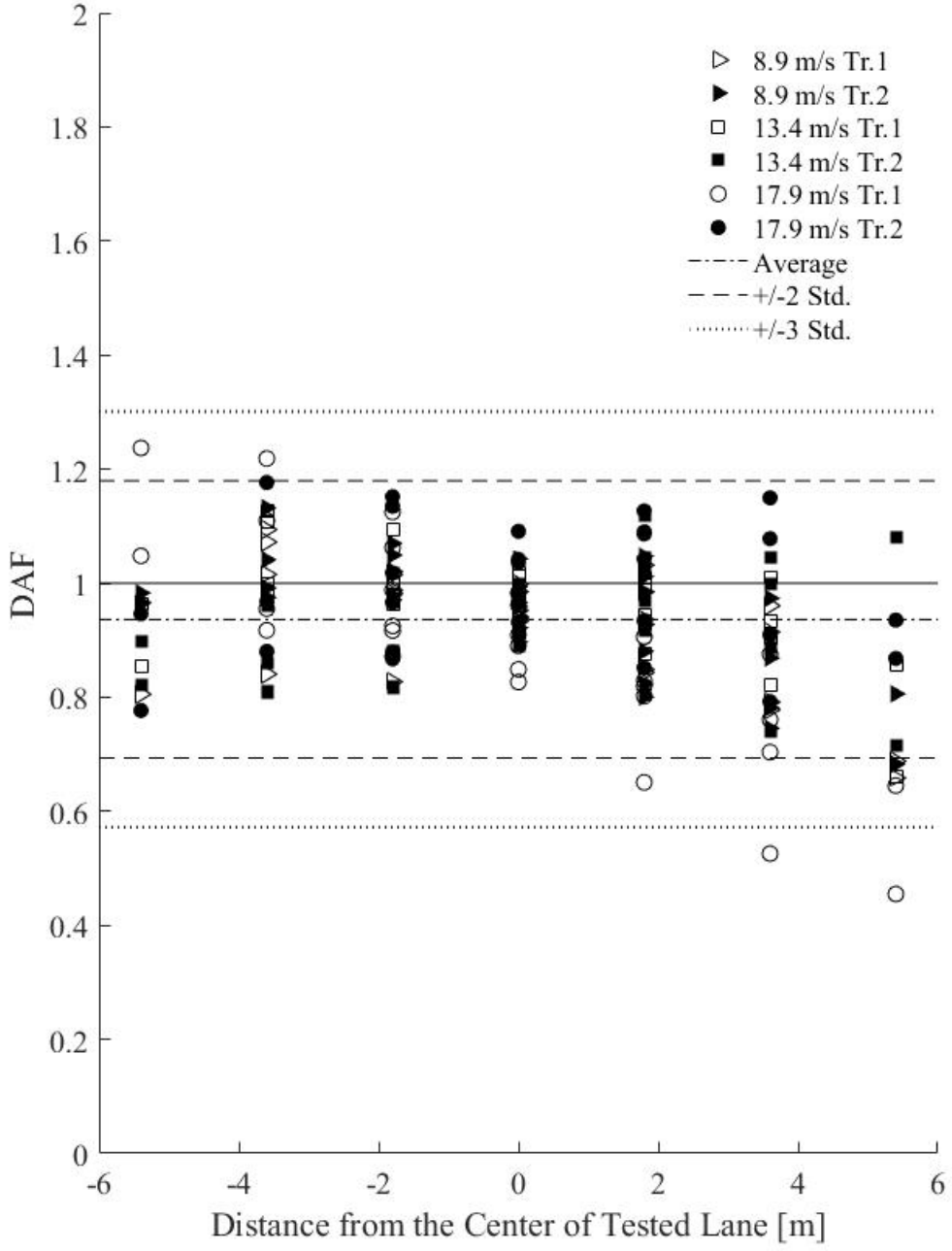

Figure 4.20 Culvert 3 Results Reported Relative to the Center of the Tested Lane

4.2.4 **Culvert 4**

Culvert Description

Culvert 4 carries a two lane (one in each direction) state route over a stream. The culvert is constructed of 8 precast, three sided box sections, which are 1.37 m wide. The sections are tied together using four 5.5 m tie rods. The culvert is skewed nine degrees. Figure 4.21 shows a picture of Culvert 4. The span length is 7.7 m. While no soil fill is present between the culvert and the pavement, a 0.3 m layer of bituminous concrete base course exists in addition to the 0.14 m thick layer of asphalt pavement.

Figure 4.21 Culvert 4 Elevation

Sensors on the right edge of lane 1, center of lane 3, and right edge of lane 3 are near the edge of box sections. As a result, additional sensors are offset 0.4, 0.6 and 0.9 m, respectfully, from those three sensors. Additionally, three of the eight sensors were offset 0.3 m from the center line of the culvert due to surface cracks in the concrete. The sensor layout can be seen in Figure 4.22.

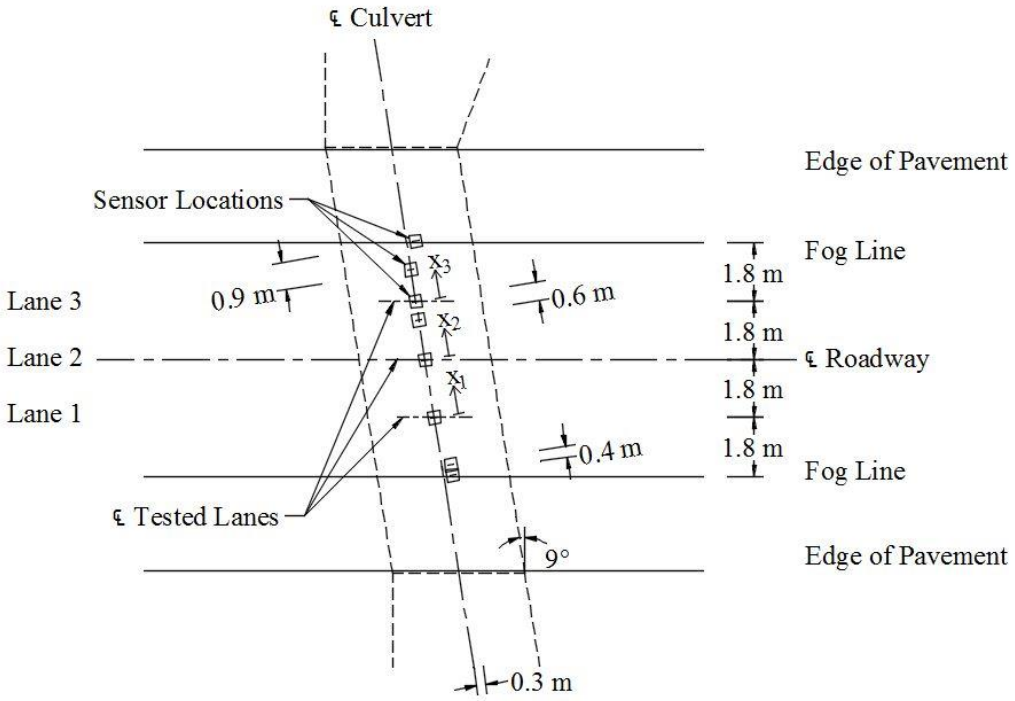

Figure 4.22 Culvert 4 Sensor Layout

Test Procedure

When testing Culvert 4, two static passes were made in each tested lane. Additionally, six dynamic passes were made in each of the three tested lanes. Dynamic passes include two passes at 8.9 m/s, two passes at 13.4 m/s and two passes

at 17.9 m/s. In total, 18 dynamic passes were completed by both trucks during the testing of Culvert 4.

Test Results

As a result of the 18 dynamic passes made by each truck and the eight sensors placed on the culvert, 288 values of *DAF* were calculated for Culvert 4. The *DAF* has been calculated for all readings, regardless of the strain magnitude. The maximum *DAF* value was 1.51, the average was 1.00 and the standard deviation was 0.17. Figure 4.23 shows *DAF* values observed at all sensors used during testing. Sensor locations are reported relative to the center of the roadway, using x_2 in Figure 4.22 as the origin. Therefore, the center of lane 1 is located at -1.8 m, the center of lane 2 is located at 0 m, and the center of lane 3 is the located at 1.8 m. Less than one percent of values calculated were in excess of three standard deviations from the average and seven percent exceeded two standard deviations from the average.

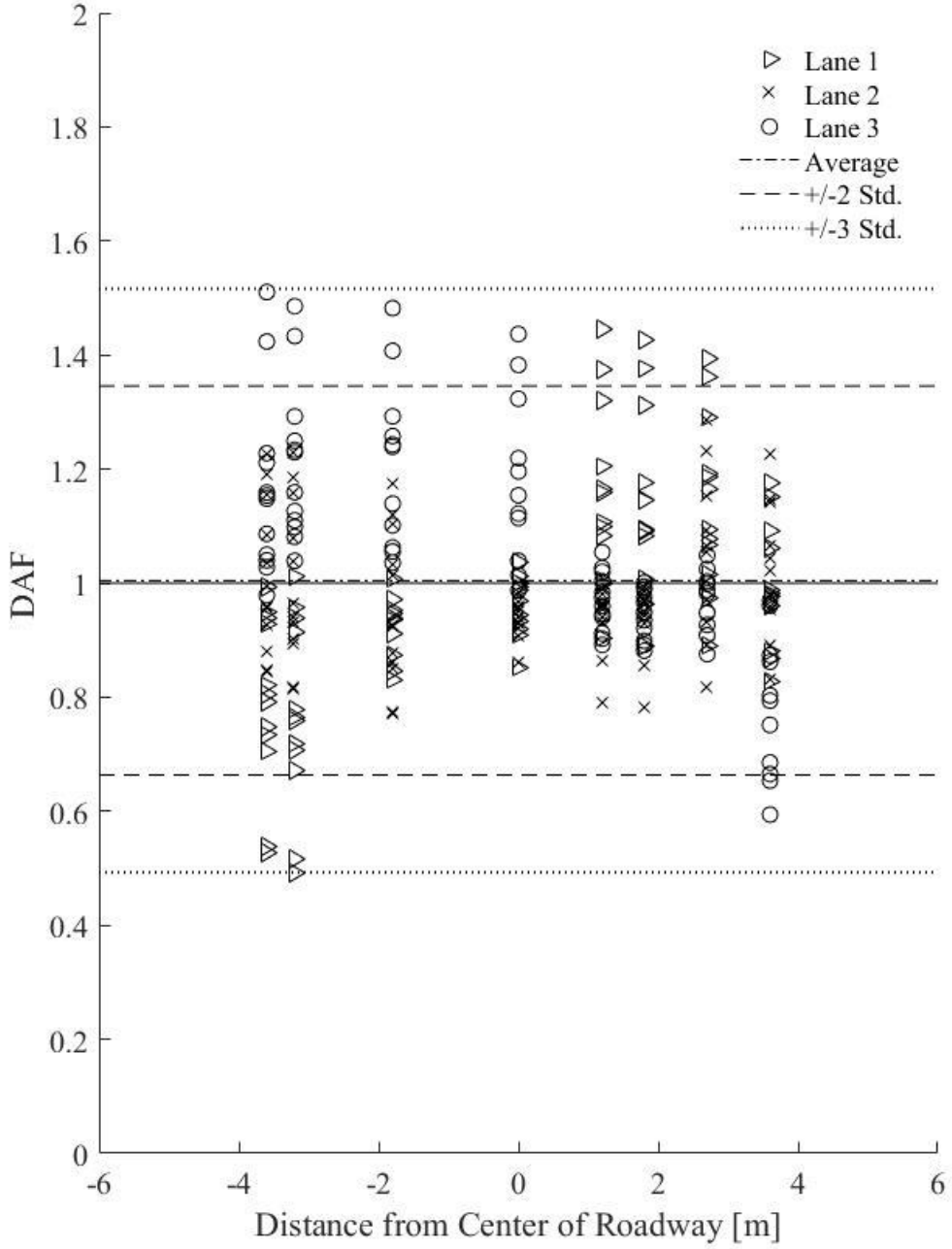

Figure 4.23 Culvert 4 Results Reported Relative to the Center of the Roadway (Center of Lane 2)

Figure 4.24 shows the *DAF* calculated at each sensor location, where the sensor's position is reported in relation to the center of the tested lane. The positive x-direction for each lane is shown in Figure 4.22; x_1 is the origin for lane 1, x_2 is the origin for lane 2 and x_3 is the origin for lane 3. As with other tests, significant variability exists in *DAF*, however, as discussed, data points are much more clustered near the center of the tested lane. Additionally, the values at these locations tend to be close to or below the average *DAF*. This is particularly dramatic in this test. It should be noted that Culvert 4 is a segmental box culvert. As a result, it is possible that the dramatic change in *DAF* at approximately +/- 2 m is due to incomplete load transfer between precast box sections.

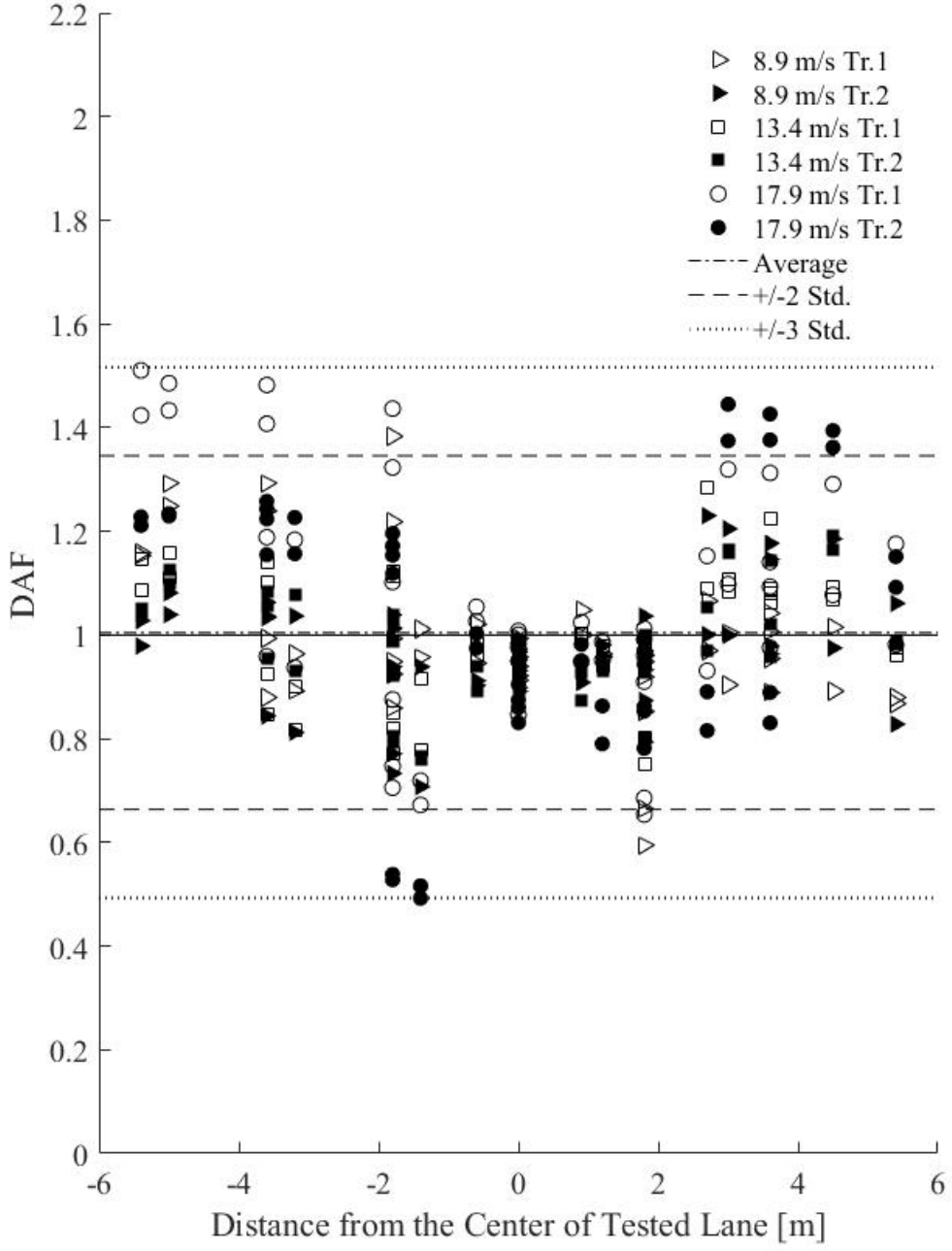

Figure 4.24 Culvert 4 Results Reported Relative to the Center of the Tested Lane

4.2.5 **Culvert 5**

Culvert Description

Culvert 5 carries a highly traveled local road with two lanes of travel over a small creek. Figure 4.25 shows an elevation view of Culvert 5. The culvert is constructed of 12, 1.28 m wide, three-sided precast box sections that are tied together using four 7.7 m tie rods. Additionally, a 0.4 m concrete parapet exists on top of the culvert slab. The span length is 6.4 m and no fill is present between the parapet and pavement. The pavement layer is 0.07 m thick. As shown in Figure 4.26, additional sensors are offset 0.3 and 0.6 m from the center of lane 1 and lane 2, respectively, because those locations are near the edge of precast sections. In total, seven strain transducers were used to test Culvert 5.

Figure 4.25 Culvert 5 Elevation

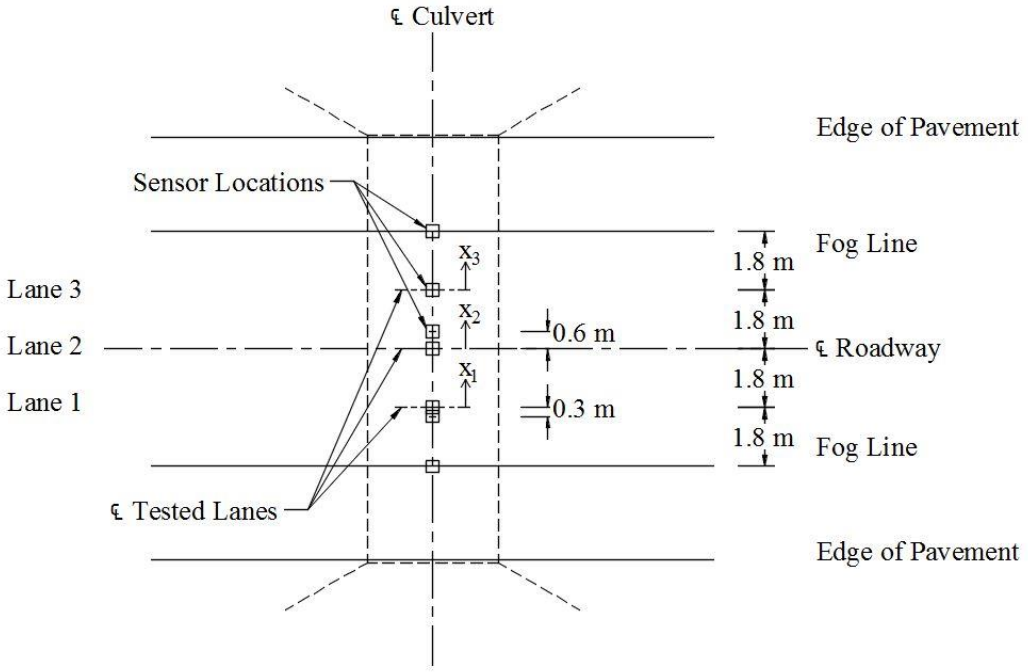

Figure 4.26 Culvert 5 Sensor Layout

Test Procedure

When testing Culvert 5, two static passes and six dynamic pass were made in each lane. Dynamic passes include two passes at 8.9 m/s, two passes at 13.4 m/s and two passes at 17.9 m/s. An error occurred in the data acquisition software during the first dynamic pass in lane 1 at 8.9 m/s. Consequently, no data was recorded for this pass. In total, 17 dynamic passes were completed by both trucks.

Test Results

Due to the 34 combined truck passes and seven sensors, 238 *DAF* values were calculated for Culvert 5. The *DAF* has been calculated for all readings, regardless of the strain magnitude. The maximum *DAF* calculated is 1.25, the average *DAF* is 0.96

and the standard deviation of results is 0.09. The standard deviation of results for Culvert 5 is significantly less than other precast box sections. This may be due to the cast-in-place parapet which allows for a more even distribution of load along the width of the roadway.

Figure 4.27 shows *DAF* values observed at all sensors used during testing. Sensor locations are reported relative to the center of the roadway, using x_2 in Figure 4.26 as the origin. Therefore, the center of lane 1 is located at -1.8 m, the center of lane 2 is located at 0 m, and the center of lane 3 is the located at 1.8 m. Only two *DAF* values (less than 1 percent) were greater than three standard deviations from the average. Six percent of values are greater than two standard deviations from the average.

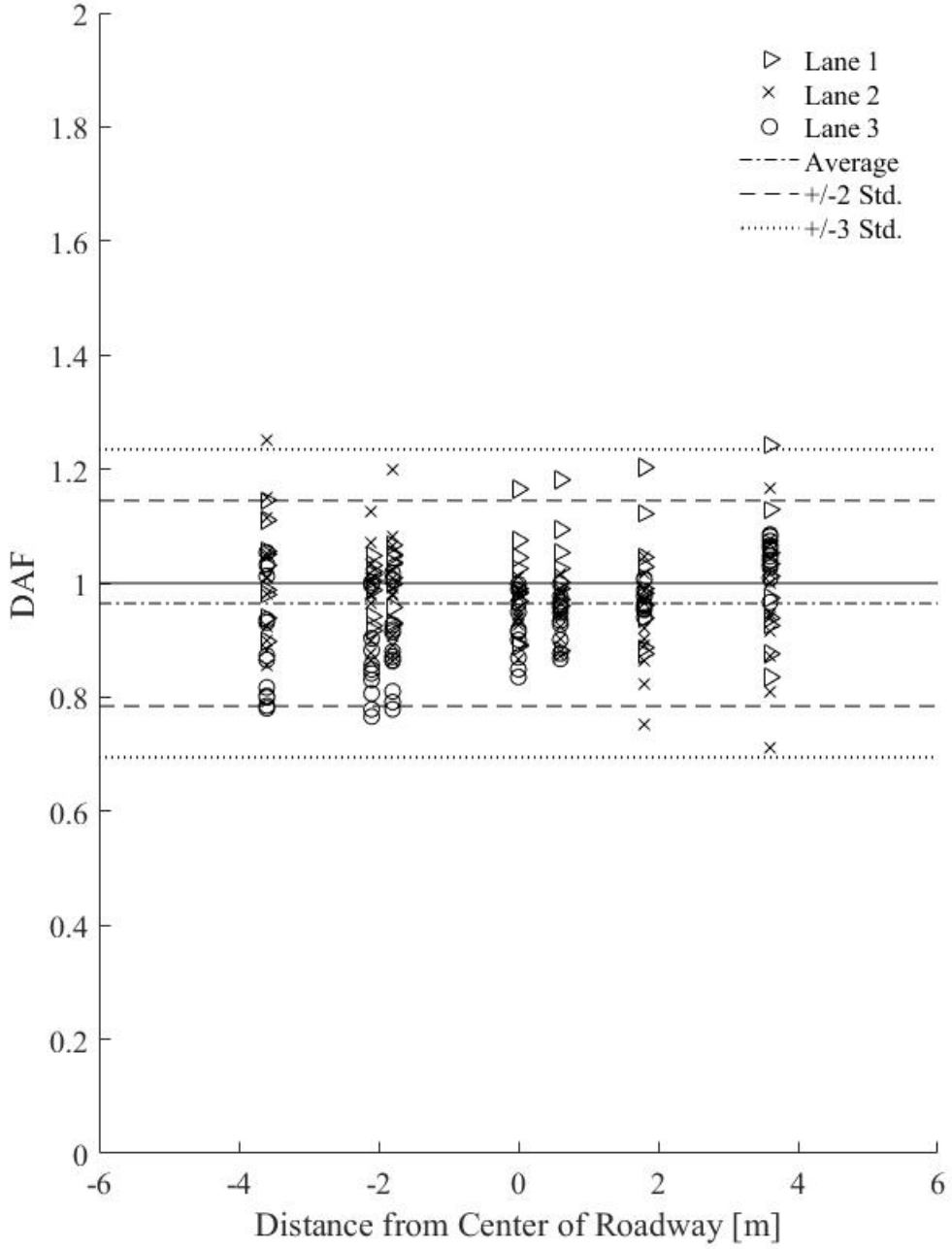

Figure 4.27 Culvert 5 Results Reported Relative to the Center of the Roadway (Center of Lane 2)

Figure 4.28 shows the *DAF* calculated at each sensor location, where the sensor's position is reported in relation to the center of the tested lane. The positive x-direction for each lane is shown in Figure 4.26; x_1 is the origin for lane 1, x_2 is the origin for lane 2 and x_3 is the origin for lane 3. The least amount of variation occurred between -1.2 and 0.6 m from the center of the tested lane.

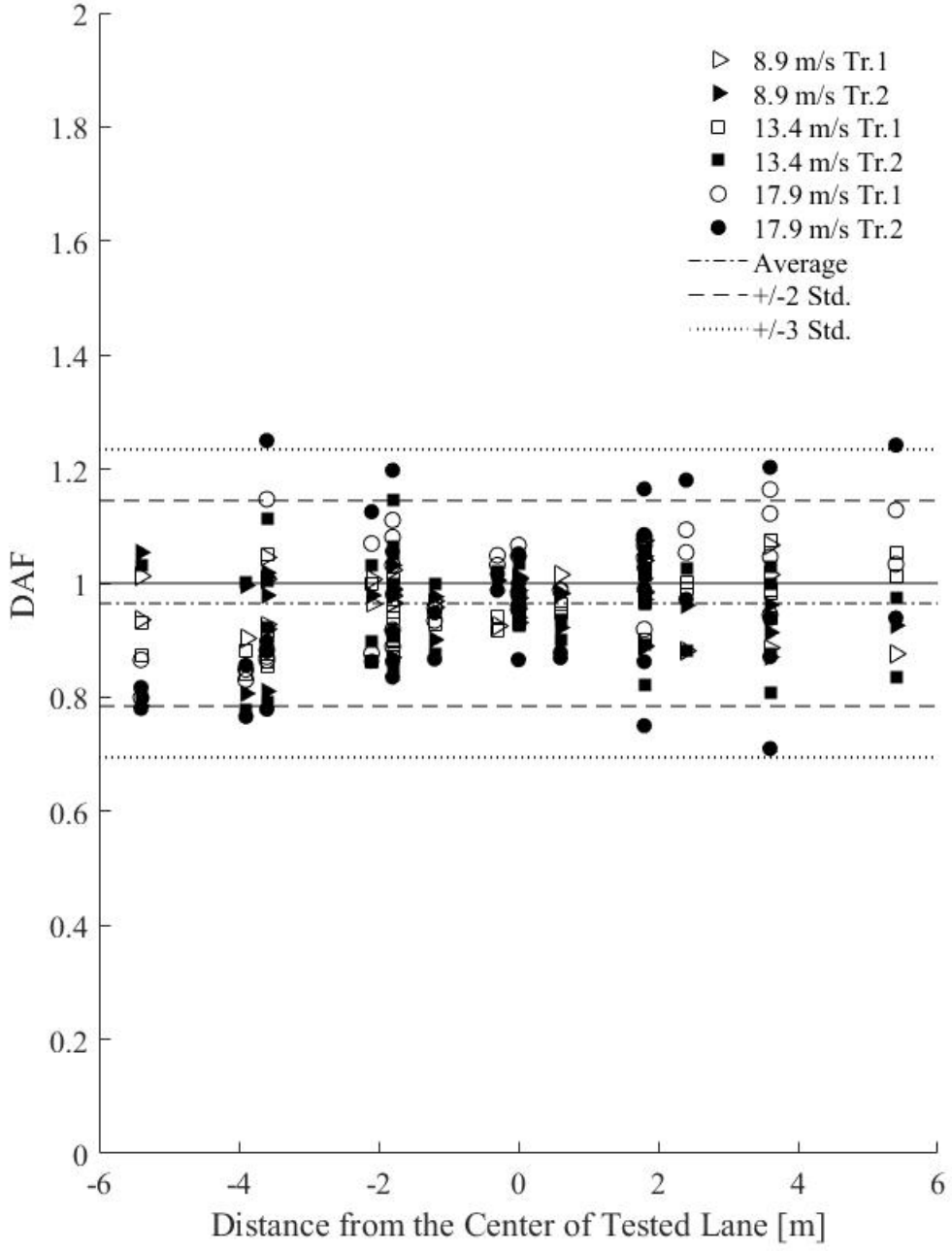

Figure 4.28 Culvert 5 Results Reported Relative to the Center of the Tested Lane

4.3 Combined Field Test Results

Over the course of this study, five culverts in the state of Delaware were tested. For each culvert, the roadway was broken into three tested lanes that were subject to quasi-static and dynamic truck loads. In total, 42 individual truck passes were completed at 8.9 m/s, 54 passes were completed at 13.4 m/s and 49 passes were completed at 17.9 m/s for a total of 145 dynamic passes. Culverts were instrumented with strain transduces at various points of interest and the *DAF* is calculated at each sensor location as a ratio of the dynamic strain to the static strain.

Table 4.5 shows the average, maximum, standard deviation, the average plus two standard deviations and the average plus three standard deviations of *DAF* values calculated at all sensor locations during each test. In the previous sections, results were reported for all *DAF* values regardless of the recorded strains used to calculate them. One observation made was that lower strains, or those further from the center of the tested land, tended to have more variability. This is because small variations in recorded strain due to ambient vibrations, a slight shift in truck location (i.e. the truck is not exactly in the center of the tested lane) or improper load transfer through joints can have large impacts on the *DAF* calculated at lower strain levels. Additionally, the *DAF* at higher strain levels is of more consequence because these areas are the most highly loaded and are the areas that control the load rating of the culvert. For this reason, Table 4.5 also shows the average, maximum, standard deviation, average plus two standard deviations and the average plus three standard deviations of *DAF* values that meet a minimum strain threshold for the static strain; the minimum strain threshold is shown in the second column of the table, listed under “Threshold Strain”. If the average of the two quasi-static strain readings recorded by a sensor is below the strain threshold indicated, *DAF* values recorded at that sensor are not included in the

calculation of the statistics. The number of "measurements" (or number of *DAF* values) used to calculate statistics are also indicated. All results reported in previous sections are listed in the rows labeled "No Limit" of Table 4.5.

It can be seen that increasing the threshold strain decreases the maximum *DAF* and decreases the standard deviation (i.e. decreases the overall variability of the results). The average *DAF* for all strain thresholds is less than or equal to one. By enforcing a minimum strain threshold of only 5 microstrain the maximum *DAF* for the five tests decreases by 0.23 on average and the standard deviation decreases by 0.03 on average.

It is also worth noting the decrease in the number of measurements as a result of increasing the minimum strain threshold. Culvert 1 and Culvert 3 see almost a 50 percent decrease in the number of measurements by imposing a strain threshold of only five microstrain. The number of measurements used for Culvert 2, Culvert 4 and Culvert 5 are reduced by 82, 69 and 71 percent, respectively, when a 20 microstrain threshold is enforced. At the same time, the maximum *DAF* for the five tests decreases by 14, seven, 48, 30 and 16 percent, respectively, when those same limitations are enforced.

Table 4.5 *DAF* Results Restricted by a Minimum Strain Threshold

Culvert	Threshold Strain (με)	Avg. DAF	Max DAF	Std. Dev.	Avg. +2 Std.	Avg. +3 Std.	No. of Measure-ments
1	No Limit	0.97	1.37	0.14	1.25	1.39	50
	5	0.96	1.18	0.11	1.18	1.30	28
	10	0.90	0.94	0.05	1.01	1.06	2
	15	-	-	-	-	-	0
	20	-	-	-	-	-	0
2	No Limit	0.99	2.13	0.22	1.43	1.65	232
	5	0.95	1.40	0.15	1.25	1.39	160
	10	0.93	1.34	0.13	1.20	1.34	122
	15	0.93	1.34	0.12	1.17	1.29	79
	20	0.93	1.10	0.08	1.10	1.18	41
3	No Limit	0.94	1.24	0.12	1.18	1.30	180
	5	0.96	1.15	0.09	1.13	1.22	96
	10	-	-	-	-	-	0
	15	-	-	-	-	-	0
	20	-	-	-	-	-	0
4	No Limit	1.00	1.51	0.17	1.35	1.52	288
	5	0.96	1.45	0.16	1.28	1.44	204
	10	0.93	1.44	0.14	1.20	1.34	156
	15	0.93	1.05	0.09	1.11	1.20	108
	20	0.95	1.05	0.05	1.05	1.09	90
5	No Limit	0.96	1.25	0.09	1.14	1.23	238
	5	0.96	1.20	0.08	1.13	1.21	194
	10	0.98	1.20	0.07	1.11	1.18	136
	15	0.97	1.20	0.07	1.11	1.17	98
	20	0.99	1.20	0.06	1.12	1.18	68

Table 4.6 shows the same fields described in Table 4.5, however values are only calculated based on the sensor that recorded the maximum static strain in each pass. As discussed, this is done to minimize the effect of small variations between passes and report the *DAF* at the most critical points in the culvert cross-section. As can be seen, the maximum *DAF* values in Table 4.6 are less than or equal to those calculated in Table 4.5 for the largest strain threshold with the exception of Culvert 1. This is because only one of the five passes made by each truck (two total) during the testing of Culvert 1 recorded static strains in excess of 10 microstrain.

Table 4.6 Results Calculated Using only the Location of Maximum Stain in Each Pass

Culvert	Avg. *DAF*	Max *DAF*	Std. Dev	Avg. +2 Std.	Avg. +3 Std.	No. of Measurements
1	0.98	1.10	0.09	1.17	1.26	10
2	0.92	1.03	0.06	1.04	1.10	29
3	0.97	1.13	0.07	1.11	1.19	36
4	0.96	1.05	0.05	1.05	1.10	36
5	1.01	1.20	0.07	1.15	1.22	34
All Culverts	0.97	1.20	0.07	1.11	1.18	145

4.4 Individual Parameters

Each culvert tested has a unique fill depth, span length, slab thickness, and asphalt pavement thickness. The following sections will examine the influence of those four geometric properties on the *DAF*. Results are discussed in terms of the trends of the maximum, average, and average plus two standard deviations of *DAF* values calculated at the location of maximum recorded static strain in each lane (Table 4.6). Assuming the data is normally distributed, the average plus two standard

deviations captures 97.5 percent of possible *DAF* values. For this research, 2.5 percent is deemed an acceptable level of exceedance. Trend lines of the maximum, average and average plus two standard deviations are determined using the values recorded in Table 4.6 and the geometric properties outlined for each culvert in Table 4.2.

4.4.1 Fill Depth

Figure 4.29 shows the *DAF* values calculated for each culvert as a function of fill depth. Based on the linear fit, the *DAF* tends to decrease as fill depth increases. The slope of the linear fit lines to the average, maximum and average plus two standard deviations is -0.081, -0.11 and -0.024 1/m, respectively. It should be noted that the slope obtained using the maximum *DAF* for each culvert is over four times larger than that obtained using the average plus two standard deviations. It can be clearly seen that this large discrepancy is caused by one *DAF* from Culvert 5. This value is the only *DAF* recorded at the location of maximum static strain during the testing of Culvert 5 that is more than two standard deviations greater than the average and one of three values more than one standard deviation greater than the average. For this reason, the slopes of the average and the average plus two standard deviation trend lines may be more representative of the data set.

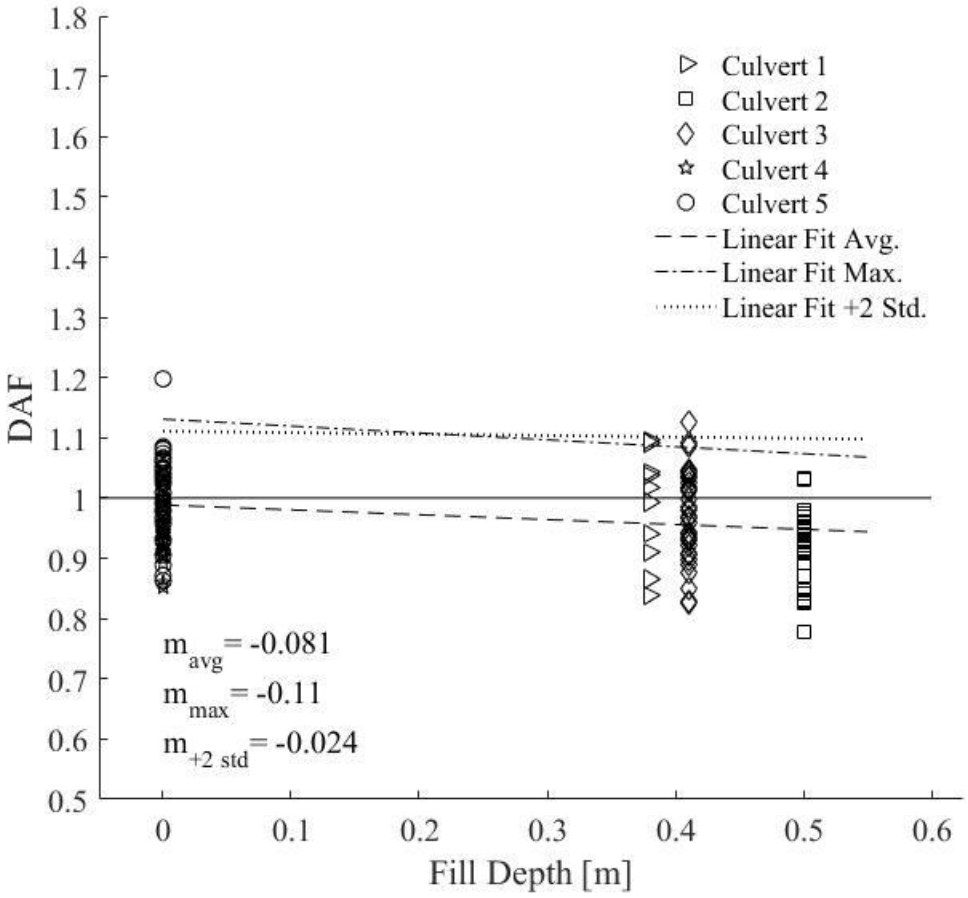

Figure 4.29 Field Test Results as a Function of Fill Depth Compared to AASHTO (2012) Specifications (Linear Fit Trend Lines Constructed from Data in Table 4.6)

In order to assess the adequacy of AASHTO (2012) specifications, Figure 4.30 compares the average, maximum and average plus two standard deviations for each test as a function of fill depth to the line specified by AASHTO. Values for each culvert are taken from Tables 4.2 and 4.6. As can be seen, the slope of maximum *DAF* trend line reasonably approximates that prescribed by AASHTO. However, the slope of the average plus two standard deviations does not. Over 2.44 m (the fill depth at which AASHTO specifies a *DAF* equal to one), the slope of the average plus two standard deviations linear fit only predicts a 0.06 decrease in *DAF*. Over the same increase in fill depth, the slope of the average trend line predicts a decrease in *DAF* of 0.20.

It is worth noting that all values shown in Figure 4.30 are more than 0.10 below the AASHTO curve. This indicates that AASHTO is conservative at the fill depths studied. However, if trends are in keeping with the linear fit of the average plus two standard deviations this may not be the case for all fill depths.

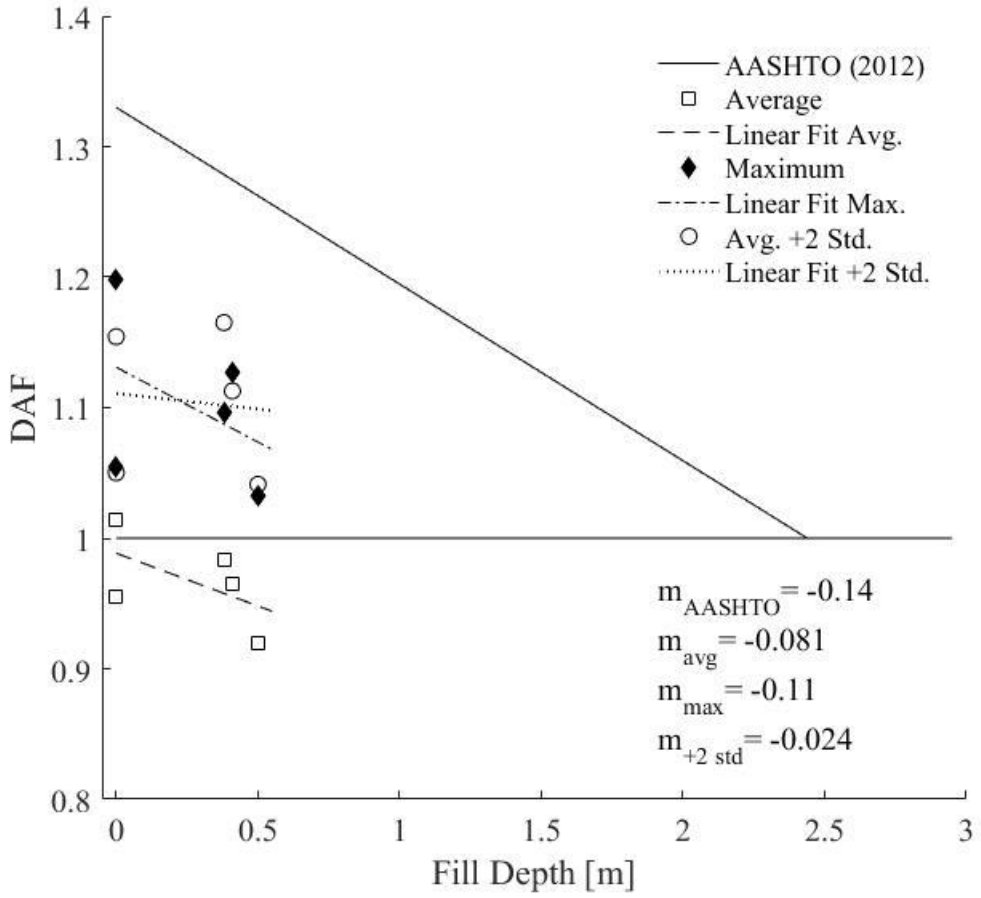

Figure 4.30 Field Test Results in Comparison to AASHTO (2012) (Linear Fit Trend Lines Constructed from Data in Table 4.6)

Because it is common practice to consider asphalt pavement as soil fill for the purposes of live load attenuation and *DAF* calculation during load rating, Figure 4.31 shows results as a function of fill depth plus asphalt pavement thickness. By including the thickness of asphalt pavement as fill, the slope of the linear fit line for the maximum *DAF* increases to -0.20 1/m, the slope of the average plus two standard deviations increases to -0.086 1/m and the slope of the average increases to -0.11 1/m. By these three measures, the slope of the average plus two standard deviations is significantly closer to that prescribed by AASHTO. Figure 4.32 shows the average, maximum and average plus two standard deviations for each test as a function of fill depth plus asphalt pavement thickness and compares results to the curve specified by AASHTO (2012). Again all results shown in Figure 4.32 are more than 0.10 below AASHTO specifications.

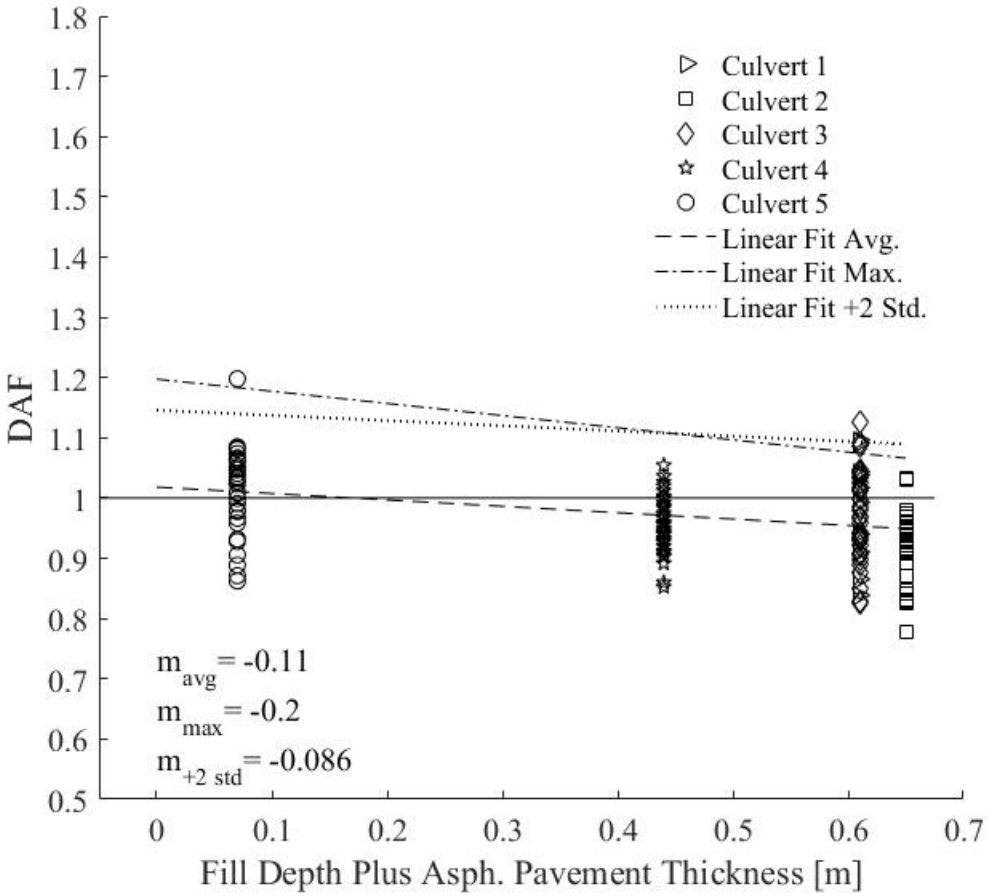

Figure 4.31 Field Test Results as a Function of Fill Depth Plus Asphalt Pavement Thickness (Linear Fit Trend Lines Constructed from Data in Table 4.6)

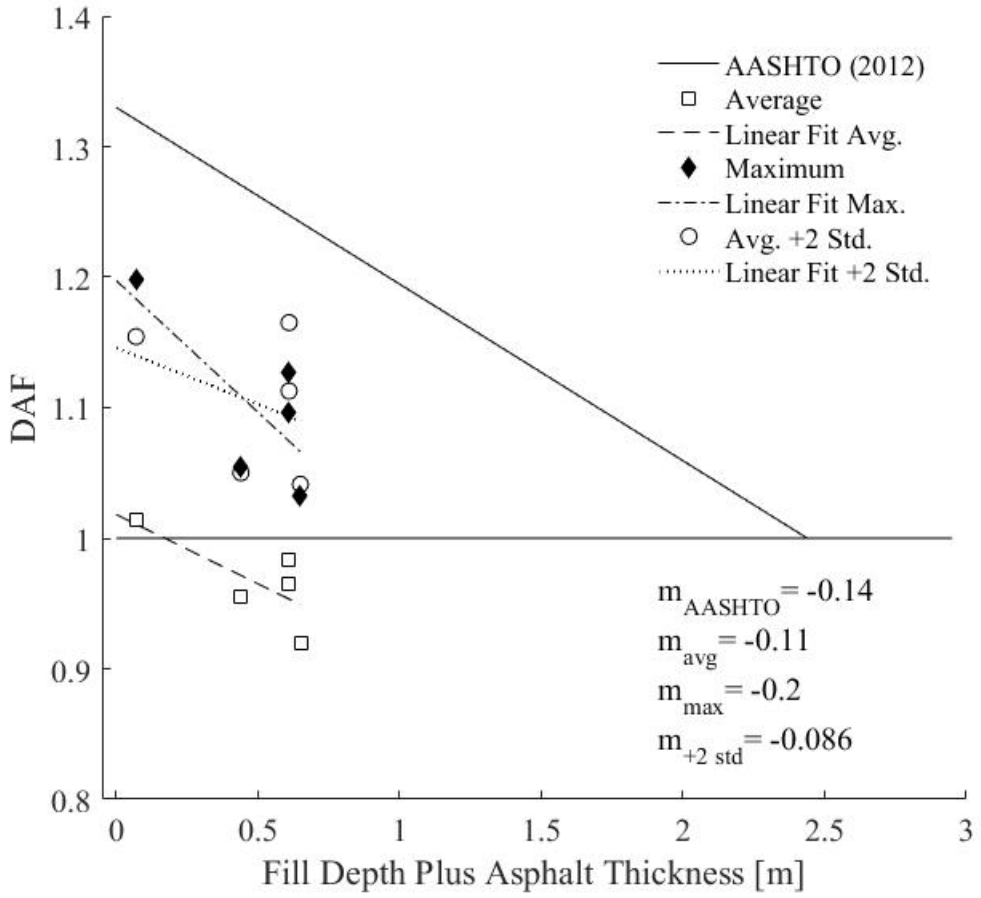

Figure 4.32 Field Test Results in Comparison to AASHTO (2012), Including Asphalt Thickness as Fill (Linear Fit Trend Lines Constructed from Data in Table 4.6)

4.4.2 Span Length

Figure 4.33 shows the *DAF* values calculated for each culvert as a function of span length. Based on the linear fit, *DAF* increases with increasing span length when the maximum *DAF* is considered, decreases with increasing span length when the average *DAF* plus two standard deviations is considered and increases with increasing span length when the average *DAF* is considered. The slopes of the linear fit lines are 0.0061, -0.011 and 0.0026 1/m, respectively. Based on these conflicting results, a common trend cannot be observed. Moreover, a simple examination of results shows that *DAF* values calculated for Culverts 2 and 4 are generally lower than those determined for other culverts; however, Culvert 4's span length is nearly double that of Culvert 2. Consequently, it does not appear that a culvert's span length is indicative of its *DAF*.

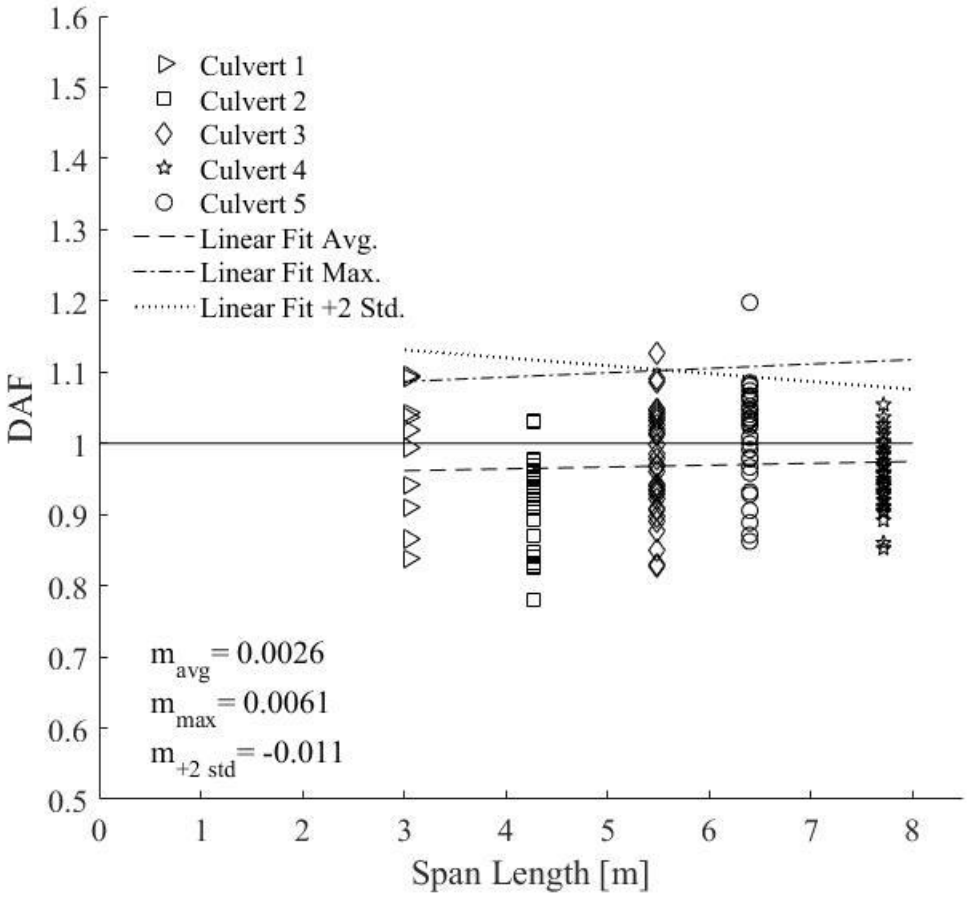

Figure 4.33 Field Test Results as a Function of Span Length (Linear Fit Trend Lines Constructed from Data in Table 4.6)

4.4.3 Slab Thickness

Figure 4.34 shows the *DAF* values calculated for each culvert as a function of culvert slab thickness. Based on the linear fit, *DAF* tends to increase as slab thickness increases. The slope of the linear fit lines for average *DAF*, maximum *DAF* and average *DAF* plus two standard deviations are 0.13, 0.31 and 0.13 1/m, respectively. The slope of the maximum *DAF* is over twice that of the average and average plus two standard deviations. As with fill depth, it may be the case that the maximum trend line is not as representative of culvert dynamic behavior as the average and average plus two standard deviations due to the large influence of one *DAF* calculated for Culvert 5. The slope of the maximum *DAF* predicts an increase of 0.14 over the range of slab thicknesses studied, while the average and average plus two standard deviations only predict an increase of 0.06.

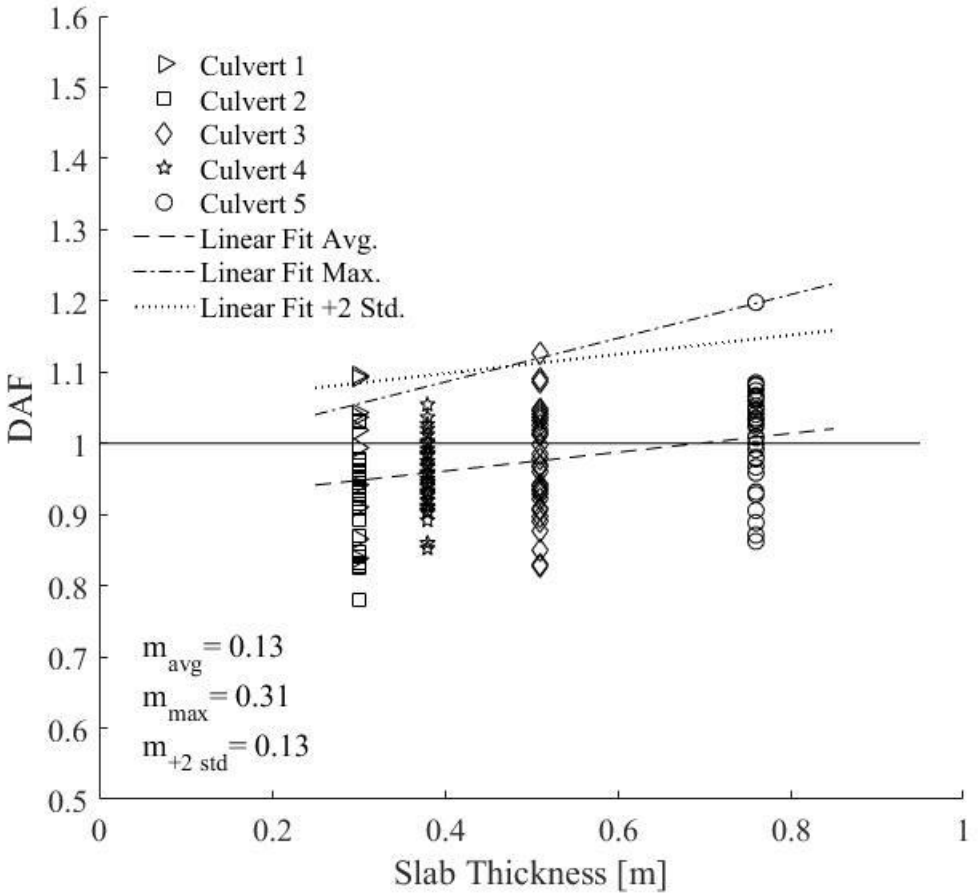

Figure 4.34 Field Test Results as a Function of Slab Thickness (Linear Fit Trend Lines Constructed from Data in Table 4.6)

4.4.4 **Asphalt Pavement Thickness**

Figure 4.35 shows the *DAF* values calculated for each culvert as a function of asphalt pavement thickness. The slopes of the linear fit lines for maximum *DAF*, average *DAF* plus two standard deviations and average *DAF* are -0.27, -0.19 and -0.08 1/m, respectively. From these results it appears that *DAF* tends to decrease with increasing asphalt pavement thickness. However, it should be noted that Culvert 2 has the lowest average and maximum *DAF* of all five culverts and has the second lowest asphalt pavement thickness.

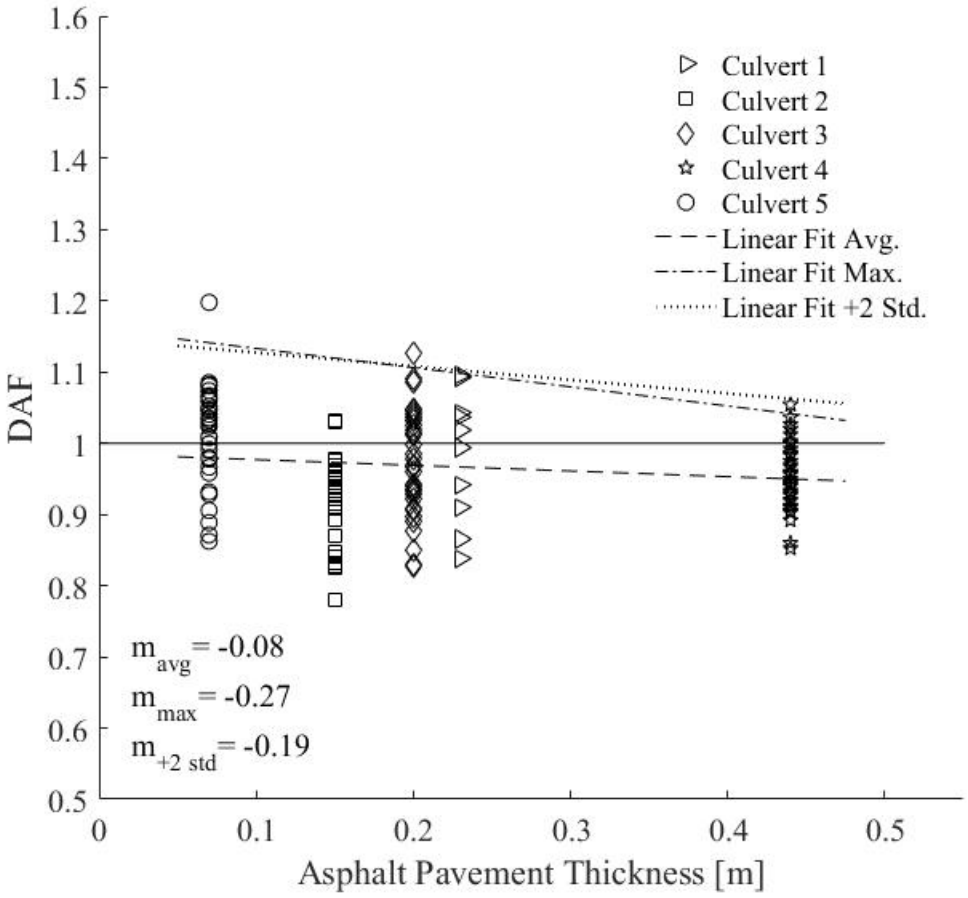

Figure 4.35 Field Test Results as a Function of Asphalt Pavement Thickness (Linear Fit Trend Lines Constructed from Data in Table 4.6)

4.4.5 **Vehicle Speed**

The three vehicle speeds tested in this study are 8.9, 13.4 and 17.9 m/s. Figure 4.36 combines the results from each culvert and shows *DAF* as a function of vehicle speed. Based on the linear fit, the *DAF* tends to increase as vehicle speed increases when the maximum *DAF* and average *DAF* plus two standard deviations are considered. However, *DAF* appears to decrease as vehicle speed increases if the average *DAF* for each culvert is considered. The slopes of the linear fit lines are 0.0017, 0.0019 and -0.0017 s/m, respectively. That suggests that *DAF* could potentially decrease by -0.02 or increase 0.02. Due to these conflicting trends and vehicle speed's relatively little overall influence, it is difficult to say that any correlation exists between vehicle speed and *DAF*.

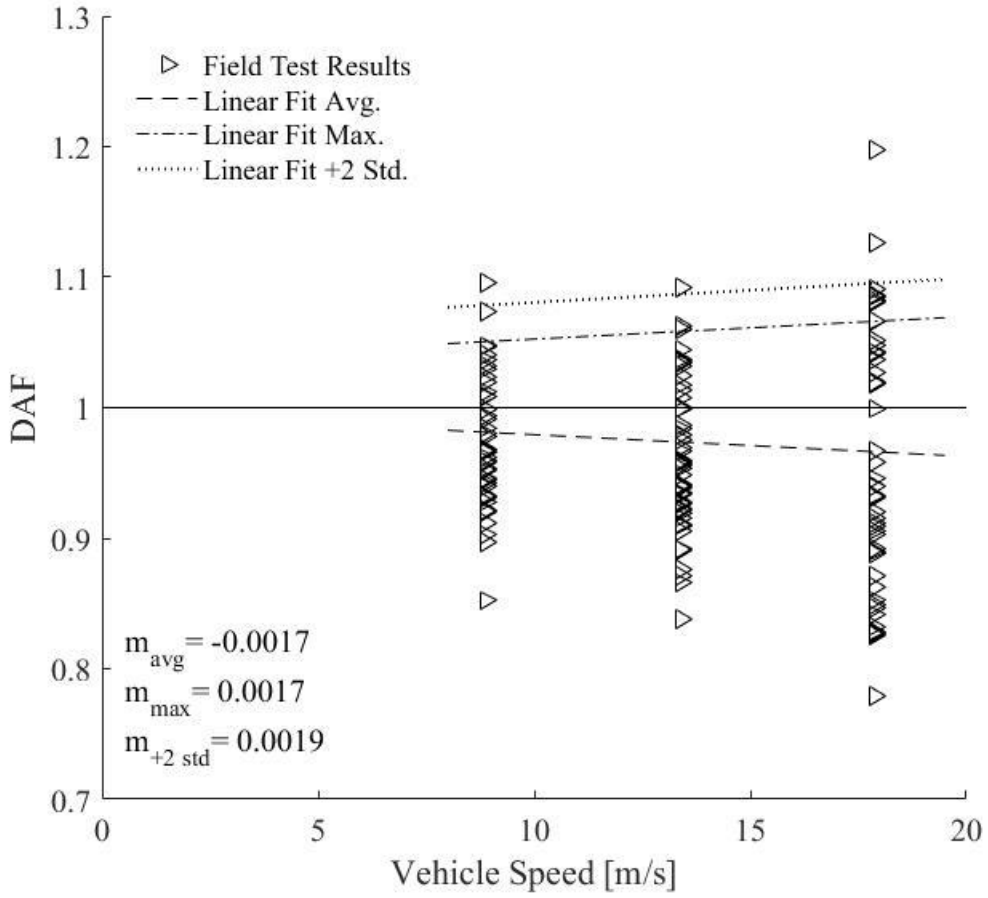

Figure 4.36 Field Test Results as a Function of Vehicle Speed

Chapter 5

COMPARISON OF RESULTS

According to AASHTO (2012) specifications the *DAF* decreases linearly as fill depth increases. At zero meters of fill *DAF* is specified as 1.33, meaning that the dynamic affects amplify loads to 1.33 times their static load. The purpose of this thesis is to attempt to verify that specification and possibly identify other parameters that significantly influence the *DAF*.

Over the course of this study 324 finite element model configurations were analyzed and five field tests were conducted to assess the dynamic behavior of reinforced concrete box culverts (RCBC). Results obtained through finite element modeling represent the theoretical maximum *DAF* for each of the 324 model configurations, given reasonable constraints on vehicle speed. Results suggest that RCBC behave in a similar manner to the single degree of freedom system solution. This finding subsequently suggests that the response of the culvert is a function of the speed at which a truck crosses the culvert, the span length, and the natural period of the structure. However, the relationship between each of these parameters is highly non-linear.

Unlike the finite element models, all results obtained through field testing do not necessarily represent the maximum *DAF* for each culvert tested. Instead the results of each pass are merely possible values for *DAF* that can then be further scrutinized to determine the appropriate maximum *DAF*. Because the location where the highest load occurs is the most critical location from an evaluation standpoint, the *DAF* values calculated at the sensor location that recorded the highest static strain are used to determine the appropriate *DAF* for each culvert. Based on results, the maximum *DAF*

is expressed in two ways: the maximum value obtained during testing at the point that recorded the highest static strain and the average plus two standard deviations of all *DAF* values calculated at the sensor that recorded the highest static strain. Assuming that results are normally distributed, the average plus two standard deviations accounts for 97.5 percent of possible *DAF* values. A 2.5 percent exceedance was deemed to give a reasonably conservative estimate of the maximum expected *DAF*.

Finite element results showed the *DAF* to be less than 1.33 for all configurations tested. The average *DAF* obtained from the finite element study was 1.15. The field test results showed no *DAF* to be higher than 1.2 at the location of maximum static strain. Furthermore, two culverts did not have a maximum *DAF* greater than 1.05. The following sections compare the results of the finite element modeling and field testing portions of this work in order to examine the influence of each geometric parameter studied. Additionally, findings are discussed in view of past research included in the literature review.

5.1 Geometric Properties

5.1.1 Fill Depth

Figure 5.1 compares the field test (FT) and finite element model (FEM) results as a function of fill depth. Additionally, the *DAF* specified by AASHTO (2012) is shown. Using the slopes as an indication of general behavior, it can be seen that the model predicts that *DAF* will increase as fill depth increases while the field test results suggest the opposite. Further comparing these results to AASHTO provisions shows good agreement between the slopes of the maximum observed *DAF* from field test results and AASHTO, while only marginal agreement when the average plus two

standard deviations of field test results is considered. The trend of finite element results is opposite those suggested by AASHTO specifications.

When comparing the data, it is important to recognize that all culverts instrumented have fill depths less than those studied as a part of the parametric finite element analysis. No experimental results were obtained for culverts having fill depths greater than 0.5 m. This is because most culverts in the Delaware Department of Transportation database do not have large fill depths. Given trends shown in the finite element results, the addition of higher fill depths may influence the trends observed during field testing.

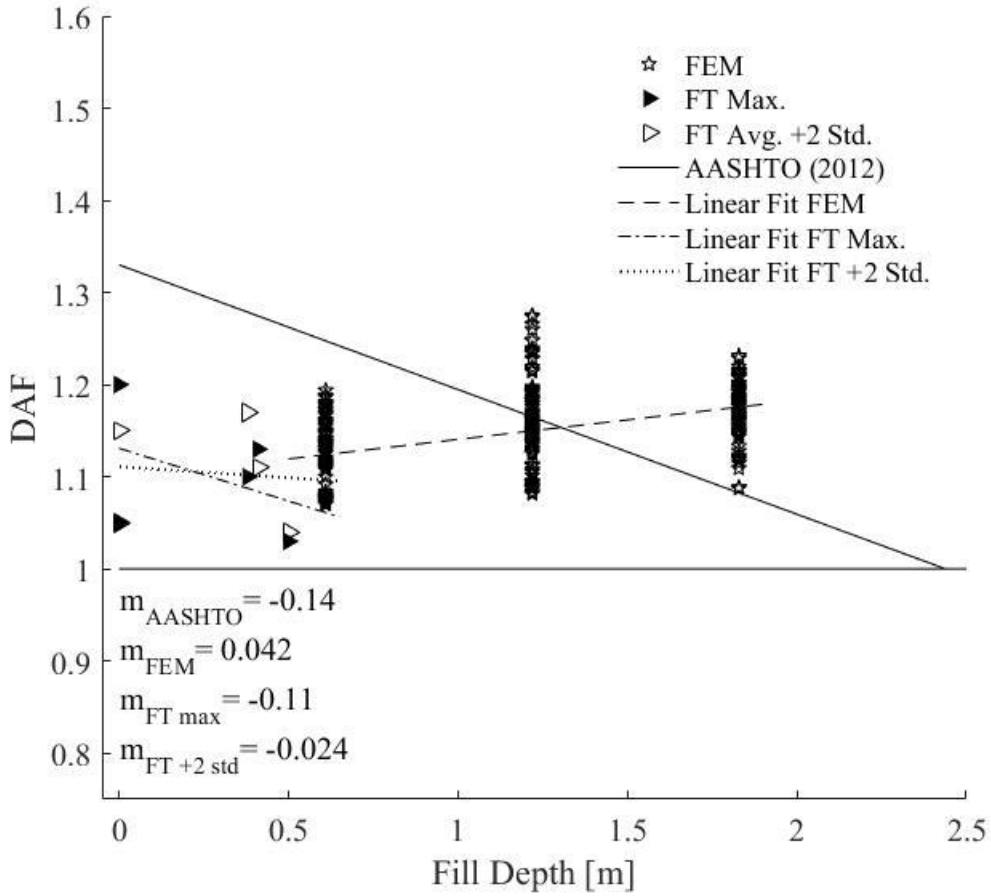

Figure 5.1 Comparison of Results as a Function of Fill Depth and AASHTO (2012) Specifications

5.1.2 **Span Length**

Figure 5.2 compares the field test and finite element model results as a function of span length. When examining the results of both methods, it does not appear that a trend exists. The slope of the finite element results is inconsequential for the span lengths studied and thus can be considered to be zero. Additionally, the trend lines for the maximum and average plus two standard deviations of the field tests have slopes of the opposite direction.

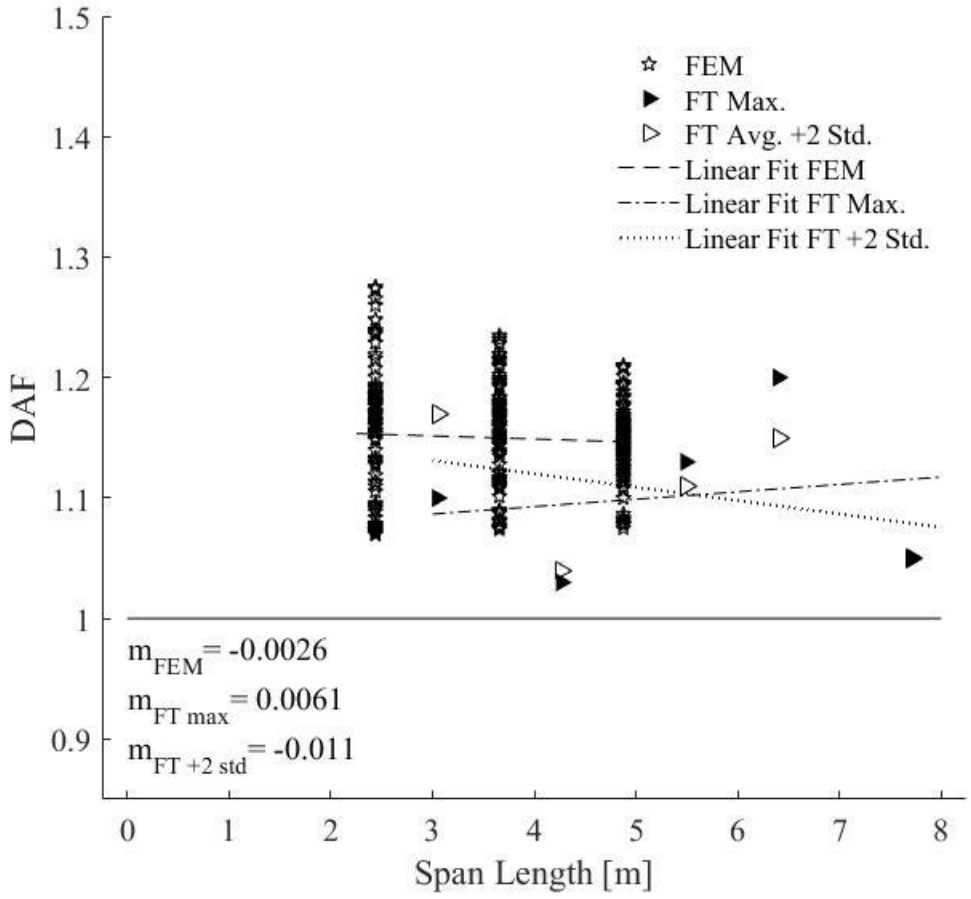

Figure 5.2 Comparison of Results as a Function of Span Length

5.1.3 Slab Thickness

Figure 5.3 compares the field test and finite element model results as a function of slab thickness. As can be seen, the finite element results suggest a decrease in *DAF* as slab thickness increases, while the field test results suggest the opposite. Moreover, the slope of the linear fit to the finite element results is much more gradual than the field test results. Over an increase of 0.6 m (roughly the range of results), the finite element model study predicts a 0.04 decrease in *DAF*. Conversely, the field test results predict between a 0.08 and 0.18 increase in *DAF*.

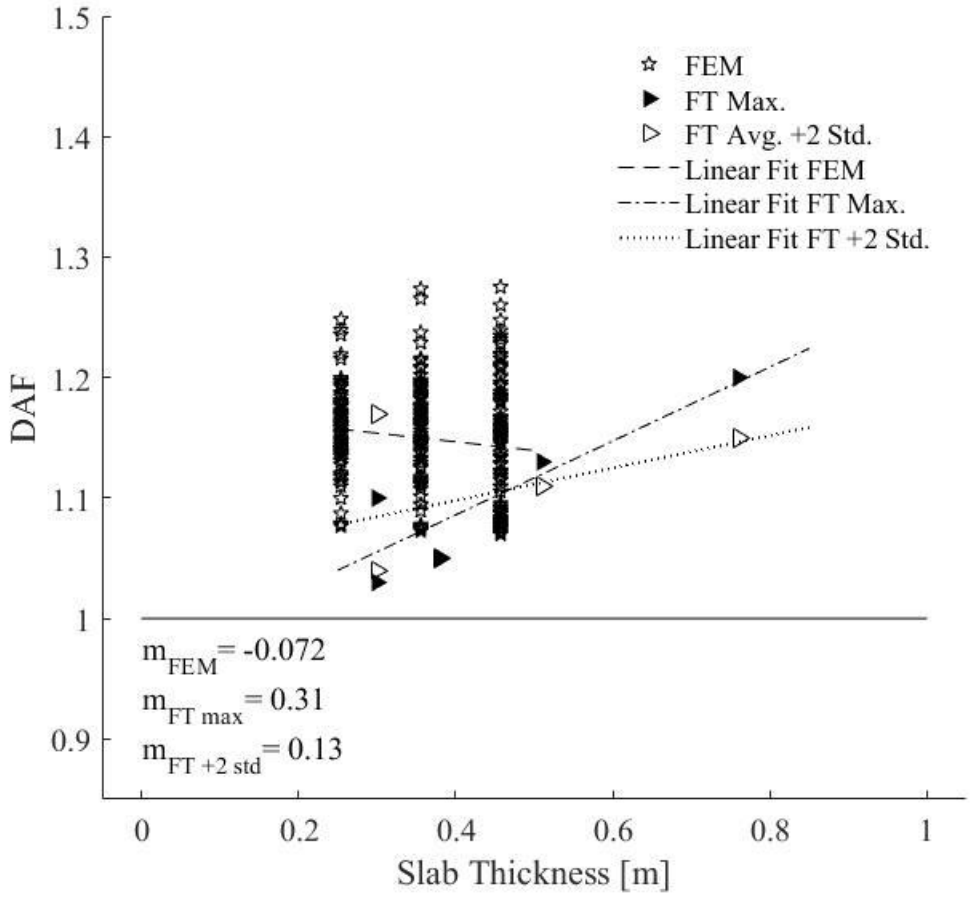

Figure 5.3 Comparison of Results as a Function of Slab Thickness

5.1.4 Asphalt Pavement Thickness

Figure 5.4 compares the field test and finite element model results as a function of asphalt pavement thickness. As can be seen, the two methods have conflicting results. The finite element model indicates that *DAF* increases slightly as pavement thickness increases, while field test results indicate that *DAF* decreases as pavement thickness increases. Over a 0.5 m increase in asphalt pavement thickness, the finite element models predict an increase in *DAF* of 0.01, while the field test results suggest a decrease in *DAF* between 0.10 and 0.14.

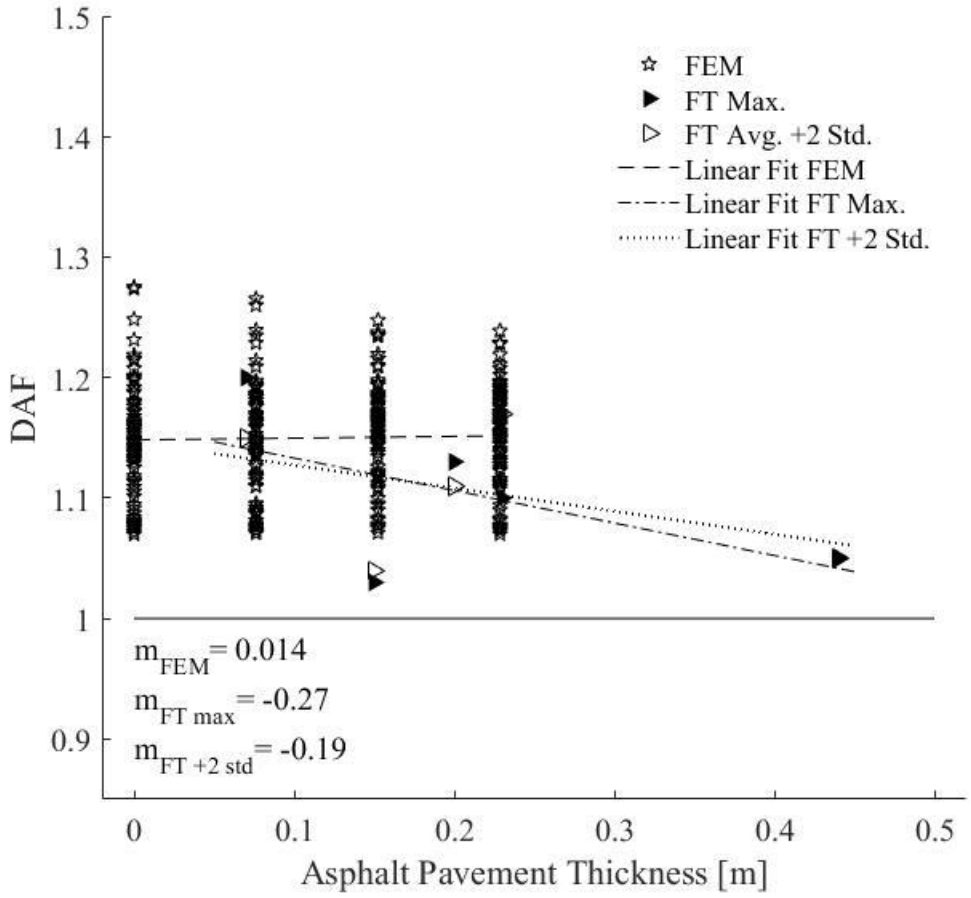

Figure 5.4 Comparison of Results as a Function of Asphalt Pavement Thickness

5.2 Discussion of Findings

Comparing the results obtained in the finite element modeling and field testing portions of this study revealed conflicting results for all four geometric parameters studied. This is concerning as the theory should resemble real behavior in the field. However, it is important to recognize that the parametric finite element study is the result of 324 model configurations, while only five culverts were instrumented and tested in the field. Given that finite element modeling revealed the dynamic behavior of box culverts to vary considerably depending on the portion of the parameter space examined, it may be necessary to conduct more field tests to corroborate trends.

When comparing AASHTO (2012) specifications to field test results, it does appear that the code has some basis, however the extent to which results corroborate a *DAF* of 1.33 that decreases with a slope of -0.14 between zero and 2.44 m of fill is presently unclear. Depending on the method used to determine the maximum *DAF*, field tests suggest a slope between -0.024 and -0.11. Furthermore, no culvert tested had a fill depth greater than 0.5 m. Consequently, it is difficult to determine at what fill depth the *DAF* becomes effectively zero or if *DAF* becomes zero at any fill depth.

McLean and Marsh (1998) observed that tests conducted by multiple researchers often reveal different and contradictory trends in *DAF*. This is due to the complexity of the soil-structure-pavement system. It is for this reason that AASHTO (2012) specifies a constant *DAF* value for non-buried bridge structures. Given the lack of agreement between theoretical and experimental results observed in this thesis, it may be reasonable to specify a similarly constant *DAF* for buried structures or consider there to be no difference between buried bridges and non-buried bridges when determining *DAF*.

In the literature it is widely recognized that *DAF* is primarily a function of road surface roughness, bridge natural period and vehicle suspension frequency. In this thesis, all culverts tested had smooth road surfaces, truck suspension frequency was not known and bridge natural period could not be obtained from the field tests. As a result, it is likely that the worst possible *DAF* for the tested geometric properties was not captured during field testing. This should also be considered when determining a reasonable *DAF* for design as the engineer has no knowledge of future roadway conditions.

For the purposes of load rating, where an engineer is evaluating a structure based on current conditions, the present study is applicable to structures in similar condition and with similar geometric properties to those tested. According to AASHTO (2011) specifications, a reduced *DAF* (or *IM*) can be used for bridges with span lengths greater than 12.2 m and roadways in good condition or roadways with only minor surface deviations. For roadways with minor surface deviations *DAF* is 1.20 and for roadways in good condition *DAF* is 1.10. Of the culverts tested, none recorded *DAF* values in excess of 1.20 for the maximum or average plus two standard deviations. As a result, it may be reasonable to apply a similar methodology to shorter span bridges and culverts.

It should be recognized that the ratio of culvert natural frequency to truck suspension frequency was not studied. Consequently, the effects of this ratio are currently unknown. The literature review showed that trucks have two predominant natural frequencies, one between two and five hertz and another between 10 and 15 Hz (Cantieni 1984; Csagoly et al. 1972; Tilly 1986). Natural periods of the 324 model configurations ranged between 0.013 and 0.074 s and had an average of 0.028 s. As a

result, culvert natural frequencies ranged between 13.5 and 76.9 Hz, with an average of 35.7 Hz. This finding suggests that increased dynamic effects due to resonance will not occur for a majority of culverts, but without a detailed experimental analysis of culvert natural period (or frequency) this cannot be verified.

Chapter 6

CONCLUSIONS & RECOMMENDATIONS

It has been observed that many reinforced concrete box culverts (RCBC) that appear to be in good condition upon inspection receive poor rating factors when evaluated according to current specifications. It is believed that an overconservative specification of the dynamic load allowance (*IM*), or dynamic amplification factor (*DAF*), is a contributing factor to this discrepancy. This specification defines *DAF* as 1.33 when no fill is present and allows for *DAF* to decrease linearly between zero and 2.44 m of fill, such that *DAF* is one at a fill depth equal to 2.44 m.

The goal of this thesis was to explore the influence of geometric and material properties on dynamic amplification, assess the adequacy of current specifications and give recommendations regarding the usage of the *DAF* in the load rating of RCBC. This was accomplished by performing a literature review, a parametric study employing 324 finite element models, and instrumenting and testing five culverts in the state of Delaware. The finite element analysis examined the influence of five parameters on the soil-structure-pavement system: fill depth, soil elastic modulus, span length, culvert slab thickness and asphalt pavement thickness. Similarly, field tests examined the influence of fill depth, span length, culvert slab thickness, asphalt pavement thickness and vehicle speed.

The literature revealed the dynamic behavior of conventional, non-buried bridges to be extremely complex. Many experimental tests show conflicting results regarding the influence of many variables, however *DAF* has generally been shown to be a function of the road surface roughness, culvert natural period and truck suspension frequency.

Finite element results showed no *DAF* values to be greater than 1.33. Of the five parameters studied, soil elastic modulus had the greatest influence on *DAF*. For a maximum increase of 500 MPa the linear fit trend showed *DAF* to decrease by 0.07 on average. The maximum increases in fill depth, slab thickness, span length and asphalt pavement thickness were 1.22, 0.203, 2.44 and 0.229 m, respectively. For a maximum increase in parameter value the linear fit trends for fill depth, slab thickness, span length and pavement thickness showed each to change *DAF* by 0.051, -0.015, -0.006 and 0.003, respectively, on average. These values are obtained by multiplying the slope of the linear fit trend line by the difference between extreme parameter values. Relative to soil elastic modulus and fill depth, span length, slab thickness and pavement thickness have little influence on the *DAF*.

Results also showed significant variability in *DAF* from all parameter's trend lines. This is primarily a function of inconsistent trends found throughout the parameter space. For instance, all other parameters being constant, an increase in span length may have a positive relation with *DAF* at 570 MPa soil, but may have a negative relation with *DAF* at 70 MPa soil. However, good agreement was observed between parametric finite element results and the single degree of freedom system solution. Consequently, the *DAF* was shown to be a function of the ratio of the pulse duration to the natural period of the soil-structure-pavement system.

Field tests showed no *DAF* to be higher than 1.2 at the location of maximum static strain. Furthermore, two of the five culverts did not have a maximum *DAF* greater than 1.05 when *DAF* is calculated at the location of maximum static strain. The *DAF* was shown to decrease as fill depth and asphalt pavement increase and increase as slab thickness increases. The effect of span length and vehicle speed were

inconclusive. The slope of the linear fit trend lines for the average, maximum and average plus two standard deviations of fill depth vs. *DAF* were -0.081, -0.11 and -0.024 1/m, respectively. When asphalt pavement thickness is included as soil fill, slopes were -0.11, -0.2 and -0.086 1/m, respectively. These results relate reasonably well to AASHTO (2012) specifications. The slopes of the linear fit lines for span length were -0.0026, 0.0061 and -0.011 1/m, respectively. The slopes of linear fit lines for slab thickness were 0.13, 0.31 and 0.13 1/m, respectively. And the slopes of the linear fit lines for asphalt pavement thickness were -0.08, -0.27 and -0.19 1/m.

A comparison of the finite element and field testing studies revealed the two studies to have opposite trends for fill depth, slab thickness, and asphalt pavement thickness. One possible reason for this disparity is that so few culverts were tested in relationship to the number of model configurations analyzed.

Although it appears from field test results that AASHTO specifications may be justified, finite element results suggest that more testing may prove otherwise. Due to the lack of experimental data concerning the *DAF* at high fill depths and the documented influence of road surface roughness on RCBC dynamic behavior it is conservatively recommended that buried bridge structures be subject to the same design specifications as non-buried bridges. In the case that a culvert's condition is not known it is critical that a conservative *DAF* value be chosen. However, after an inspection has been performed and a culvert's condition can be verified to match those of culverts tested in this study, it seems appropriate to allow for a reduced *DAF*.

When load rating conventional, non-buried bridges, current AASHTO (2011) specifications allow for a reduction in *DAF* based on roadway condition. For longitudinal members over 12.2 m in length a *DAF* of 1.20 can be applied if the

roadway has only minor surface deviations and 1.10 can applied if the roadway has a smooth riding surface. Culverts tested in this thesis were all in good condition and had smooth roadways. Because no test revealed a *DAF* greater than 1.2 at the location of maximum strain it is recommended that a reduction in *DAF* similar to current allowances be extended to bridges and culverts less than 12.2 m in length. If a longitudinal member is less than 12.2 m in length, the fill depth is less than 0.5 m and the road surface is in good condition, it is recommended that a *DAF* of 1.2 be applied. Further testing and analysis may prove the allowance of 1.10 for smooth road surfaces to be acceptable, however current results do not show such a value to be conservative.

Due to the current lack of research on the *DAF* for RCBC it is recommended that a significant effort be put forward in studying this topic. Current specifications for non-buried bridges have culminated from the testing of hundreds of bridge structures and many more computer analyses. To date, this study is the only one known to examine the *DAF* for concrete box culverts. Given that culverts tested all had fill depths less than 0.5 m and the results of the parametric study showed different behavior on different ends of the parameter space it is specifically recommended that more experimental tests be conducted. Additionally, the influence of road surface roughness was not included in this thesis. It is recommended that future tests examine culverts with higher fill depths and consider a rough road condition. Furthermore, experimental studies should examine the ratio of culvert natural frequency to vehicle suspension frequency and assess the potential for resonance.

Future finite element studies should consider the load as a sprung mass so that the influence of truck suspension frequency can be assessed. Three dimensional

analyses should also be conducted so that the load attenuation out of plane can be incorporated into the analysis.

REFERENCES

(2011). "National Bridge Inspection Stanards." *23 CFR § 650 C*.

AASHO (1962). "The AASHO Road Test." *Report 4, Highway Research Board, Special Report 61D*Washington, D.C.

AASHTO (2002). *Standard Specifications for Highway Bridges, 17th Edition*, American Association of State Highway and Transportation Officials, Washington, D.C.

AASHTO (2011). *Manual for Bridge Evaluation, 2nd Edition, with 2011, 2013, 2014, 2015 and 2016 Interim Revisions*, American Association of State Highway and Transportation Officials, Washington, D.C.

AASHTO (2012). *LRFD Bridge Design Specifications, 6th Edition, with 2012 and 2013 Interim Revisions*, American Association of State Highway and Transportation Officials, Washington, D.C.

Abaqus (2013). "Abaqus 6.13 Online Documentation." Dassault Systèmes, Providence, RI, USA.

ASCE "Impact on Highway Bridges, Final Report of the Special Committee." *Proc., ASCE Transactions*, 1089-1117.

Beben, D. (2013). "Dynamic Amplification Factors of Corrugated Steel Plate Culverts." *Engineering Structures*, 46, 193-204.

Billing, J. R. (1984). "Dynamic Loading and Testing of Brdges in Ontario." *Canadian journal of civil engineering*, 11(4), 833-843.

Cantieni, R. "Dynamic Load Testing of Highway Bridges." *Proc., Second Bridge Engineering Conference.*, Transportation Research Board, 141-148.

CEN (2002). *EN 1991-2, Eurocode 1: Actions on structures—Part 2: Traffic loads on bridges*, European Committee for Standardization, Brussels, Belgium.

Chen, S. S., and Harik, I. E. (2012). "Dynamic Effect of a Moving Truck on a Culvert." *Journal of Bridge Engineering*, 17(2), 382-388.

Chopra, A. K. (2012). *Dynamics of structures : theory and applications to earthquake engineering*, Prentice Hall, Upper Saddle River, N.J.

CSA (2006). *Canadian Highway Bridge Design Code*, Canadian Standards Association, Mississauga, Ontario.

Csagoly, P. F., Campbell, T. I., and Agarwal, A. C. (1972). "Bridge Vibration Study."Downsview, Ontario.

Dancygier, A. N., and Karinski, Y. S. (1999). "A simple model to assess the effect of soil shear resistance on the response of soil-buried structures under dynamic loads." *Engineering Structures*, 21(12), 1055-1065.

Deng, L., Yu, Y., Zou, Q. L., and Cai, C. S. (2015). "State-of-the-Art Review of Dynamic Impact Factors of Highway Bridges." *Journal of Bridge Engineering*, 20(5), 14.

Dhar, C. L., Chu, K. H., and Garg, V. K. (1978). "Dynamic Response of a single track railway truss bridge." *Transport Res Rec*(655), 73-80.

FHWA (1995). "Recording and coding guide for the structure inventory and appraisal of the nation's bridges." United States Department of Transportation, Washington, DC.

Hwang, E. S., and Nowak, A. S. (1991). "Simulation of Dynamic Load for Bridges." *Journal of Structural Engineering (ASCE)*, 117(5), 1413-1434.

Idham, M. K., Hainin, M. R., Yaacob, H., Warid, M. N. M., and Abdullah, M. E. (2013). "Effect of Aging on Resilient Modulus of Hot Mix Asphalt Mixtures." *Innovation and Sustainable Technology in Road and Airfield Pavement*, J. R. Chang, and S. R. Yang, eds., 291-297.

Janoo, V., Irwin, L., and Haehnel, R. (2003). "Pavement Subgrade Performance Study, Project Overview." Federal Highway Administration, Washington, D.C.

Jayawickrama, P. W., Senanayake, A., Lawson, W. D., and Wood, T. A. (2012). "Impact of variability in soil parameter on culvert load rating." *GeoStructures Congress 2012: State of the Art and Practice in Geotechnical Engineering*, American Society of Civil Engineers, Oakland, CA.

Kaliakin, V. N. (2002). *Introduction to approximate solution techniques, numerical modeling, and finite element methods*, Marcel Dekker, New York.

Lawson, W. D., Wood, T. A., Newhouse, C. D., and Jayawickrama, P. W. (2009). "Culvert rating guide." Texas Department of Transportation, Austin, TX.

Lawson, W. D., Wood, T. A., Newhouse, C. D., and Jayawickrama, P. W. (2010). "Evaluating existing culverts for load capacity allowing for soil-structure interaction." Texas Department of Transportation, Austin, TX.

Lo Presti, D. C. F., Pallara, O., and Cavallaro, A. (1997). *Damping ratio of soils from laboratory and in situ tests*.

Loulizi, A., Flintsch, G. W., Al-Qadi, I. L., Mokarem, D., and Trb (2006). "Comparing resilient modulus and dynamic modulus of hot-mix asphalt as material properties for flexible pavement design." *Bituminous Paving Mixtures 2006*, 161-170.

Mamlouk, M. S., and Sarofim, R. T. (1988). "Modulus of asphalt mixtures - an unresolved dilemma." *Transport Res Rec*(1171), 193-198.

Manko, Z., and Beben, D. (2008). "Dynamic testing of a corrugated steel arch bridge." *Canadian Journal of Civil Engineering*, 35(3), 246-257.

McGrath, T., Selig, E. T., and Beach, T. J. (1996). "Structural behavior of three-sided arch span bridge." *Transport Res Rec*(1541), 112-119.

McGrath, T. J., Liepins, A. A., and Beaver, J. L. "Live load distribution widths for reinforced concrete box sections." *Proc., Transportation Research Board - 6th International Bridge Engineering Conference: Reliability, Security, and Sustainability in Bridge Engineering, July 17, 2005 - July 20, 2005*, Transportation Research Board, 99-108.

McGrath, T. J., and Mastroianni, E. P. (2002). "Finite element modeling of reinforced concrete arch under live load." *Transport Res Rec*(1814), 8.

McLean, D. L., and Marsh, M. L. (1998). "Dynamic Amplification Factors for Bridges." *Synthesis of Highway Practice 266*, Transportation Research Board, Washington, D.C.

Menq, F. (2003). "Dynamic properties of sandy and gravelly soils." Doctor of Philosophy Dissertation, The University of Texas at Austin.

Moore, I. D., and Brachman, R. W. (1994). "3-Dimensional analysis of flexible circular culverts." *Journal of Geotechnical Engineering-Asce*, 120(10), 1829-1844.

Muhunthan, B., and Jennings, A. T. (1994). "Finite Element Study of the Rehabilitation of Faulted Portland Cement Concrete Pavements." Washington State Department of Transportation, Olympia, WA.

Nowak, A. S. (1999). "Calibration of LRFD bridge design code." *NCHRP Report 368*, Transportation Research Board, Washington, D.C.

NZTA (2013). *Bridge Manual: Third Edition*, New Zealand Transport Agency, Wellington, New Zealand.

Orton, S. L., Loehr, J. E., Boeckmann, A., and Havens, G. (2015). "Live-Load Effect in Reinforced Concrete Box Culverts under Soil Fill." *Journal of Bridge Engineering*, 20(11).

Paultre, P., Chaallal, O., and Proulx, J. (1992). "Bridge dynamics and dynamic amplification factors - a review of analytical and experimental findings." *Canadian Journal of Civil Engineering*, 19(2), 260-278.

Petersen, D. L., Nelson, C. R., Li, G., McGrath, T. J., and Kitane, Y. (2010). "Recommended design specifications for live load distribution to buried structures." *NCHRP Report 647*, Transportation Research Board, Washington, D.C.

Robinson, S. W. (1884). "Vibration of bridges." *Annual Report of the Commissioner of Railrads and Telegraphs*Columbus, Ohio.

Seed, H. B., Wong, R. T., Idriss, I. M., and Tokimatsu, K. (1986). "Moduli and Damping Factors for Dynamic Analyses of Cohesionless Soils." *Journal of Geotechnical Engineering-Asce*, 112(11), 1016-1032.

Selig, E. T. "Soil properties for plastic pipe installations." *Proc., Symposium on Buried Plastic Pipe Technology, September 10, 1990 - September 13, 1990*, Publ by ASTM, 141-158.

Selig, E. T., and Nash, W. A. "Buried Pipeline Research Needs." *Proc., Pipeline Infrastructure, Proceedings.*, ASCE, 463-475.

Senetakis, K., Anastasiadis, A., and Pitilakis, K. (2012). "The Small-Strain Shear Modulus and Damping Ratio of Quartz and Volcanic Sands." *Geotechnical Testing Journal*, 35(6), 964-980.

Senetakis, K., and Madhusudhan, B. N. (2015). "Dynamics of potential fill-backfill material at very small strains." *Soils and Foundations*, 55(5), 1196-1210.

Spangler, M. G., Mason, C., and Winfrey, R. E. (1926). *Experimental determinations of static and impact loads transmitted to culverts*, Iowa State College, Ames, Iowa.

Tilly, G. P. (1986). *Dynamic Behaviour of Concrete Structures : Report of the RILEM 65 MDB Committee*, Elsevier, Amsterdam; New York.

Turneaure, F. E., Crandall, C. L., Cartlidge, C. H., and Schneider, C. C. "Report of Sub-committee on Impact." *Proc., Twelfth Annual Convention*, American Railway Engineering and Maintenance o Way Association.

Uddin, W. "Characterization of pavement materials and soils using gyratory shear test." *Proc., Proceedings of the 1998 Geo-Congress, October 18, 1998 - October 21, 1998*, ASCE, 59-68.

Wekezer, J., Taft, E., Kwasniewski, L., and Earle, S. (2010). "Investigation of impact factors for FDOT bridges."Tallahassee, Florida.

Whitmoyer, S. L., and Kim, Y. R. (1994). "Determining asphalt concrete properties via the impact resonant method." *Journal of Testing and Evaluation*, 22(2), 139-148.

Wills, R. (1849). "The Effects Produced by Causing Weights to Travel Over Bars with Different Velocieities." *Appendix to the Report of the Commissioners Appointed to Inquire into the Application of Iron to Railway Structures*London, England.

Appendix A

FIELD TEST RESULTS

A.1 Dynamic Amplification Factor Tables

Tables A.1 to A.10 give the *DAF* values calculated at each sensor during all passes for each of the five culverts for Truck 1 and Truck 2. Sensor location is reported with respect to the center of the roadway, using x_2 in Figures 4.10, 4.14, 4.18, 4.22 and 4.26 as the origin.

Table A.1 Culvert 1, Truck 1 *DAF*

		Sensor Location (m)				
Speed (m/s)	Lane	-3.6	1.8	0	1.8	3.6
8.9	2	1.05	1.01	1.10	0.91	0.95
13.4	1	1.01	0.94	1.12	0.95	0.87
	2	1.02	0.96	1.04	0.88	0.85
	3	0.97	0.84	0.97	0.91	0.95
17.9	2	0.90	0.89	1.02	0.92	0.92

Table A.2 Culvert 1, Truck 2 *DAF*

		Sensor Location (m)				
Speed (m/s)	Lane	-3.6	1.8	0	1.8	3.6
8.9	2	0.70	0.70	0.99	0.98	1.25
13.4	1	0.75	0.87	1.18	1.25	1.37
	2	0.94	0.91	1.09	0.97	0.96
	3	0.92	0.87	0.94	0.84	0.95
17.9	2	0.75	0.75	1.04	1.08	1.31

Table A.3 Culvert 2, Truck 1 *DAF*

			Sensor Location (m)							
Speed (m/s)	Lane	Pass No.	-3.4	-2.2	-1.7	-0.5	0	1.2	1.7	3.4
8.9	1	1	1.28	0.94	0.95	0.96	0.97	0.96	0.98	1.01
	2	1	0.86	0.89	0.90	0.94	0.96	1.00	1.04	1.06
	3	1	1.42	0.89	0.89	0.90	0.93	0.97	1.02	1.02
	1	2	1.21	0.98	1.03	1.06	1.08	1.14	1.24	1.10
	2	2	1.24	0.90	0.93	0.96	0.98	1.02	1.04	1.10
	3	2	0.86	0.90	0.91	0.92	0.93	0.95	1.02	1.01
13.4	1	1	0.91	0.85	0.93	1.03	1.05	1.14	1.03	1.11
	2	1	0.90	0.82	0.86	0.95	0.97	1.11	1.14	1.25
	3	1	0.72	0.81	0.84	0.86	0.91	0.96	1.02	1.09
	1	2	0.91	0.87	0.94	1.04	1.07	1.13	1.01	1.20
	2	2	1.11	0.80	0.85	0.94	0.98	1.12	1.17	1.28
	3	2	1.40	0.91	0.93	0.94	0.95	0.98	0.98	1.03
17.9	1	1	0.96	0.80	0.89	1.06	1.08	1.16	1.16	1.25
	2	1	0.73	0.75	0.79	0.91	0.96	1.13	1.12	1.28
	3	1	1.06	0.82	0.85	0.87	0.87	0.92	0.94	0.97
	1	2	0.69	0.77	0.87	1.10	1.12	1.22	1.21	1.37
	2	2	0.85	0.64	0.68	0.84	0.93	1.18	1.18	1.47
	3	2	0.70	0.82	0.83	0.85	0.87	0.94	0.99	1.06

Table A.4 Culvert 2, Truck 2 *DAF*

			Sensor Location (m)							
Speed (m/s)	Lane	Pass No.	-3.4	-2.2	-1.7	-0.5	0	1.2	1.7	3.4
8.9	1	1	-	-	-	-	-	-	-	-
	2	1	-	-	-	-	-	-	-	-
	3	1	-	-	-	-	-	-	-	-
	1	2	-	-	-	-	-	-	-	-
	2	2	-	-	-	-	-	-	-	-
	3	2	-	-	-	-	-	-	-	-
13.4	1	1	1.06	0.99	1.03	1.07	1.08	1.07	0.95	1.14
	2	1	1.08	0.86	0.88	0.92	0.94	1.00	1.00	1.07
	3	1	0.69	0.72	0.73	0.78	0.82	0.91	0.97	1.13
	1	2	0.84	0.93	0.98	1.08	1.10	1.15	0.97	1.21
	2	2	1.33	0.93	0.95	0.95	0.97	0.99	1.02	1.00
	3	2	0.65	0.75	0.76	0.80	0.85	0.92	0.99	1.10
17.9	1	1	0.64	0.73	0.85	1.22	1.24	1.48	1.26	1.70
	2	1	0.92	0.64	0.68	0.83	0.91	1.14	1.16	1.41
	3	1	1.27	0.55	0.57	0.64	0.70	0.83	0.91	1.13
	1	2	0.62	0.70	0.83	1.34	1.40	1.93	1.65	2.13
	2	2	0.64	0.52	0.58	0.78	0.89	1.25	1.34	1.80
	3	2	-	-	-	-	-	-	-	-

Table A.5 Culvert 3, Truck 1 *DAF*

			Sensor Location (m)				
Speed (m/s)	Lane	Pass No.	-3.6	-1.8	0	1.8	3.6
8.9	1	1	1.02	0.94	0.85	0.79	0.66
	2	1	1.07	1.02	0.98	0.94	0.92
	3	1	0.80	0.84	0.83	0.93	1.03
	1	2	0.99	0.94	0.84	0.78	0.69
	2	2	1.02	1.01	1.00	0.98	0.96
	3	2	0.96	1.09	0.98	0.95	0.93
13.4	1	1	0.96	0.97	0.93	0.82	0.66
	2	1	1.13	1.09	1.02	0.94	0.90
	3	1	0.85	1.00	0.98	0.92	0.88
	1	2	0.88	0.98	1.01	0.93	0.86
	2	2	0.99	1.00	1.01	1.00	1.01
	3	2	0.96	1.11	1.00	0.96	0.93
17.9	1	1	0.99	0.83	0.65	0.53	0.45
	2	1	0.92	0.87	0.85	0.80	0.76
	3	1	1.05	1.11	1.06	0.98	0.91
	1	2	0.92	0.89	0.82	0.70	0.64
	2	2	0.96	0.92	0.91	0.91	0.88
	3	2	1.24	1.22	1.12	0.96	0.83

Table A.6 Culvert 3, Truck 2 *DAF*

			Sensor Location (m)				
Speed (m/s)	Lane	Pass No.	-3.6	-1.8	0	1.8	3.6
8.9	1	1	1.07	0.92	0.82	0.78	0.81
	2	1	0.98	0.97	0.97	0.99	0.97
	3	1	0.97	0.99	1.02	1.04	1.05
	1	2	1.05	0.90	0.80	0.75	0.68
	2	2	1.13	1.05	0.96	0.88	0.87
	3	2	0.98	1.04	0.98	0.99	1.01
13.4	1	1	0.88	1.00	1.12	1.05	1.08
	2	1	0.86	0.88	0.92	0.97	1.00
	3	1	0.90	0.81	0.82	0.91	1.02
	1	2	1.02	0.89	0.81	0.74	0.72
	2	2	0.96	0.97	0.93	0.92	0.89
	3	2	0.82	0.81	0.82	0.92	1.04
17.9	1	1	1.02	0.93	0.85	0.79	0.87
	2	1	1.18	1.13	1.09	1.04	1.08
	3	1	0.95	0.88	0.88	0.97	1.09
	1	2	1.15	1.04	0.93	0.91	0.94
	2	2	0.97	0.97	1.04	1.09	1.15
	3	2	0.78	0.88	0.87	0.98	1.13

Table A.7 Culvert 4, Truck 1 *DAF*

			Sensor Location (m)							
Speed (m/s)	Lane	Pass No.	-3.6	-3.2	-1.8	0	1.2	1.8	2.7	3.6
8.9	1	1	0.99	1.01	0.91	0.85	0.90	0.89	0.89	0.88
	2	1	0.88	0.89	0.86	0.96	0.96	0.96	1.06	1.04
	3	1	1.16	1.29	1.29	1.38	0.95	0.92	1.00	0.59
	1	2	0.95	0.96	0.94	0.92	1.00	1.01	1.02	0.87
	2	2	0.99	0.96	0.92	0.94	0.96	0.95	0.97	0.95
	3	2	1.15	1.25	1.24	1.22	1.02	0.99	1.05	0.67
13.4	1	1	0.93	0.91	0.95	0.99	1.08	1.08	1.07	0.98
	2	1	0.93	0.90	0.85	0.93	0.94	0.95	1.09	1.06
	3	1	1.09	1.11	1.10	1.11	0.96	0.95	1.00	0.80
	1	2	0.82	0.78	0.94	0.97	1.11	1.09	1.09	0.96
	2	2	0.85	0.82	0.77	0.96	0.98	0.98	1.28	1.23
	3	2	1.15	1.16	1.14	1.12	0.98	0.97	0.99	0.75
17.9	1	1	0.75	0.72	1.01	1.01	1.32	1.31	1.29	1.18
	2	1	1.19	1.18	1.10	0.95	0.95	0.96	0.93	0.98
	3	1	1.42	1.43	1.41	1.32	1.03	0.98	0.95	0.69
	1	2	0.71	0.67	0.85	0.91	1.10	1.09	1.08	0.98
	2	2	0.96	0.94	0.88	0.98	0.99	0.99	1.15	1.14
	3	2	1.51	1.49	1.48	1.44	1.05	1.00	1.02	0.65

Table A.8 Culvert 4, Truck 2 *DAF*

			Sensor Location (m)							
Speed (m/s)	Lane	Pass No.	-3.6	-3.2	-1.8	0	1.2	1.8	2.7	3.6
8.9	1	1	0.73	0.71	0.97	1.04	1.20	1.18	1.19	1.06
	2	1	0.84	0.81	0.77	0.93	0.96	0.97	1.23	1.15
	3	1	0.98	1.08	1.06	1.04	0.91	0.89	0.91	0.79
	1	2	0.94	0.94	0.95	0.93	1.00	0.96	0.97	0.83
	2	2	1.03	1.04	1.01	0.97	0.98	0.97	1.00	0.98
	3	2	1.03	1.04	1.04	1.01	0.90	0.90	0.91	0.87
13.4	1	1	0.79	0.76	0.95	1.00	1.16	1.14	1.19	0.99
	2	1	1.08	1.08	1.03	0.93	0.93	0.93	0.97	0.96
	3	1	1.04	1.13	1.06	1.04	0.89	0.88	0.88	0.80
	1	2	0.81	0.77	0.95	1.00	1.16	1.15	1.16	0.98
	2	2	0.96	0.93	0.92	0.92	0.94	0.94	1.05	1.02
	3	2	1.05	1.10	1.06	0.99	0.94	0.94	0.93	0.96
17.9	1	1	0.54	0.52	0.87	0.99	1.45	1.43	1.39	1.15
	2	1	1.15	1.16	1.12	0.91	0.86	0.85	0.89	0.89
	3	1	1.21	1.23	1.24	1.15	1.00	0.99	0.98	0.97
	1	2	0.53	0.49	0.83	0.94	1.37	1.38	1.36	1.09
	2	2	1.22	1.23	1.17	0.86	0.79	0.78	0.82	0.83
	3	2	1.23	1.23	1.26	1.20	0.97	0.95	0.95	0.86

Table A.9 Culvert 5, Truck 1 *DAF*

			Sensor Location (m)						
Speed (m/s)	Lane	Pass No.	-3.6	-2.1	-1.8	0	0.6	1.8	3.6
	1	1	-	-	-	-	-	-	-
	2	1	1.05	1.01	1.02	1.01	1.01	0.99	1.07
	3	1	1.01	0.90	0.92	0.97	0.97	1.01	1.04
	1	2	0.99	0.92	0.93	0.89	0.88	0.89	0.88
	2	2	1.01	0.96	0.98	0.97	0.98	0.98	1.01
	3	2	0.94	0.90	0.93	0.96	0.96	1.01	1.07
	1	1	0.90	0.92	0.93	0.97	0.99	0.98	1.01
	2	1	0.85	0.86	0.87	0.94	0.95	1.02	1.08
	3	1	0.93	0.88	0.91	0.95	0.96	0.98	1.06
	1	2	0.94	0.94	0.96	0.98	1.00	0.99	1.05
	2	2	1.05	1.00	1.01	0.95	0.96	0.90	0.94
	3	2	0.87	0.84	0.86	0.90	0.93	0.96	1.03
	1	1	1.11	1.05	1.07	1.04	1.05	1.05	1.03
	2	1	0.88	0.88	0.89	0.99	0.99	1.04	1.16
	3	1	0.87	0.83	0.86	0.92	0.96	0.95	1.08
	1	2	1.03	1.03	1.05	1.07	1.09	1.12	1.13
	2	2	1.15	1.07	1.08	0.98	0.99	0.92	0.94
	3	2	0.80	0.85	0.87	0.92	0.93	0.96	1.07

Table A.10 Culvert 5, Truck 2 *DAF*

			Sensor Location (m)						
Speed (m/s)	Lane	Pass No.	-3.6	-2.1	-1.8	0	0.6	1.8	3.6
	1	1	-	-	-	-	-	-	-
	2	1	1.01	0.98	0.98	0.94	0.92	0.89	0.87
	3	1	0.78	0.81	0.81	0.87	0.90	0.96	1.05
	1	2	1.03	1.01	1.01	0.98	0.96	0.96	0.93
	2	2	0.98	0.98	0.99	0.99	0.98	0.97	0.91
	3	2	1.05	1.00	1.02	0.99	0.98	0.99	1.01
	1	1	1.05	1.01	1.04	1.02	1.03	1.03	0.97
	2	1	1.11	1.03	1.06	0.92	0.90	0.82	0.81
	3	1	1.03	1.00	1.01	1.00	1.00	0.96	0.97
	1	2	1.14	1.02	1.03	0.89	0.88	0.88	0.83
	2	2	0.92	0.90	0.91	0.93	0.94	0.96	1.00
	3	2	0.80	0.78	0.79	0.85	0.88	0.94	1.06
	1	1	1.06	0.99	1.00	0.99	0.97	0.94	0.94
	2	1	1.25	1.13	1.20	0.95	0.88	0.75	0.71
	3	1	0.78	0.77	0.78	0.84	0.87	0.96	1.09
	1	2	0.98	1.02	1.05	1.17	1.18	1.20	1.24
	2	2	0.90	0.86	0.86	0.87	0.87	0.86	0.87
	3	2	0.82	0.86	0.88	0.91	0.95	0.98	1.03